UNCLASSIFIED

AD NUMBER

AD462521

LIMITATION CHANGES

TO:

Approved for public release; distribution is unlimited.

FROM:

**Distribution authorized to U.S. Gov't. agencies and their contractors;
Administrative/Operational Use; MAR 1965. Other requests shall be referred to Ballistic Div., Det 4, RTD, Eglin AFB, FL.**

AUTHORITY

AFATL ltr 3 Oct 1977

THIS PAGE IS UNCLASSIFIED

THIS REPORT HAS BEEN DELIMITED
AND CLEARED FOR PUBLIC RELEASE
UNDER DOD DIRECTIVE 5200.20 AND
NO RESTRICTIONS ARE IMPOSED UPON
ITS USE AND DISCLOSURE.

DISTRIBUTION STATEMENT A

APPROVED FOR PUBLIC RELEASE;
DISTRIBUTION UNLIMITED.

UNCLASSIFIED

AD 462521

DEFENSE DOCUMENTATION CENTER

FOR

SCIENTIFIC AND TECHNICAL INFORMATION

CAMERON STATION ALEXANDRIA, VIRGINIA

UNCLASSIFIED

NOTICE: When government or other drawings, specifications or other data are used for any purpose other than in connection with a definitely related government procurement operation, the U. S. Government thereby incurs no responsibility, nor any obligation whatsoever; and the fact that the Government may have formulated, furnished, or in any way supplied the said drawings, specifications, or other data is not to be regarded by implication or otherwise as in any manner licensing the holder or any other person or corporation, or conveying any rights or permission to manufacture, use or sell any patented invention that may in any way be related thereto.

DISCLAIMER NOTICE

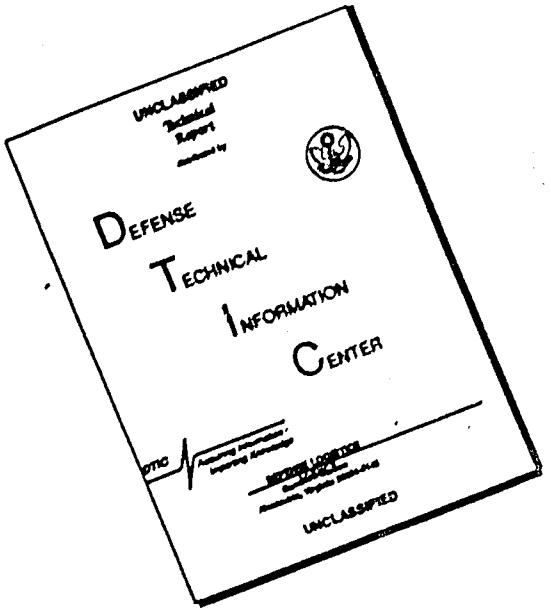

THIS DOCUMENT IS BEST QUALITY AVAILABLE. THE COPY FURNISHED TO DTIC CONTAINED A SIGNIFICANT NUMBER OF PAGES WHICH DO NOT REPRODUCE LEGIBLY.

462521

CATALOGED BY: DDC
AS AD NO. 462521

ATI-TR-65-24

CONSTANT VELOCITY JETS FOR QUANTITATIVE ULTRA - HIGH VELOCITY CRATERING STUDIES

By

Douglas H. Pack
Intermountain Research and Engineering Co., Inc.

DDC
RECEIVED
MAY 11 1965
DDC-IRA E

March 1965

Directorate of Armament Development
Det 4, Research and Technology Division
Air Force Systems Command
Eglin Air Force Base, Florida

Constant Velocity Jets For Quantitative Ultra - High Velocity Cratering Studies

By

Douglas H. Pack
Intermountain Research and Engineering Co., Inc.

FOREWORD

This theoretical and experimental investigation of shaped charge design was conducted under Air Force Contract AF 08 (635)-3668 between 5 June 1963, and 28 January 1965 by Intermountain Research and Engineering Co., Inc., Salt Lake City, Utah.

The work was administered under the direction of the Terminal Ballistics Branch, Det. 4, Research and Technology Division, Eglin Air Force Base with Mr. A.G. Bilek and Lt. M.S. Harris as Project Engineers.

PUBLICATION REVIEW

This technical documentary report has been reviewed and is approved.

CHARLES E WOOD
Major, USAF
Chief, Ballistics Division

ABSTRACT

Experiments were carried out to produce a constant velocity jet from shaped charges. Tests were conducted in atmosphere and at reduced pressures. Liner geometries, types of explosive, and wave shaping techniques were varied systematically to produce an elongated jet which approached a velocity of 14.0 km/sec.

CONTENTS

ILLUSTRATIONS

CONSTANT VELOCITY JETS FOR QUANTITATIVE ULTRA-HIGH VELOCITY CRATERING STUDIES

FINAL TECHNICAL DOCUMENTARY REPORT

RESUME OF THE STATE OF THE ART

Methods of accelerating hypervelocity projectiles fall into two general categories:

1. Acceleration, by various means, of single particles or pellets as unit projectiles, and

2. Formation of a jet from the liner in an explosive shaped charge.

Although the latter method results in considerably higher-velocity projectiles, the jet has extended axial length and consists of a train of particles having a rather wide range of velocities. This contract was concerned with refining the second method to produce shaped charge jets made up of particles all having the same velocity.

STATEMENT OF THE PROBLEM

When the explosive of a shaped charge detonates, the resulting pressures on the liner causes the formation and emergence of a jet having the inherent characteristic of possessing a spectrum of velocities for the various elements comprising the jet. This characteristic of jets is very effective in causing spectacular deep-hole penetration of targets, but on the other hand ambiguous results occur when these jets are used in basic cratering studies. What is desired for the latter application is a single particle or group of particles having the following characteristics:

1. Velocities in the range from 10 to 14 km/sec,

2. All portions of the jet having the same velocity.

3. Sufficiently large jet mass to cause appreciable cratering.

4. Good cohesion of particles out to practical standoff distances.

All of these requirements are not independent of each other; for example, the jet velocity may be increased by reducing the liner angle, but this reduces the jet mass.

METHODS OF PROBLEM SOLUTION

Prior Methods

Previous efforts to reduce the velocity gradient in shaped charge jets have consisted of (1) unsymmetrical initiation of the shaped charge which resulted in a dispersed pattern of particle impact on the target (each particle having a single velocity)[1], and (2) inhibiting the slower portion of the jet to allow only the higher velocity elements of the jet to reach the target[2]. Neither of these approaches made any effort to alter the basic structure of a shaped charge jet, but rather manipulated the jet to obtain the desired effects.

Methods Used in this Contract

The following parameters were varied in efforts directed towards reducing the velocity gradients in the jets from shaped charges:

1. Liner size, configuration, and material.
2. Shaped charge explosive.
3. Size and configuration of charge.
4. Wave shaping of detonation front.
5. Inhibition of jet by various configurations.

Initial work consisted of devising a method of accurately determining the velocity structure of shaped charge jets. This method was then used to analyze the performance of jets emerging from various conic and paraboloid liners cast in conventional cylindrical charges. The final phase of investigation consisted of developing a disc-shaped charge and a suitable initiator to provide symmetrical peripheral initiation of the charge.

VELOCITY MEASUREMENT TECHNIQUES

Framing Camera

The first attempts to measure jet velocities were made with a framing camera setup as shown in Figure 1. Vacuum tight seals were made between the plastic tubing and the shaped charge on one end, and the steel target on the other. The plastic tubing chamber was then evacuated to a pressure of a few microns to prevent the jet from becoming self luminous during its high velocity excursion from liner to target. A backlighting light bomb was used to provide illumination for sequential silhouette pictures of the jet. Jet velocities were then calculated from the geometry of the system and the frame rate of the framing camera. Information on the jet was also obtained from the extent of target penetration. This

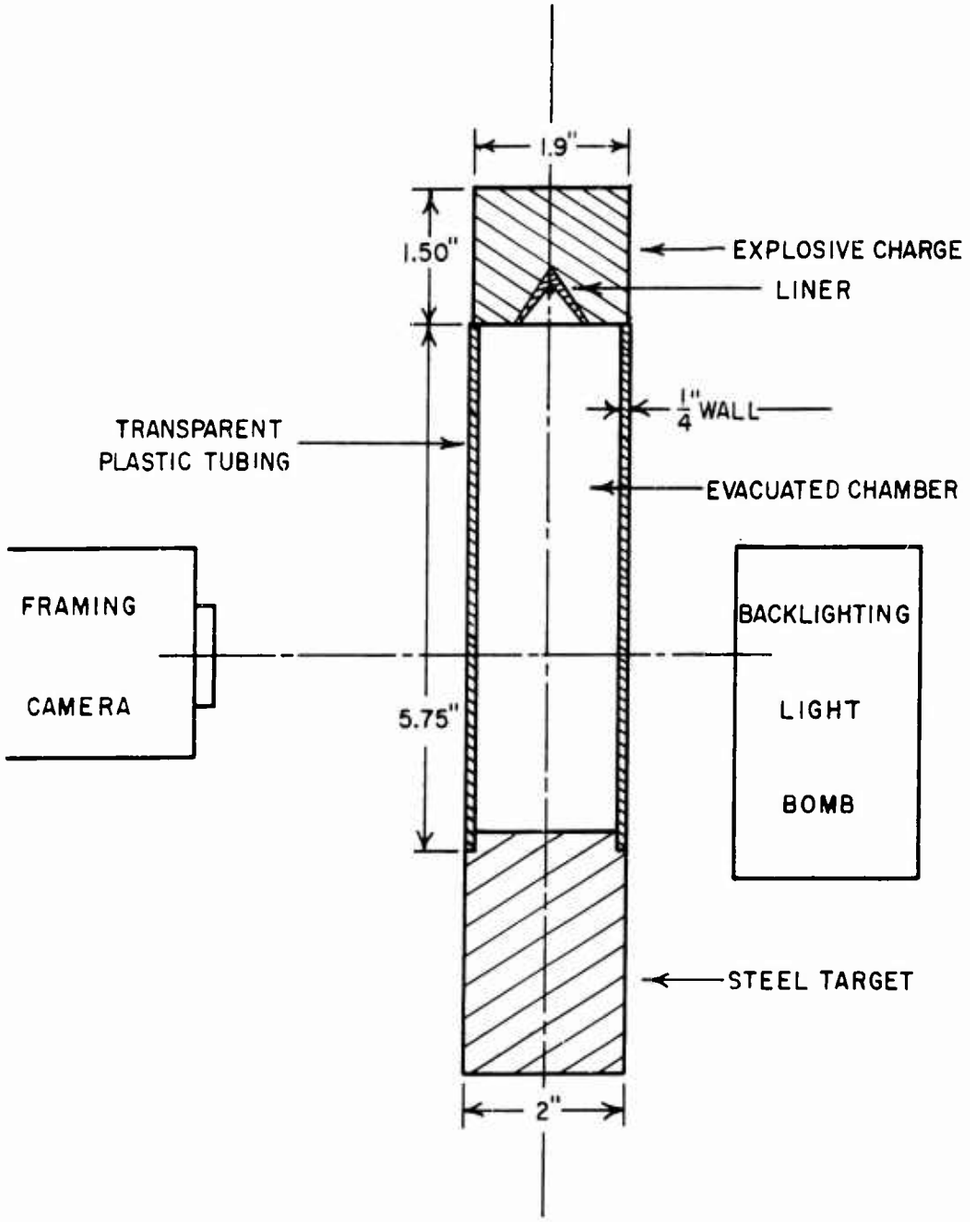

FIGURE 1. Sectional view of framing camera method designed to measure shaped charge jet velocities.

SCALE = ½

arrangement would therefore theoretically provide data on jet velocity, jet dimensions, and jet penetration capabilities. However difficulties were experienced in obtaining satisfactory vacuum seals and proper back-lighting illumination levels.

Pin Set Technique

The second method used to obtain jet velocity data consisted of a series of pin sets as shown in Figure 2. Each target plate was covered with an insulating film of Mylar; aluminum foil was then placed over the top and bottom surfaces of each plate and electrical leads were brought out from the plate and from the two foil surfaces. These leads were connected to the pin set circuitry so that penetration of Mylar film at any point would short circuit an aluminum foil to its grounded target plate and this would result in a pip appearing on an oscilloscope raster. Timing marks on the latter permitted determination of time intervals between jet penetrations of various target foils; then jet velocities, both between and through plates, could be calculated by taking into consideration the vertical displacements between plates as well as plate thicknesses. The streak camera was used in conjunction with the foregoing setup to measure the initial velocity of the jet between the charge and the first plate. Some difficulties were encountered in realizing adequate insulation and proper circuit adjustments, but prior to correcting these problems it was noted from the streak camera record that jet velocity traces appeared between plates as well as for the initial velocity. This actually eliminated the need for pin sets to determine jet velocities as may be seen from the following section.

Multiple Plate Technique

Figure 3 shows a sketch of a multiple plate test setup as viewed by the streak camera, while Figure 4 is a photograph of a typical charge ready to be fired. As the jet leaves the liner it first becomes visible to the camera when it passes the lower edge of the charge-centering block. And since the jet is self luminous in passing through the air, sufficient light is produced by the leading edge of the jet to produce a velocity trace on the streak camera film. Figure 5 is a photographic reproduction of a streak camera record of Test Shot No. E-211 and shows the analytical and graphical methods used to reduce the data to the several velocities of the jet elements at various distances from the leading edge of the jet. The photograph contains streak traces corresponding to several velocities. The first trace at the left results from the shaped charge itself and gives an approximate measure of the detonation velocity of octol of which the charge was comprised. This (as well as the other streak traces on the film) is translated into a velocity magnitude as follows. The inverse magnification is determined by dividing a measured distance on the scale image in the static image by the indicated number of units within the measured distance. In Figure 5 the inverse magnification turns out to

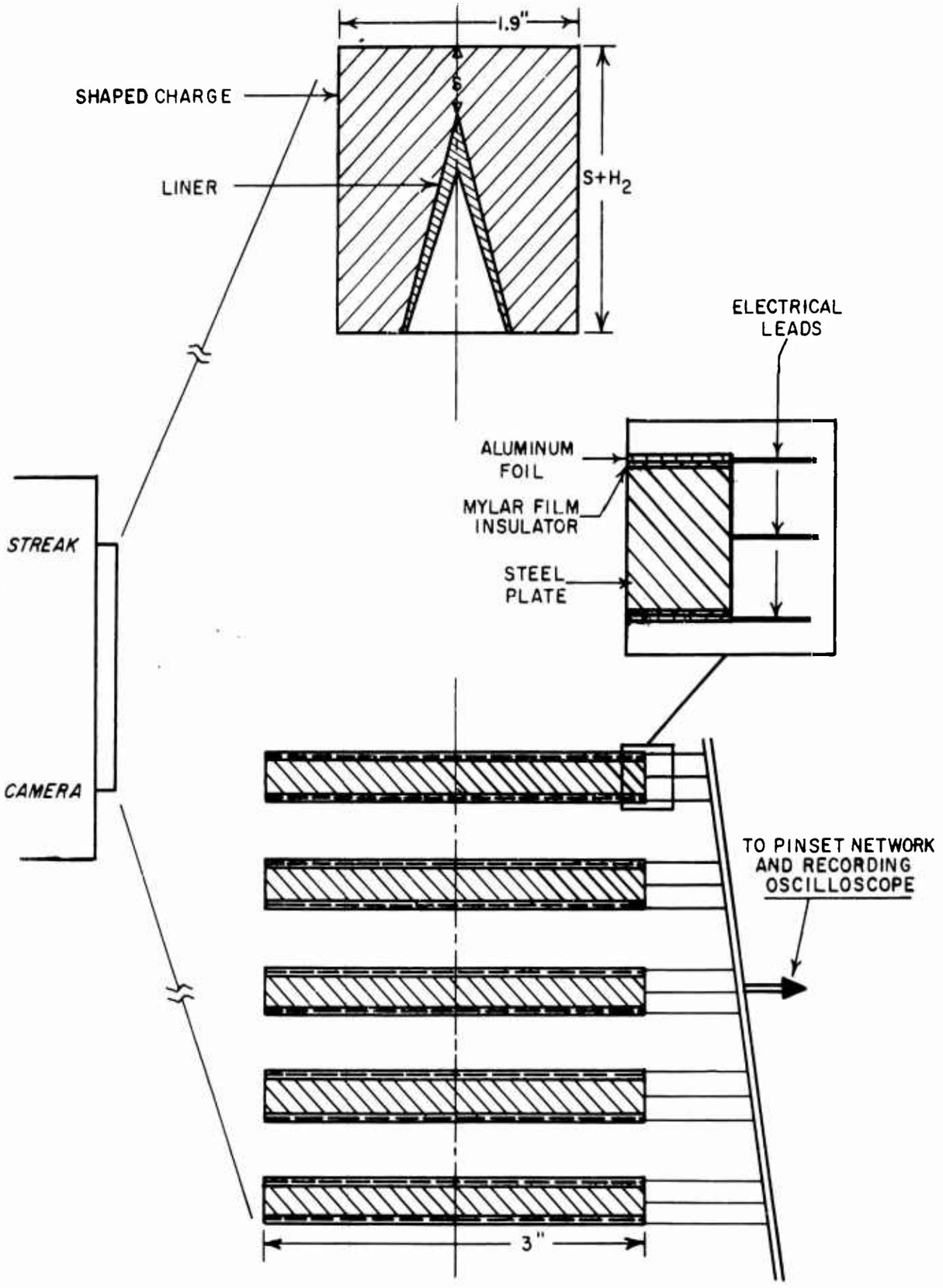

FIGURE 2. Pin set method of determining jet velocities.

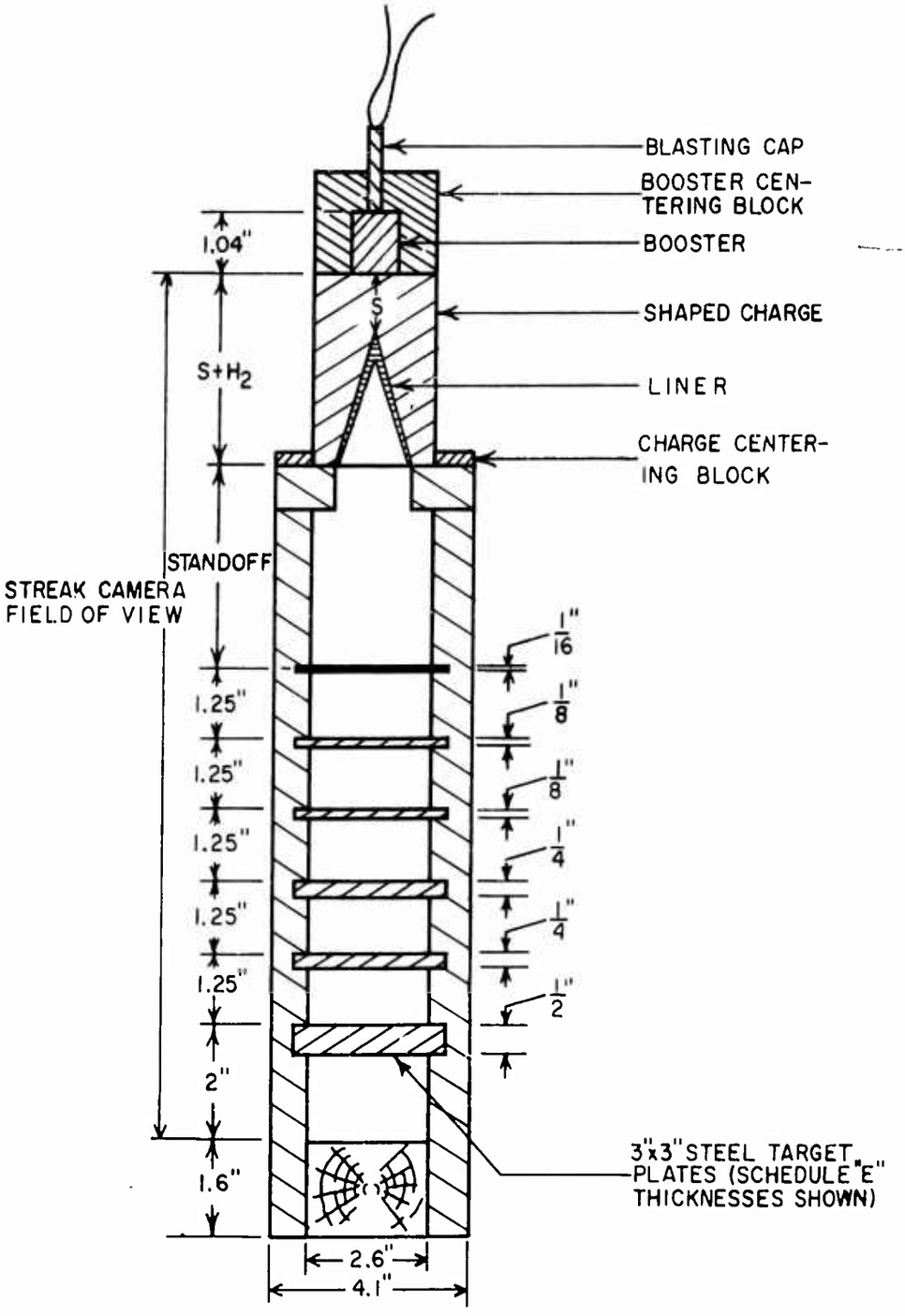

FIGURE 3. Sectional view of multiple plate setup for determining jet velocities.

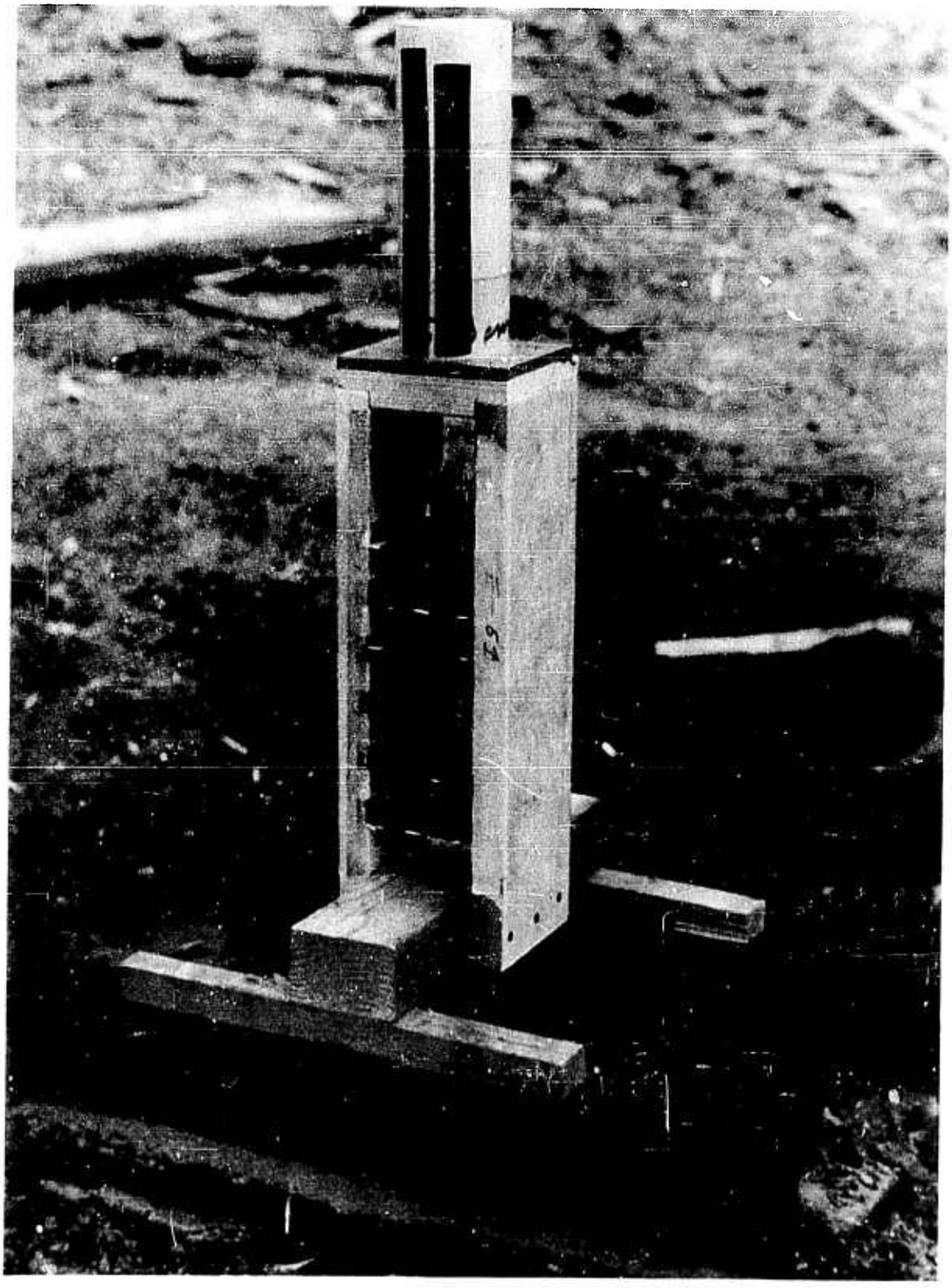

FIGURE 4. Multiple-plate setup for Test No. E-61.

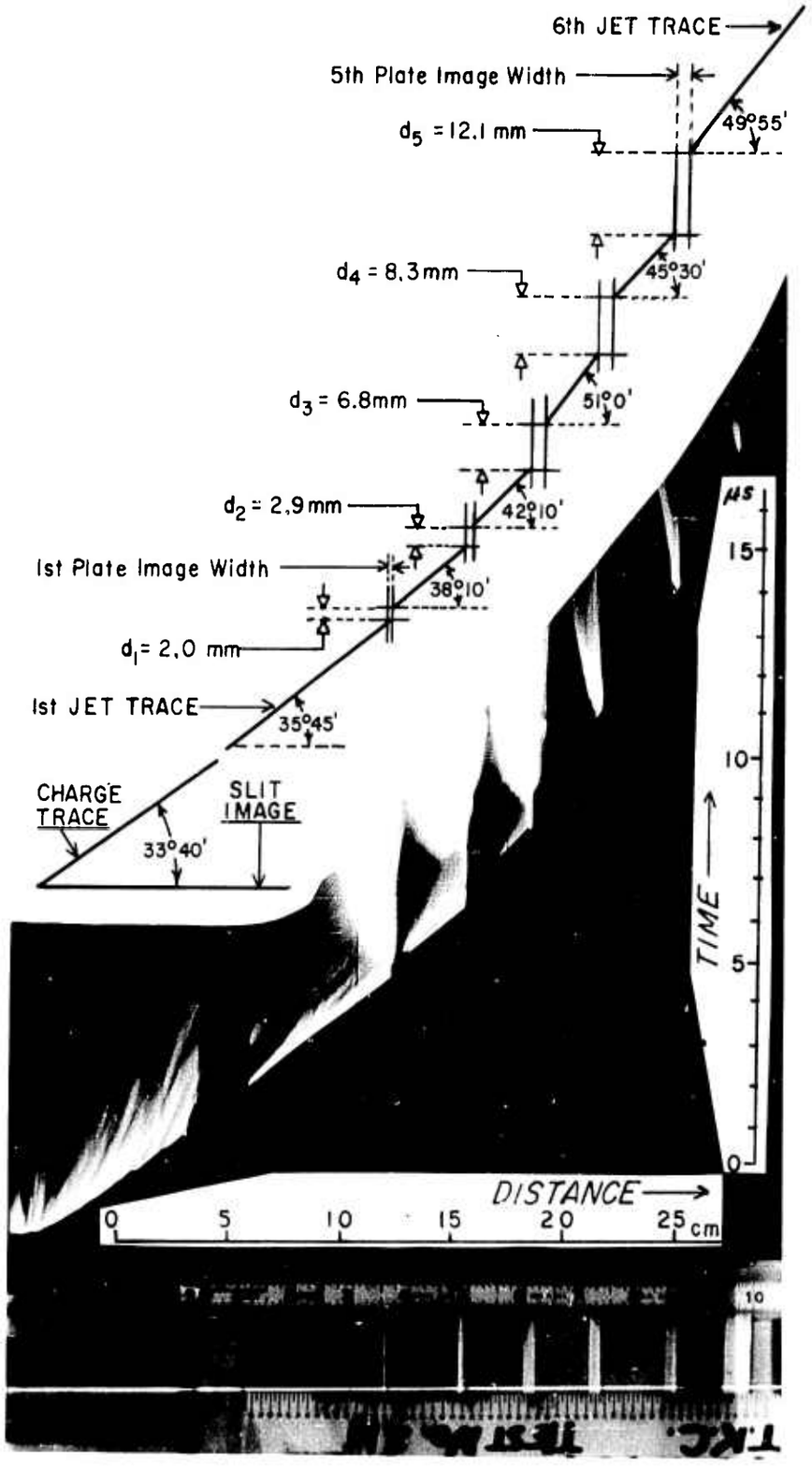

FIGURE 5. Streak camera velocity traces and graphical method of data reduction for Test No. E-211.

be:

$$M^{-1} = 9"/3.31" = 2.72$$

The rotating mirror of the streak camera had an angular velocity of 300 rps for test No. E-211 of Figure 5, and from the geometry of the camera this represents an image velocity writing speed, W, of 2.25mm/μsec along the film in the TIME direction. But in order to determine the object velocity at the event, the film writing speed velocity is multiplied by the inverse magnification:

$$M^{-1} W = 2.72 \ (2.25) = 6.12 \text{ mm/}\mu\text{second}$$

Thus, distance along the film in the TIME direction represents an object velocity of 6.12 mm/μsec = 6.12 km/sec for the particular camera parameters used to obtain the streak record of Figure 5. In the following construction the rotating mirror moves the object image a distance equal to OA during the same time interval that the object

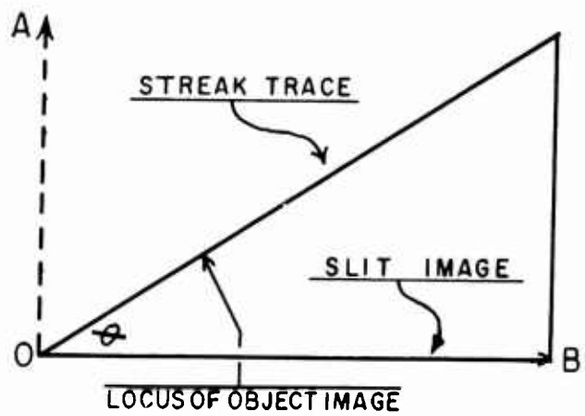

image (of the leading edge of the detonation front on the side of the charge) moves through a distance equal to OB. And since OA represents a velocity of 6.12 mm/μsec, the object velocity is determined as:

$$V = OA \ (\cot \theta) = (6.12) \cot 33°40'$$

$$= 9.2 \text{ mm/}\mu\text{s} = 9.2 \text{ km/sec}$$

This apparent detonation velocity, incidentally, is higher than the normal 8.1 to 8.4 km/sec for octol because of central initiation by a

relatively small booster and the short length of the charge. The following sketch of booster and charge shows how the detonation front on the side of the charge (which produces the streak recorded by the camera) travels from c to d while the detonation travelling normal to the camera moves over the shorter path from e to f. Thus, due to the

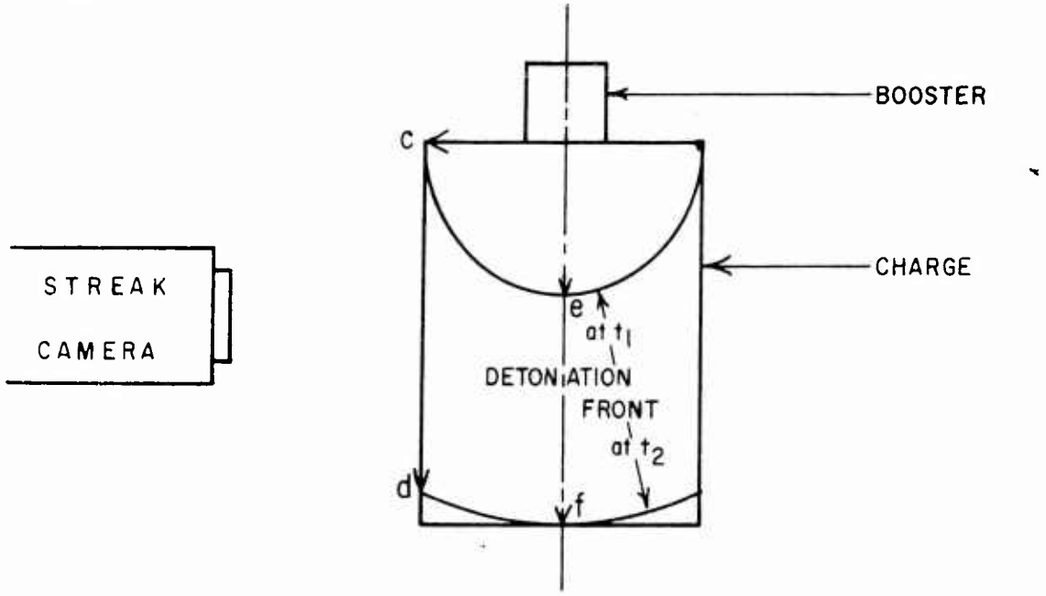

geometry of the booster and charge, and to the curved detonation front, the camera records an apparent velocity higher than the true velocity by the approximate ratio: cd/ef. Of course the greater the axial length of a charge the closer this ratio approaches one.

Since the streak traces on the film of Figure 5 resulting from the shaped charge jet are already up to maximum velocity before coming into view of the camera, the measured velocities are correct since they do not have the foregoing discrepancy.

The second trace from the left in Figure 5 corresponds to the velocity of the leading element of the jet from the time it emerges into view below the charges centering block until it strikes the first target plate. The same procedure as used above to obtain the indicated octol detonation velocity results in a velocity of 8.50 km/sec for the leading element of the jet as listed in Table 1. When the leading elements of the jet reach the first target plate a finite length of the jet is dissipated in making a hole through the first plate. The time required for the jet to penetrate the first plate is determined from the graphical construction of Figure 5. The image thickness of the first target plate is superimposed upon streak traces corresponding to the jet velocities before and after passing through the plate. Then the vertical distance d_1 between the intersection of the initial jet velocity trace with the entrance surface of the plate, and the intersection of the second jet velocity trace with the exit surface

TABLE 1. Values obtained from Figure 5 used to calculate velocities and ΣL_i distances for test E-211.

j	θ	cot θ	V_j (mm/μs)	$\bar{V}_j$ (mm/μs)	d (mm)	t=d/W (μsec)	$L=V_j t$ (mm)	S_i (mm)	$L_i=L-S_i$ (mm)	ΣL_i (mm)	$U_i=S_i/t$ (mm/μsec)
e	33°40'	1.501	9.19								
o	35°45'	1.389	8.50								
1				8.15	2.0	0.89	7.26	1.78	5.5	5.5	2.00
2	38°10'	1.272	7.79								
3				7.27	2.9	1.29	9.38	3.25	6.1	11.6	2.52
4	42°10'	1.104	6.76								
5				5.86	6.8	3.02	17.7	6.35	11.4	23.0	2.10
6	51°0'	0.810	4.96								
7				5.48	8.3	3.69	20.2	6.35	13.8	36.8	1.72
8	45°30'	0.983	6.01								
9				5.58	12.1	5.38	30.0	6.35	23.6	60.4	1.18
10	49°55'	0.842	5.15								

U_i: Effective jet velocity through target plate.

of the plate, is proportional to the time required for the jet to penetrate the first plate. And since this distance d is parallel to the TIME axis, the penetration time of the first plate is

$$t = \frac{d}{W} = \frac{2.0 \text{ mm}}{2.25 \text{ mm/}\mu\text{sec}} = 0.89 \ \mu\text{sec}$$

The distance which the leading elements of the jet travel during the time required for penetration of the first plate may be closely approximated by assuming a jet velocity $\overline{V}_i$ during penetration that is an average of the jet velocities before and after penetration. For the first plate this would be 8.15 km/sec (Table 1). The jet travel distance, L, is therefore:

$$L = V_i t = 8.15 \text{ mm/}\mu\text{s} \ (0.89 \ \mu\text{sec})$$

$$= 7.24 \text{ mm}$$

This distance is actually the length of the jet from its initial front to the element that first emerges from the exit side of the first plate.

This new leading front of the jet passed through the thickness, S_i, of the first plate without any resistance due to the hole that had already been made by the preceding jet elements. Therefore the calculated length L is longer than the jet segment "used up" in penetrating the first plate by an increment equal to the plate thickness, since this increment is equal to the jet element length that passed unimpeded through the plate hole before the emerging trace became visible on the exit side of the plate. Hence the length L_i of the jet that was dissipated in passing through the first plate may be determined:

$$L_i = L - S_i = 7.26 - 1.78$$

$$= 5.5 \text{ mm}$$

It has thus been determined that the new leading front of the jet which emerged from the first target plate to produce the third streak trace from the left in Figure 5 was 5.5 mm from the initial front of the jet. Therefore the third velocity trace of Figure 5 provides a measure of the velocity of the jet element which was 5.5 mm from the initial front of the jet.

The succeeding velocity traces of Figure 5 have been analyzed to provide jet element velocities at the various increments from the initial front of the jet as listed under the ΣL_i column of Table 1. Figure 6 contains a plot of these velocities as a function of the ΣL_i increments for Test No. E-211.

Finer resolution of the velocity structure within the jet may be obtained by using a greater number of thinner target plates which are more closely spaced. The limit to this approach would consist of allowing the target plates to merge into a continuous medium to provide a smooth continuous plot of velocity vs position in the jet. The following sub-section analyzes the results of firing a jet into air as a continuous medium.

Continuous Medium Technique

Several shots were made over an air range of sufficient length to cause radical jet velocity attenuation due to progressive continuous attrition of the jet (as well as frictional drag on the jet) by the air, instead of the stepwise method of steel target plates. Figure 7 is a photographic reproduction of a streak camera record that was made of this type shot (Test No. E-134). The streak trace shows a continuous change in jet velocity from the charge to a steel target plate 13-1/3 feet away.

In the following analysis, arbitrary 1-foot thick increments of air were chosen to simulate the steel target plates of the preceding section. Instantaneous velocity values were read from the streak trace at the 1-foot intervals to provide entrance and exist velocities for each foot-thick "air target plate". These values are listed under the V_j column of Table 2. The mean velocity (not a continuously integrated true average velocity) through each 1-foot air increments $(V_j+V_{i+1})/2$ was next calculated and these values are listed under the $\bar{V}_i$ column. Distances, d, were then measured on the film corresponding to the 1-foot increments of jet travel (see bottom of Figure 7). These distances were then divided by the camera writing speed, 0.375 mm/μsec, to obtain jet transit times, t, across the 1-foot increments. Then the theoretical jet travel distance, L, during calculated transit time, t, at average velocity $\bar{V}_i$ was determined for each 1-foot increment. And the magnitude of jet erosion, L_i, was then assumed to be the difference between the calculated jet travel distance, L, which would have occurred had there been no erosion nor air drag and S_i the actual jet travel distance. And finally the L_i distances are summed under the ΣL_i column to give the apparent integrated jet length which includes any air drag influence that would make the erroded jet length appear longer than it actually was.

When the jet length of E-134 is compared to an identical shaped charge (Test No. E-86, Figure 29) the indicated integrated jet erosion

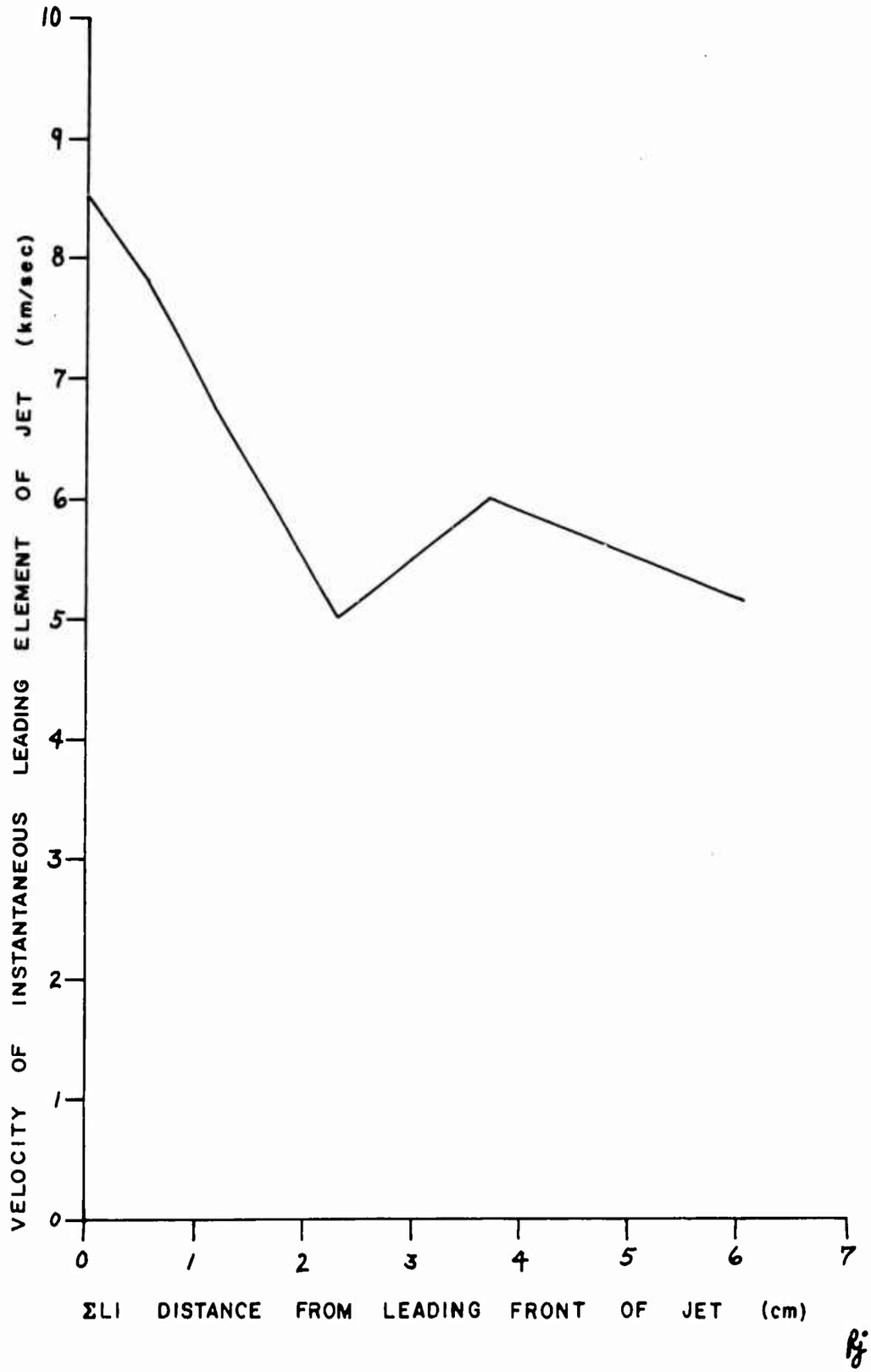

FIGURE 6. Jet segment velocity vs segment distance from initial front of jet, Test E-211.

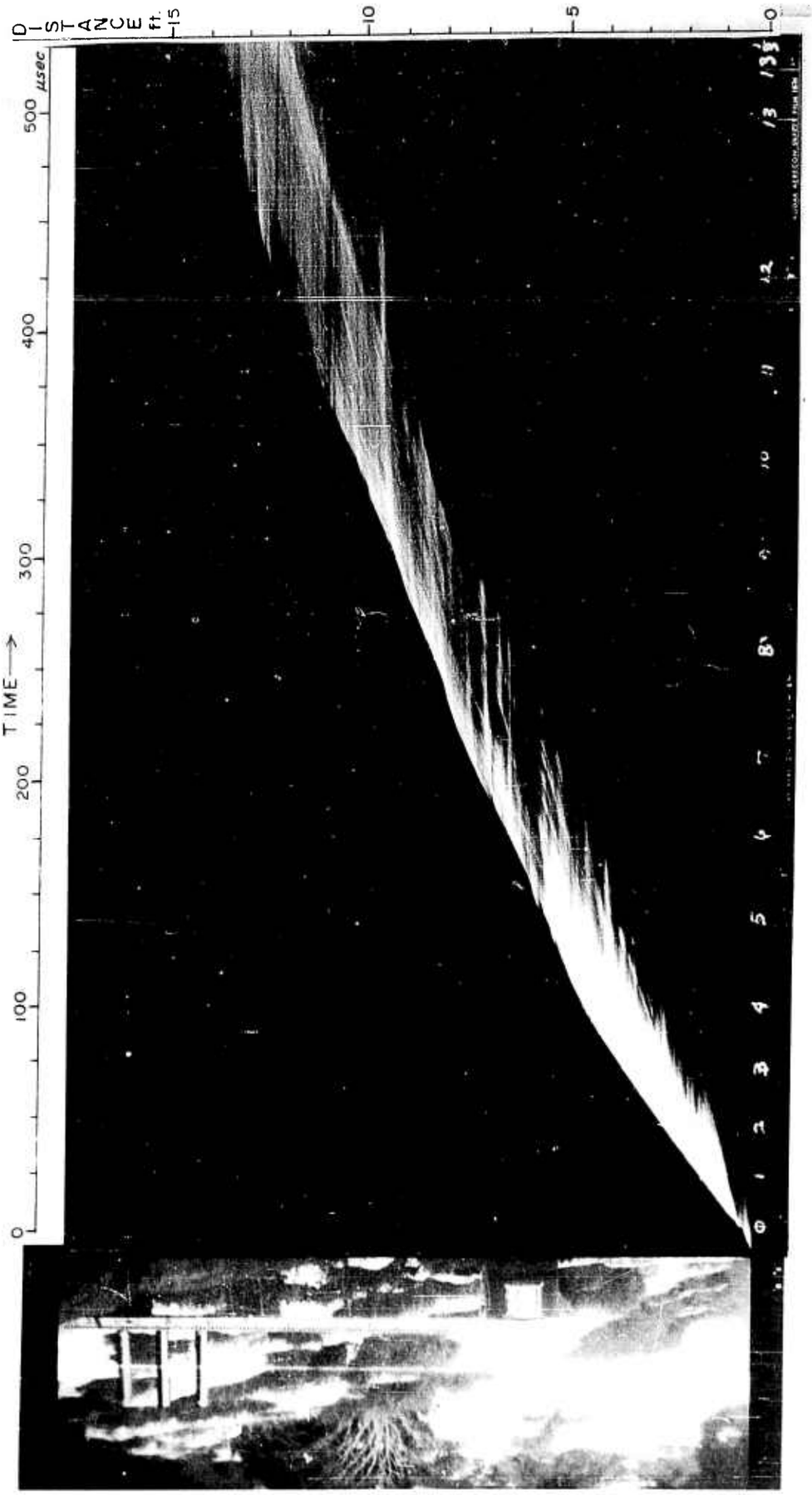

FIGURE 7. Photographic reproduction of streak camera record showing air erosion of jet in Test E-184.

TABLE 2. Values obtained from Figure 7 with resulting velocity and distance values for E-134.

j	θ	cot θ	V_j (mm/μs)	V_i (mm/μs)	d (mm)	t=d/W* (μsec)	$L=\bar{V}_i$ t (mm)	S_i (mm)	$L_i=L-S_i$ (mm)	ΣL_i (mm)
e**	64°	0.488	7.8							
o	47°	0.933	14.6							
1				13.8	8.3	22.2	305	305	0	0
2	50-1/2°	0.824	12.9							
3				12.8	8.7	23.2	297	305	-	0
4	51°	0.810	12.7							
5				12.5	9.3	24.8	310	305	5	5
6	52°	0.781	12.2							
7				11.2	10.3	27.6	309	305	4	9
8	57°	0.649	10.2							
9				9.2	13.8	36.8	339	305	34	43
10	62-1/2°	0.521	8.1							
11				8.3	14.9	39.7	329	305	24	67
12	61-1/2°	0.543	8.5							
13				8.1	12.9	34.4	279	305	-	67
14	64°	0.488	7.6							
15				7.4	17.9	47.7	353	305	48	115
16	65-1/2°	0.456	7.1							
17				6.9	16.2	43.2	298	305	-	115
18	67°	0.425	6.6							
19				6.8	15.8	42.1	286	305	-	115
20	66°	0.445	7.0							
21				7.3	14.4	38.4	280	305	-	115
22	64°	0.488	7.6							
23				7.1	15.9	42.4	301	305	-	115
24	67°	0.425	6.6							
25				5.9	26.4	70.4	416	305	109	224
26	72°	0.325	5.1							
27				3.8	8.6	22.9	87	107	-	224
28	81°	0.158	2.5							

* At a camera speed of 500 rps, the image writing speed was: W = 0.375 mm/μsec.

** Charge detonation velocity.

length, ΣL_i, was found to be longer for the continuous-medium method of Test E-134 than for the multiple plate method of E-86 in which the air travel distances are so short that air drag is negligible. For Test E-86 the ΣL_i valuve at 7.2 mm/μsec was 74 mm, while for test E-134 the value at 7.4 mm/μsec was 115 mm which is about 1-1/2 times as long as from the multiple-plate method. It might therefore be assumed that the additional apparent eroded jet length was due to air drag.

A formula has been developed to calculate the air drag on meteorites[3]:

$$\text{Drag} = -\Gamma\rho_a v^2 A (1+0.16s \Lambda/\Gamma) \text{ dynes},$$

in which Γ and Λ are assumed to be constants, each equal to 1, ρ_a is the air density, v is the meteor velocity, A is the effective cross-sectional area of the meteor, and s is the meteor velocity in units of km/sec. In order to obtain at least a first order effect value of drag magnitude, let it be assumed that the cross-sectional area of the leading jet element of Test No. E-134 was about one-fourth the size of those shown in the radiographs by Kronman and Merendino[4] (using the liner size scaling method shown in their Figure 6). This would give a jet leading element diameter of 0.2 cm, a cross-sectional area of about 0.03 cm^2, and a mass of about 0.004 gm, assuming a sphere of aluminum. Using these assumptions in the air drag formula results in the following value of air drag at a jet element velocity of 10 km/sec.

$$\text{Drag} = -\rho_a v^2 A (1.16) = -0.001 (10^6)^2 (0.03) 1.16$$

$$= -3.5 \times 10^7 \text{ dynes}$$

From which the deceleration, a, may be calculated:

$$a = F/m = 3.5 \times 10^7/.004 \simeq 10^{10} \text{ cm/sec}^2$$

Change in jet element velocity during a 1-foot jet travel increment may now be calculated. The increment nearest the v = 10 km/sec assumed above will be used. In Table 2 this will be the increment in which the velocity dropped from V_8 = 10.2 to V_{10} = 8.1 mm/μsec in 36.8 μsec. Decrease in velocity due to drag will be:

$$\Delta V = at = (10^{10}) 36.8 \times 10^{-6} \text{ cm/sec} = 0.368 \text{ mm/μsec}$$

Thus 0.368 mm/μsec of the $V_8 - V_{10}$ = 2.1 mm/μsec was due to air drag while the remaining 1.7 mm/μsec was due to erosion of the 10.2 mm/μsec

leading element appearing at the 4' mark to permit an 8.1 mm/μsec element to form the velocity trace at the 5' mark.

Due to the assumptions made in the foregoing analysis, the calculated numerical values are somewhat qualitative to show the trend of effects. Also the erratic behavior of the L values in Table 2 (falling below the magnitude of S_i) may be attributed to choosing 1-foot increments of jet travel. A close inspection of the undulating streak trace of Figure .7 reveals that the velocity wasn't continuously decreasing in a smooth manner, but actually increased momentarily in several places as later faster jet elements passed slower earlier elements. Thus, some of the arbitrarily chosen 1-foot points on the curve were probably unfortunate choices to analyze the jet behavior in the preceding and ensuing 1-foot increments. This could be overcome by choosing smaller increments down to the limit of infinitesimals. Therefore an improvement in the photography of jets in a continuous medium to provide larger streak traces that could be read more accurately, and refinement in curve analysis could result in a practical technique to provide a means of determining continuous velocity data throughout the length of the jet.

Figure 8 is a plot of jet element velocities plotted as a function of distance from the charge rather than as a function of the ΣL_i distance from the leading front of the jet, because of the erratic nature of the ΣL_i values in Table 2. In addition to containing results of Test E-134, Figure 8 contains plots for Tests E-132, E-133, and E-135 discussed later.

Since the extended air range method failed in its initial purpose of determining jet cohesion, due to air attrition of the jet, it was deemed necessary to shoot the jets into a vacuum.

Vacuum Range Method

Another method of determining velocity of the leading jet element, as well as jet cohesion at extended standoff distances, consisted of shooting the jet into an evacuated chamber. Virtual elimination of a resistive medium permitted the jet to travel from entrace orfice to target without appreciable deceleration or erosion. The extended distance to the target also provided a check on lateral dispersion within the jet which gave a measure of cohesion of the jet elements. However this technique gave mainly a measure of the leading element of the jet and provided less information on the velocity structure within the jet than did the multiple plate method. Two spaced target plates were provided within the chamber; arrival of the jet at the first plate gave velocity data on the leading element of the jet, and the second plate gave velocity data on the leading portion of the jet which penetrated the first plate.

An example of a streak camera record from a vacuum range shot is shown in the photographic reproduction of Figure 9 for Test No. E-162. In order to realize increased accuracy in reducing the data, the

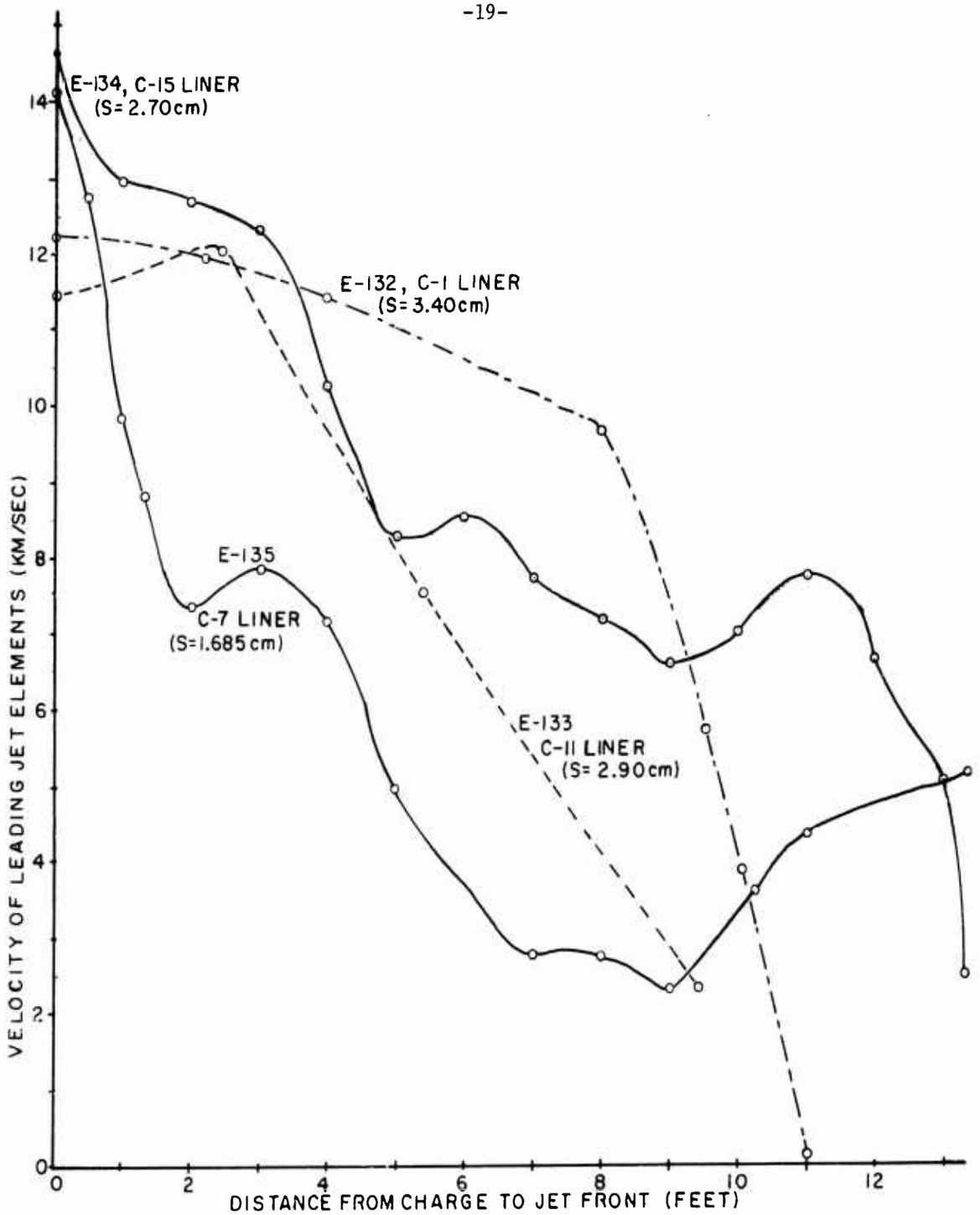

FIGURE 8. Jet element velocity vs distance from charge for extended air range tests.

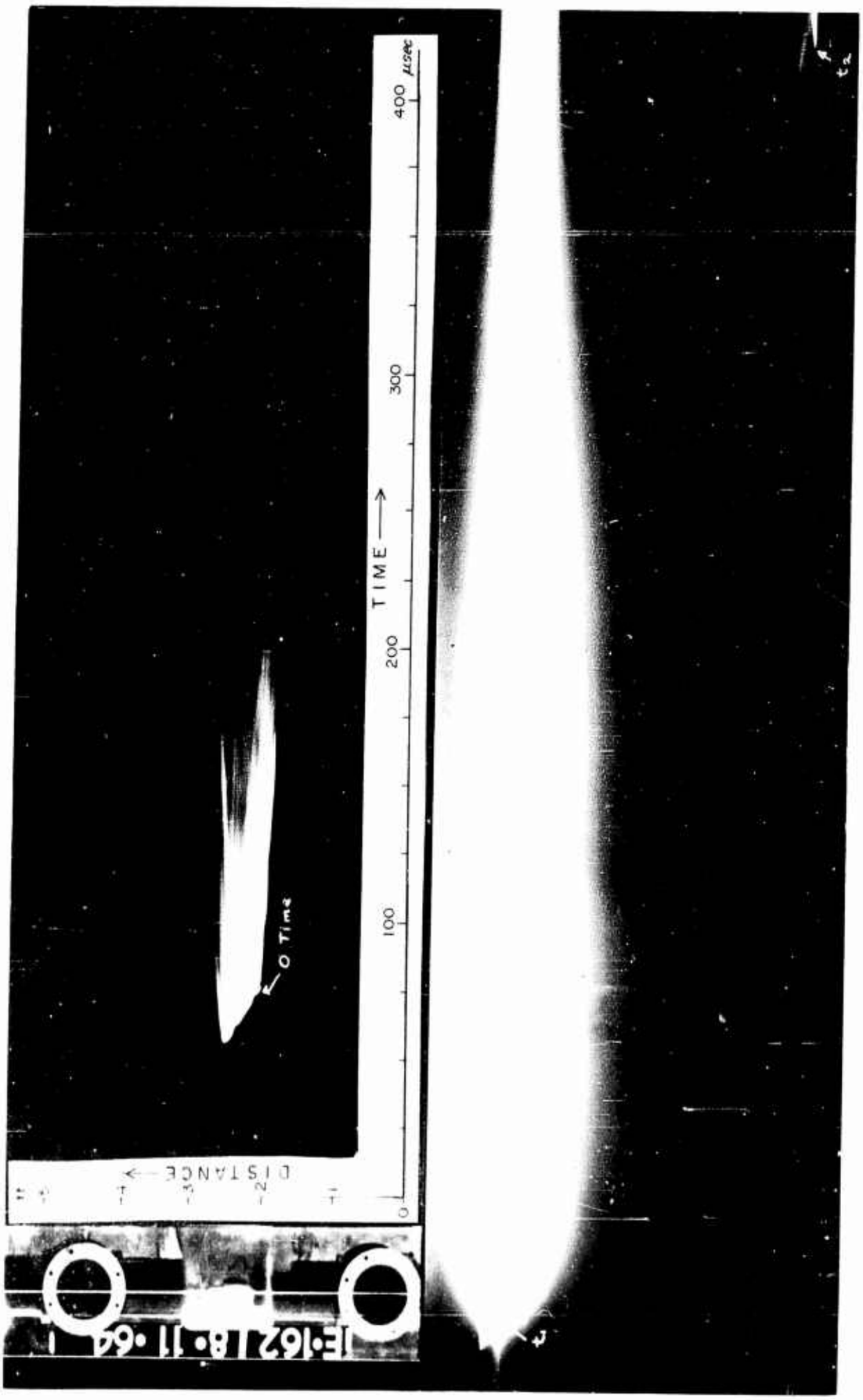

FIGURE 9. Photographic reproduction of streak camera record of Test No. E-162 vacuum range shot.

streak traces on the film were made as large as practical. This was accomplished by focusing on the two observation ports as shown in the static image of Figure 9, instead of on the full 21-foot length of the vacuum tube and barricade. However it was important that the event of the detonation of the shaped charge also be recorded, and this was accomplished without loss in magnification by reflecting with two mirrors an image of the charge into the space between the observation ports as may be seen in the static image.

The original 5" x 30" streak camera film was cut into two equal lengths and mounted in Figure 9 so that the right side of the upper half is continued, timewise, at the left side of the lower half. The first event on the film is the streak record of the detonating charge and the brief appearance of the jet leaving the liner at the point designated on the film as "0-TIME". Elapsed time between the latter point and t_1 was:

$$t_1 = \frac{287.2\text{mm}}{0.75\ \text{mm}/\mu\text{s}} = 382\ \mu\text{s}$$

where t_1 was the time at which the leading element of the jet reached the first target plate. And since the distance from charge to the first plate was 14'1", the jet velocity of the jets leading element was:

$$V_1 = 4260/382 = 11.2\ \text{mm}/\mu\text{sec}$$

This velocity agrees reasonably well with the initial velocity (12.3 km/sec) of the jet from an identical charge (Test No. E-155) shot into multiple plates to determine velocities. The initial velocity of Test E-162 was also determined from the streak trace appearing in the first observation port as shown in Figure 9. As near as the trace angle could be read at that camera-to-object distance, the calculated velocity was about 10 km/sec.

Use of the foregoing procedure with data from the second observation port produced a velocity of 6.50 km/sec, for the portion of the jet that got through the first plate, by the linear method, compared to 5.1 km/sec by the trace angle method.

The vacuum range proved useful in determining jet velocities, especially the initial velocity, as well as for obtaining information on the cohesion of jets at extended standoff distances.

TESTS CONDUCTED

Tooele Ordnance Depot Test Site

All framing camera test shots were made at the University of Utah test facility at Tooele Ordnance Depot, Tooele, Utah by special lease arrangements. The framing camera used produced 25 individual pictures for each test shot and the experiment was designed to show silhouette pictures of the jet progressing down the evacuated chamber of Figure 1. The seven test shots made with the framing camera method of determining velocities are described in the July 1963 report of this contract.

In addition to the test shots mentioned above, three other framing camera shots were made to check the symmetry of initiation of a special type of peripheral initiator. These tests are outlined in the August 1964 report with further details given in the EXPERIMENTAL RESULTS section of this final report.

IRECO Test Site

All test shots which involved use of the streak camera were conducted at the IRECO test facility near Lehi, Utah. These tests included those employing the pin technique, multiple plate technique, extended standoff air range, and extended standoff vacuum range. These various test shots are listed in the monthly reports extending from August 1963 through October 1964, with additional discussion in the EXPERIMENTAL RESULTS section of this report.

Eglin Air Force Base Terminal Effects Tests

Four sets of tests were made at the test facility at Eglin Air Force Base. Efforts were made there to obtain additional data with equipment that was not available at either the Tooele Ordnance Depot nor the IRECO test facilities. This included x-ray methods of photographing shaped charge jets in flight, and Kerr cell framing camera methods with front-lighting and backlighting techniques to observe the shaped charge jets in flight. These tests are outlined in the January 1964, August 1964, and October 1964 reports for this contract, in addition to further information contained under the RESULTS section of this final report.

EXPERIMENTAL PARAMETERS

Shaped Charge Factors

Several factors affect the characteristics of the jets which emerge from shaped charges. These consist of the type of explosive comprising the charge, the shape and symmetry of the initiating wave as controlled

by waveshaping techniques and booster symmetry, degree of confinement of the charge, shape and size of the charge, configuration and size of the liner, material of the liner, and degree of inhibition of the jet. Variations of these factors were employed in efforts to attain the desired constant-velocity jets at the required velocities of 10 km/sec or more.

Types of Explosives

Since high velocity, as well as constant velocity, jets were desired it was advantageous to use an explosive having detonation velocity and pressure as high as practical. Octol was used for most of the test shots (shaped charges and waveshaping charges) as follows:

For all charges from June through December 1963:(Tests E-1 through E-112)

OCTOL: Composition - HMX/TNT/Wax = 69.7/29.8/0.5
Density - ρ_c = 1.74 gm/cm^3
Detonation Velocity - D = 8.1 km/sec

This explosive was made by mixing the proper ratios of the individual ingredients.

For most charges from January through December 1964: (E-113 through E-235)

OCTOL: Composition - HMX/TNT = 75/25 (wax content unknown)
Density - ρ_c = 1.77 - 1.80 gm/cm^3
Detonation Velocity - D = 8.4 km/sec

This latter material was received in pre-mixed chip form and was remelted for casting.

For some charges from August through December 1964: (see ensuing text)

BARATOL:

I Composition - $Ba(NO_3)_2$/TNT = 70/30
Density - ρ_c = 2.37 gm/cm^3
Detonation Velocity - D = 4.78 km/sec

II Composition - $Ba(NO_3)_2$/TNT = 65/35
Density - ρ_c = 2.35 gm/cm^3
Detonation Velocity - D = 5.09 km/sec

III Composition - $Ba(NO_3)_2$/TNT = 60/40
Density - ρ_c = 2.31 gm/cm^3
Detonation Velocity - D = 5.22 km/sec

TNT: Form - granular, cast into charges
Density - ρ_c = 1.6 gm/cm^3
Detonation Velocity - 6.9 km/sec

The foregoing lower-velocity explosives were used on certain charges to determine the feasibility of developing a two-component charge. The test charges which used these variations from the standard octol explosive are listed in the monthly reports and discussed under the EXPERIMENTAL RESULTS section of this report.

In addition to all the above charge explosives, a special initiator explosive was used:

DETASHEET*: Composition - Plasticized PETN
Density - 1.45 - 1.50 gm/cm^3
Detonation Velocity - 7.50 km/sec

The test shots using Detasheet are listed in the August, September, and October 1964 monthly reports, and listed in Table 7 of this report.

Waveshaping Techniques

Two factors affect the velocity of liner wall collapse: detonation pressure and detonation impulse. Since pressure is a scalar quantity the direction of the detonation wave relative to the liner wall has little effect upon liner wall acceleration. On the other hand detonation impulse is a vector quantity having a direction parallel to the direction of detonation. The closer to normal incidence that detonation impulse has with the liner wall, the greater the wall collapse acceleration and subsequent jet velocity.

Figure 10 shows cross-sectional views of shaped charges fired with and without a waveshaper. The arc lines drawn across the charges represent the progression of the detonation front through the explosive. In the charge without the waveshaper the detonation impulse is virtually parallel to the liner wall throughout the length of the latter. Therefore the detonation pressure is mainly responsible for liner wall collapse acceleration and the magnitude of the resulting jet velocity values. However when a waveshaping charge is used the steel waveshaper directs the detonation from the waveshaping charge to the shaped charge through a relatively thin annular ring around the periphery at the top of the shaped charge. The resulting detonation pattern is analogous to refraction of light around an obstacle, since each point on the annular ring now acts as a new source of "point" initiation from which the detonation front spreads out as shown on the right side of Figure 10. As a result the detonation impulse reaches the upper

---

* duPont EL-506A flexible sheet explosive.

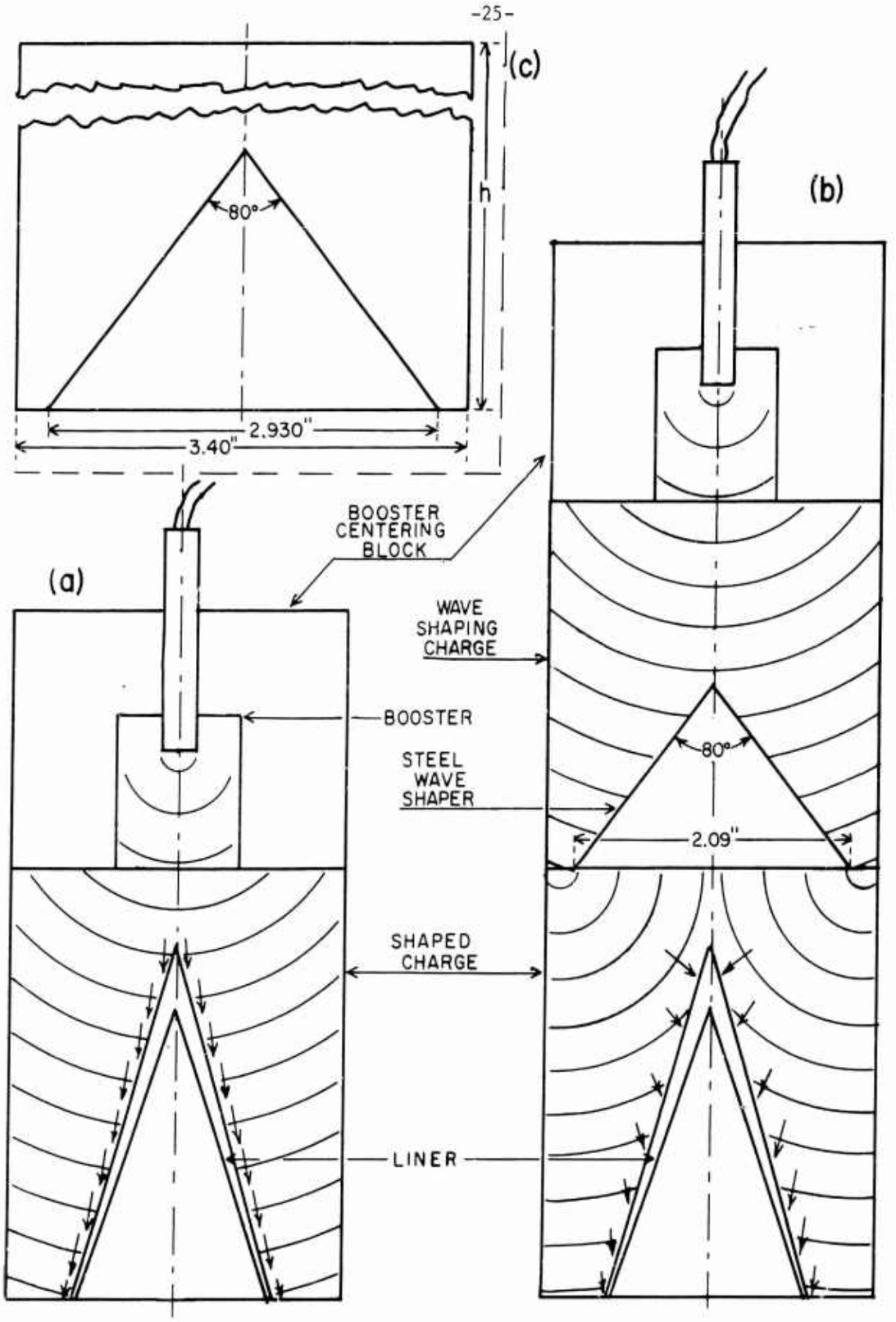

FIGURE 10. Sectional views of typical shaped charges shot without (at the left) and with (at the right) waveshaping charge. Upper left: waving shaping charge for larger diameter charges.

portions of the liner wall at a more advantageous angle than in the case at the left. But as the detonation front progresses down the charge, this angle rapidly approaches the values shown towards the bottom of the charge at the left.

Most of the charges were shot with waveshapers of the size shown in Figure 10 so that the waveshaping charge had the same diameter as the shaped charge. When a larger diameter charge was used (3.40" diameter instead of the nominal 2.43") a proportionately larger waveshaping charge was used as shown in the upper left of Figure 10.

As indicated in the monthly reports, a few shaped charges were shot without waveshaping to obtain comparative results of shooting certain charges with and without waveshapers. These results are discussed further on in this final report.

Charge Confinement

Nearly all of the shaped charges were fired unconfined. In order to determine the effects which confining a shaped charge has upon the jet velocity, tests were made with the configuration shown in Figure 11. Results were encouraging, but insufficient time prevented pursuing this approach to obtain conclusive results.

Charge Size and Shape

Initial work was done with shaped charges having a diameter of 1.90". Soon afterwards charge diameter was standardized at 2.43" since this was the inside diameter of 2-1/2" O.D. aluminum tube that made convenient molds for casting the explosive. Also, with the lengths of charges used, the resulting shaped charge and waveshaping charge combined weight was within the limit that could be fired in the test chamber at Eglin Air Force Base.

The length range of the charges was determined by the axial length of the various liners used and the "S" distance between the apex of the cone and the top of the charge. Overall length varied between about 1-1/2" and 6".

Late in the program a larger diameter cone was tested. This required a 3.40" diameter charge, but since the base of the cone and the charge had the same diameter the final weight of the charge was still within the Eglin Air Force Base test chamber limitation.

Practially all of the charges tested were of cylindrical shape. The only exception was the disc-shaped charge shown in Figure 12 with its associated peripheral initiator. This departure from charges of conventional shape was made in an effort to improve the time relationship between arrival of the detonation front along various sections of

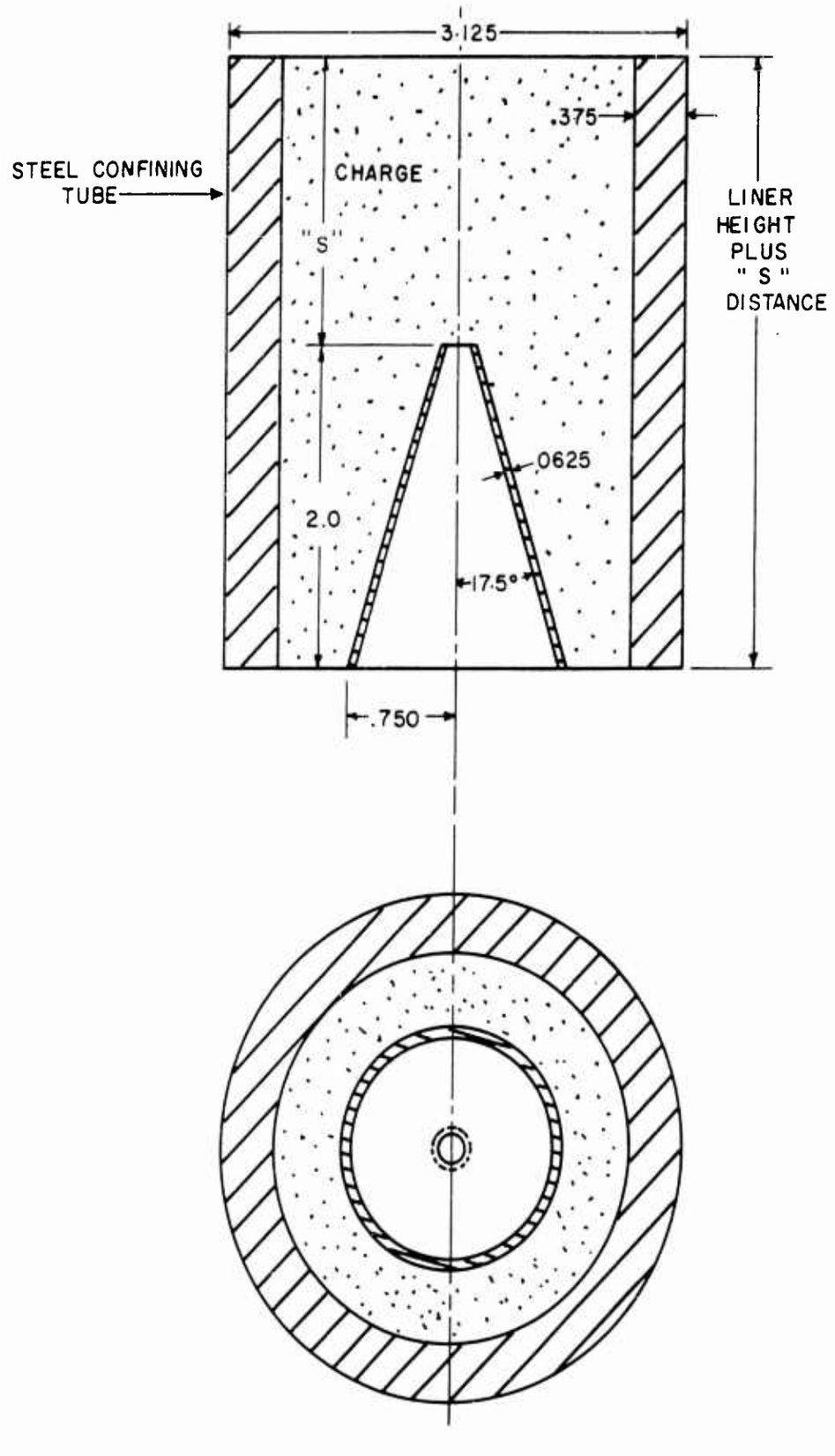

FIGURE 11. Sectional and bottom views of confined charge configuration.

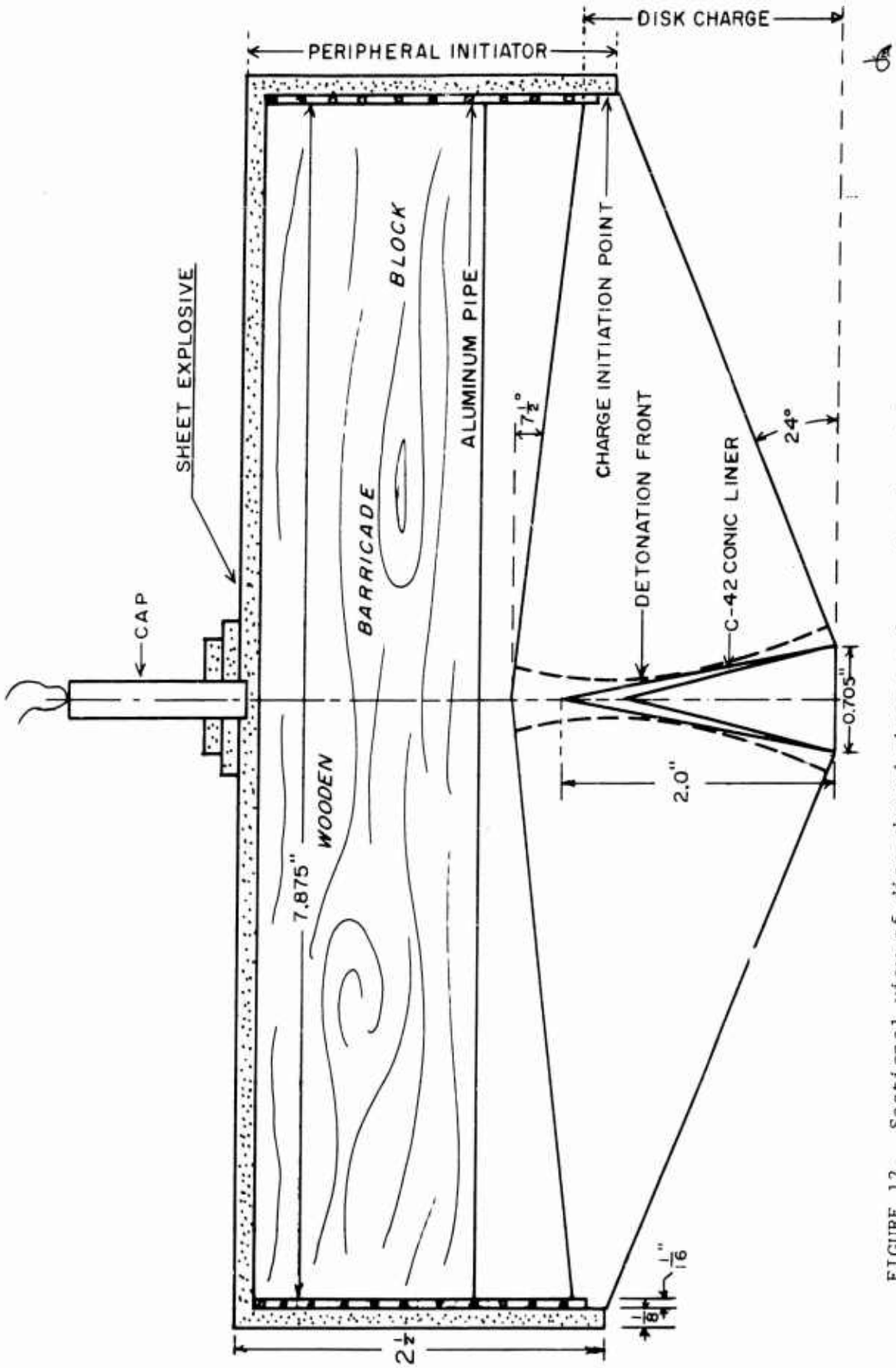

FIGURE 12. Sectional view of disc-shaped charge and associated peripheral initiator.

the liner wall. Figure 10 indicates how the detonation wave progresses from apex to base of the liner in a cylindrical charge. This results in progressive collapse of the cone in a manner to cause the jet from the apex to form the leading element of the jet, with liner sections from apex to base forming successive elements strung out behind. Moreover the wall collapse velocity of the liner is a small fraction of the jet velocity which augments the foregoing effect as the liner wall to axis distance increases from apex to base, and this causes the jet to be further elongated.

Peripheral initiation of the charge depicted in Figure 12 causes the detonation wave to progress symmetrically towards the liner until it reaches the position indicated by the dashed lines just touching the liner. Thus the detonation front is designed to reach the liner wall from apex to base almost simultaneously. This causes virtually coincident collapse of the liner wall throughout its length. This shortens the jet-forming time by an amount approximately equal to the time it takes the charge to detonate over the axial length of the liner, but does not shorten the jet forming time attributable to variable wall collapse time. Furthermore this shape of charge raises the theoretical maximum jet velocity from twice the detonation velocity of the explosive for cylindrical charges to an indefinitely large velocity as the liner angle is decreased[4]. Shortening of the jet length and increasing the maximum jet velocity is thus simultaneously achieved in going from the cylindrical charge to the disc-shaped charge.

Liner Design

Most of the liners used in the experimental testing were aluminum conic liners of varying sizes and shapes as shown in the various monthly reports. Some of these configurations departed from a true cone by truncation and other variations. Conic liners are perhaps the easiest to machine, but one of their undesirable features is the constantly increasing mass they present to the detonation front as it progress from apex to base. This is not as serious a problem when the jet is being used for maximum target penetration, but when a constant velocity jet is desired this characteristic of a conic liner compounds the problem. An approach to improving the configuration consists of departing from constant thickness liner walls to tapered walls which become progressively thinner from apex to base. However one ultimate liner design which presents a constant wall mass to be accelerated from apex to base is the paraboloid shape. Several configurations and sizes of this type liner were tested in the shaped charges as reported in the November 1963 through March 1964 reports and discussed in the RESULTS section of this report.

Several of the conic liners were made of copper to make a comparison between liners having identical size and shape, but with the copper liner having a density nearly three times that of the aluminum liner. The several shaped charges which contained the copper liners are indicated in the monthly reports; all other liners may be assumed to

be aluminum. Comparative results are discussed later on in this report.

Jet Inhibitors

As noted under the "Waveshaping Techniques" subsection, waveshapers act to improve the impulse angle with the upper part of the liner (Figure 10). This results in an increase in the velocity of the fore part of the jet at the expense of creating a larger velocity gradient in the overall jet, since the velocities of the trailing elements are not appreciably helped by the waveshaper.

An approach towards taking advantage of the velocity increase afforded by waveshaping, and at the same time minimizing the undesirable increase in velocity gradient, is accomplished by using jet inhibitors as developed by Kronman and Merendino[2]. The general type of inhibitor which they employed is shown on the left side of Figure 13. Variations of thiswere used in numerous test shots as listed in the monthly reports for this contract. The plastic inserts in these inhibitors prevented the base portion of the liner from forming a jet, while the excess explosive on one side of the base swept aside the base portion of the liner, the inhibitor, and the slug thereby preventing them from affecting the target. A modification was made in the charge configuration used by Kronman and Merendino. Instead of using excess explosive around one side of the charge base, an explosive deficiency around one-half of the base was designed as shown in the center of Figure 13. The resulting charge was simpler to cast and the effects appeared to be the same.

These inhibitors performed satisfactorily by succeeding to cut off the slower trailing elements of the jets after permitting the initial higher velocity elements to pass through. Good results were noted when the inhibitors were used in charges shot over the relatively short distances of the multiple plate setups. However it was noted on the long range vacuum shots that the inhibitors seemed to aggrevate the jet lateral dispersion problem. Therefore in an effort to minimize this effect which the inhibitor seemed to have on the fore part of the jet, while still preserving the desirable function of the inhibitor, a further modification was made as shown on the right side of Figure 13. This design kept the plastic insert as far out of the way of the fore part of the jet as if the normal cone thickness continued clear to the bottom of the liner, but still inhibited formation of jet elements from the base portion. Also the latter was kept as thin as practical, consistent with sufficient mechanical strength to hold the liner in place during casting of the charge, which provided very little liner wall material to form a jet in the first place.

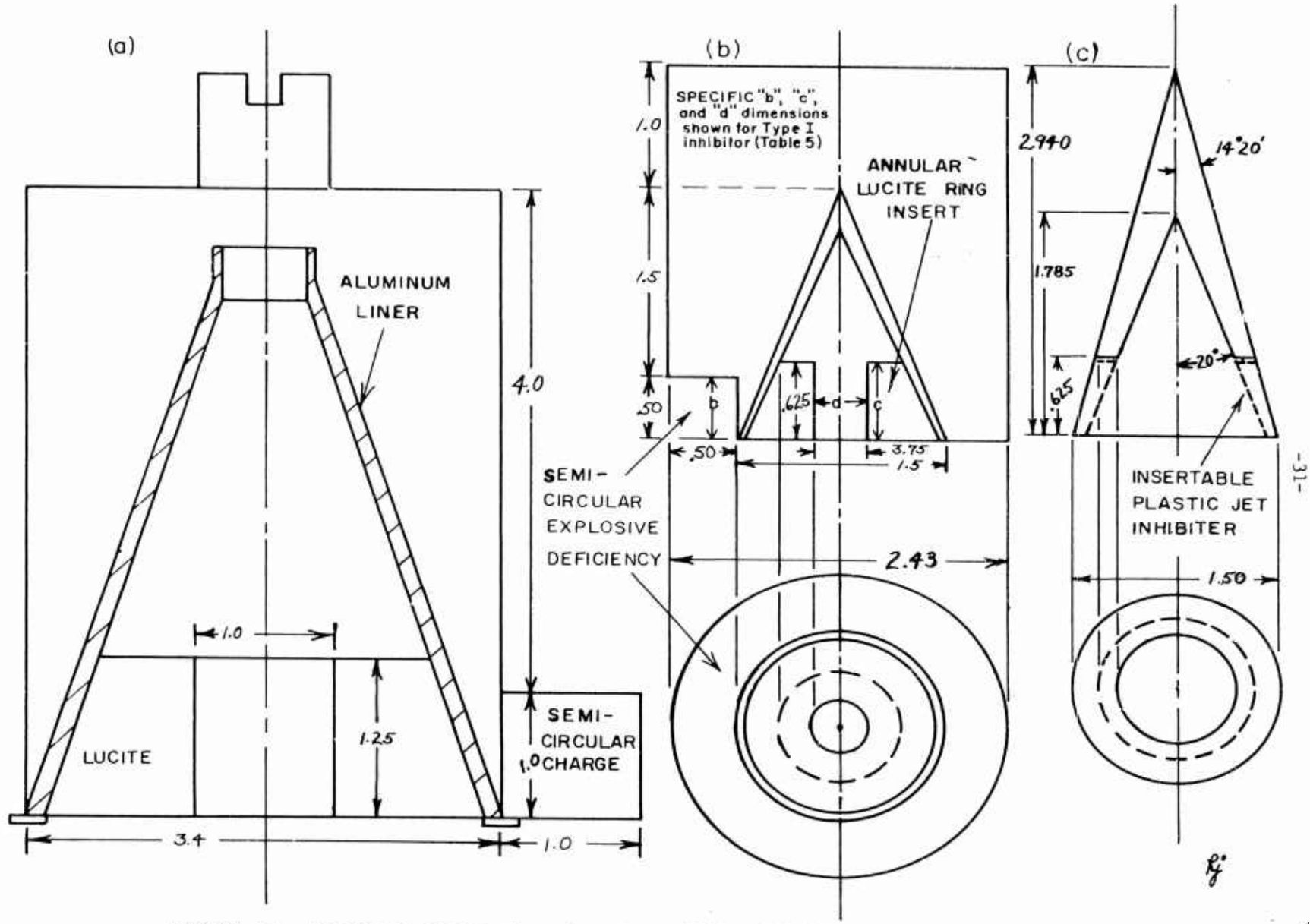

FIGURE 13. Sectional views of various type of jet inhibitors.

EXPERIMENTAL RESULTS

Reporting of Results

Most of the test shots which have been made under this contract are listed in detail in the monthly reports starting with E-1 in the July 1963 report and ending with E-211 in the October 1964 report. The only tests not reported were two made at the IRECO test late in November and the shots made during the last field trip to Eglin Air Force Base in early December. Details on these tests are contained further on in this report.

The following subsections contain discussion of results of pertinent test shots in the various categories of liner size, shape, and material, charge shape and material, charge confinement, etc.

Test Shots at Tooele Ordnance Depot

Cylindrical Charges

Test shots E-1 through E-7 were made with the framing camera method of determining jet velocities. Sectional views of the several liners used in these tests are shown in Figure 15. These tests were exploratory in nature, using a rather wide range of apex angles in the conical liners to correlate that parameter with jet velocity and target penetration. Imperfections in experimental techniques indicated a need for modifications in jet velocity measuring methods. However, a definite trend in jet velocity vs. apex angle was noted in which jet velocity (Fig. 14) was inversely proportional to apex angle. The liner for test E-7 had

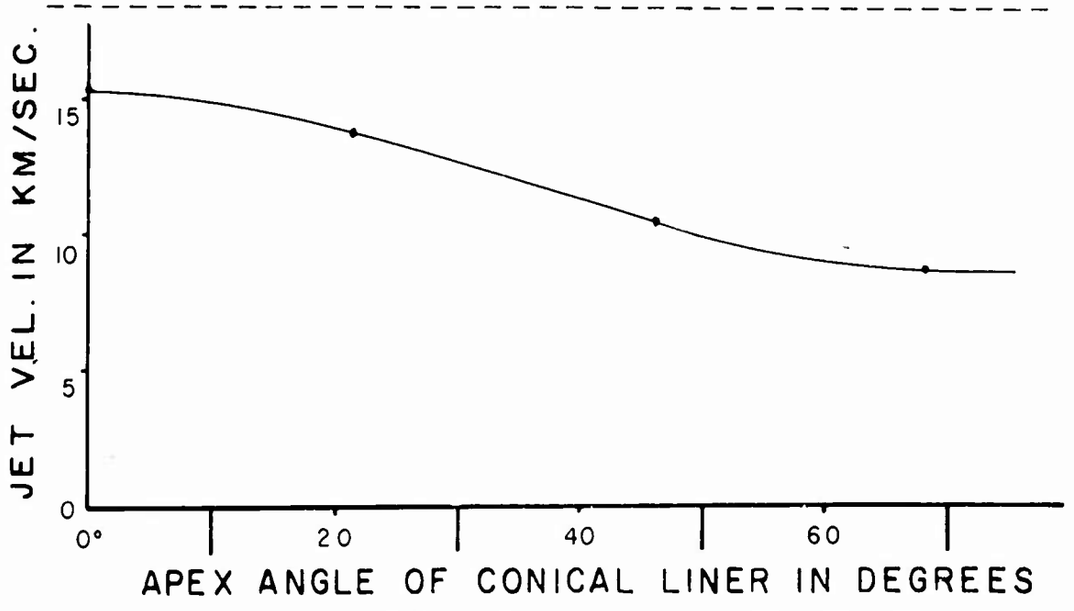

FIGURE 14. Jet velocities as a function of inside apex angle of liner.

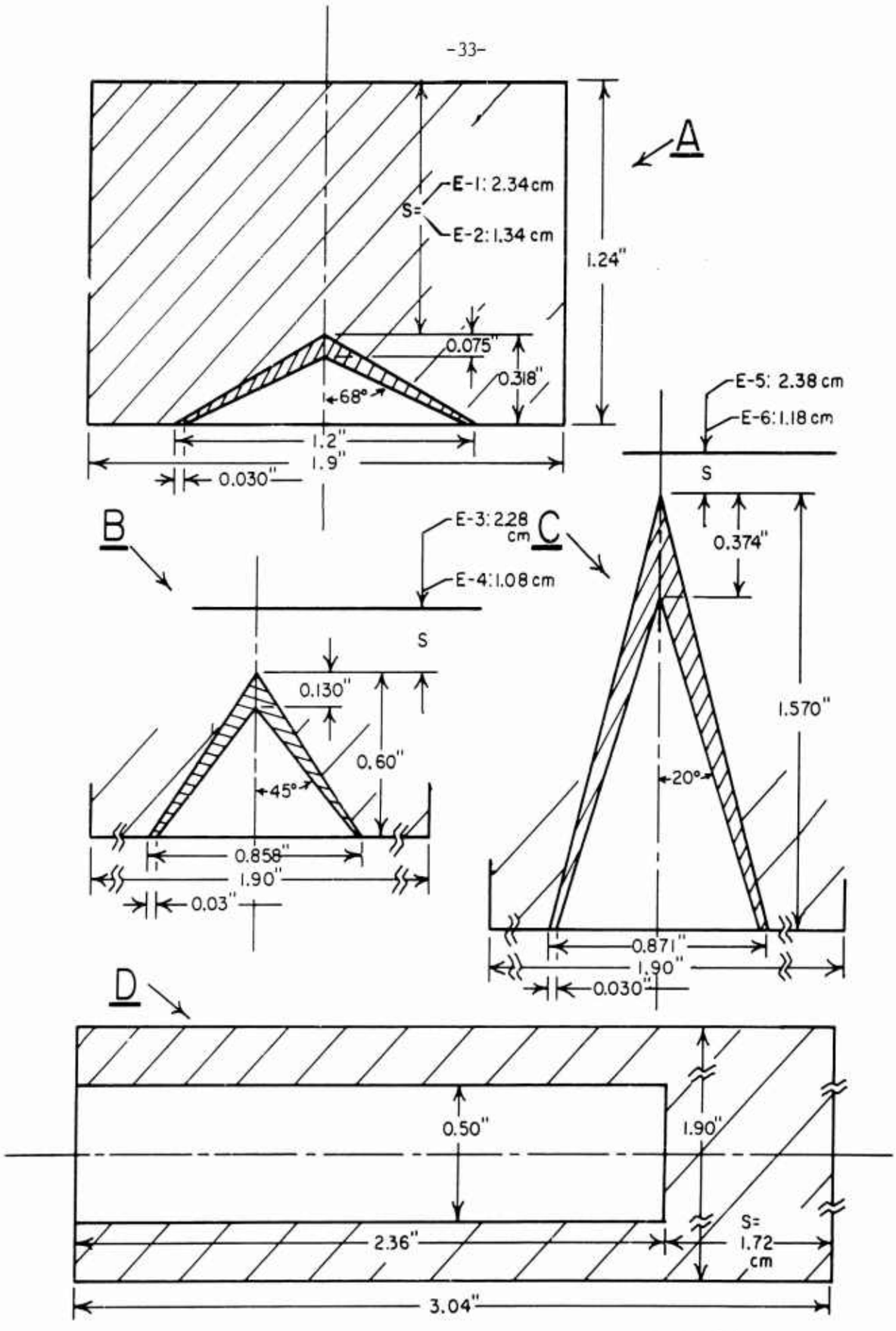

FIGURE 15. Sectional views of liners used in the following tests: A: E-1 and E-2; B: E-3 and E-4; C: E-5 and E-6; and D: E-7.

an apex angle of 0° which represents the limit in reducing this angle as the cone degenerates into a cylinder. At this apex angle the theoretical jet velocity is twice the detonation velocity[4], and this proved to be reasonably true with test E-7 which had a velocity of 15.2 km/sec compared to the theoretical value of 16.2 km/sec.

In general the jets were quite scattered which resulted in unimpressive target penetration and dictated changes in liner design. This method of testing provided no data on velocity gradient within the jet.

Peripheral Initiator

Figure 16 shows the physical setup used to check the degree of symmetry of the peripheral initiator which was used with the disc-shaped charge of Figure 12. The dashed lines and arrows indicate the detonation path which started with the cap, at the rear center of the initiator, from which it progressed radially towards the circumference of the rear plane, thence longitudinally along the surface of the cylinder, and finally radially inward towards the center of the front plane. For normal use the initiator terminated at the circumference of the front plane where it made contact with the disc-shaped charge as shown in Figure 12. However for this special test the front plane was added to provide an accurate means of determining symmetry.

Figure 17 is a photographic reproduction of typical test results. Due to an assumed detonation velocity of Detasheet that was lower than its actual value, the detonation had progressed over half way inwardly on the front plane before the No. 1 framing picture was taken. The black central circle is the unreacted Detasheet, and this circle had progressively smaller diameters in the sequential exposures Nos. 2, 3, 4, etc. The light dot at the center of the front plane was a white circle of paper placed there as a reference to spot the center of the plane. Degree of symmetry was determined by the concentricity of the ingressing black circle and the white dot. Frame No. 4 is perhaps the best of the sequence to ascertain symmetry. Precise measurements on the original film showed that the black "circle" of Frame No. 4 had a maximum differential radius of less than 2-1/2% of the front plane's outer radius. This was assumed to be sufficiently symmetrical for initial tests with the disc-shaped charge, and various test shots using this type of initiator produced results which indicated satisfactory initiation.

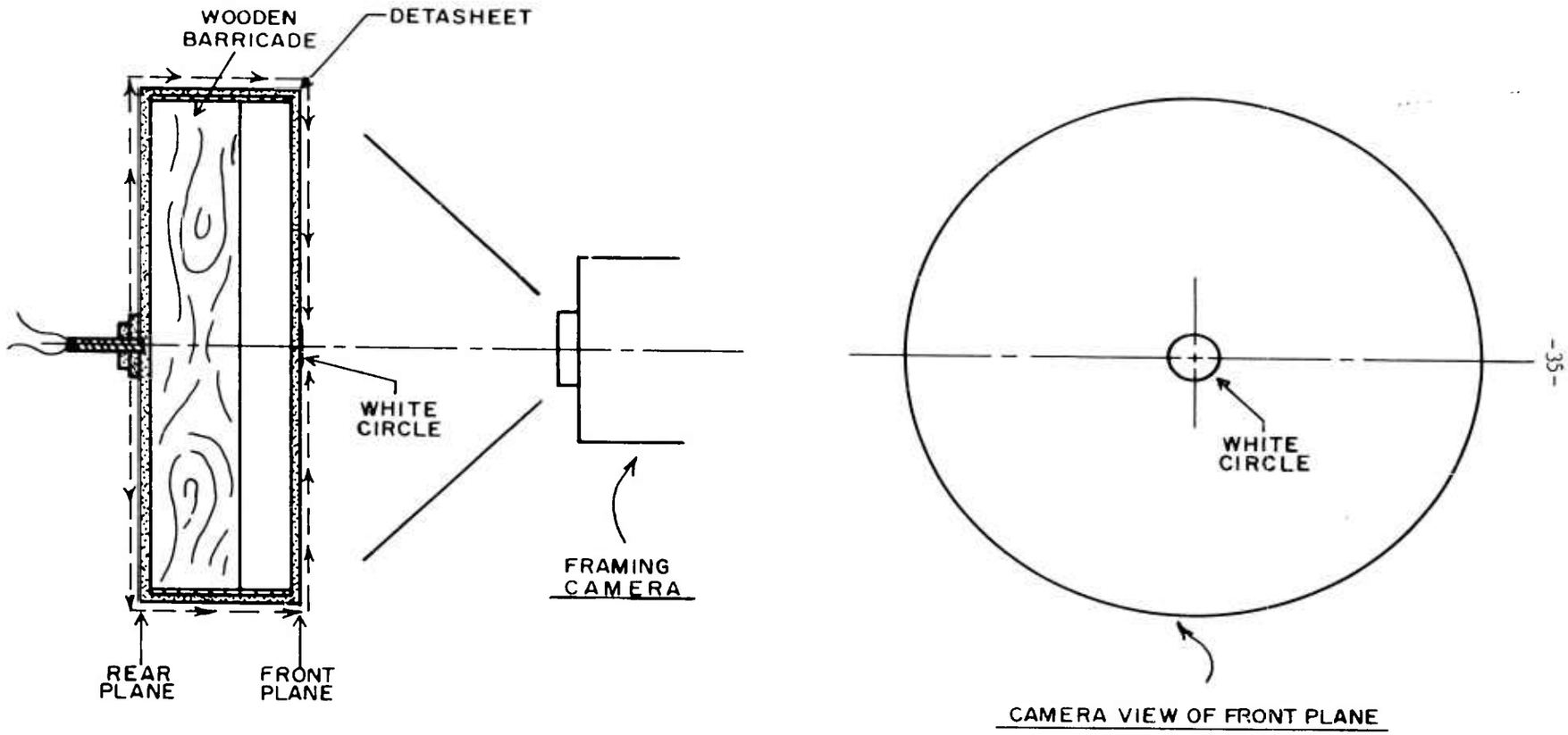

FIGURE 16. Experimental arrangement for checking initiation symmetry of peripheral initiator.

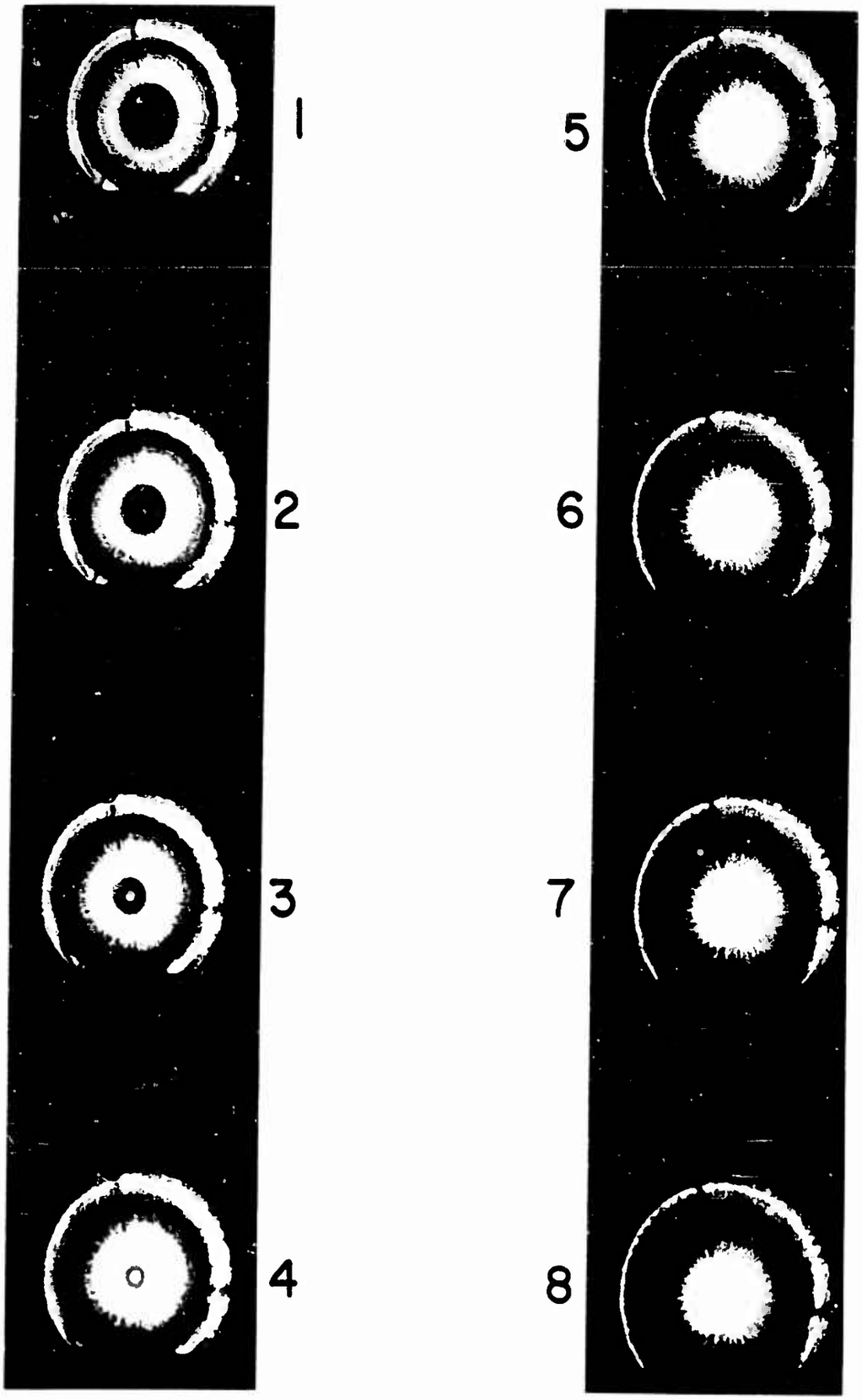

FIGURE 17. Photographic reproduction of first eight frames from test arrangement shown in Figure 16 showing degree of symmetry of peripheral initiator.

TESTS CONDUCTED AT IRECO FACILITIES

Conventional Cylindrical Charges

Multiple-Plate Targets

Conic Liners - The first series of tests using the multiple-plate method of determining jet velocity gradient used conical liners of the type shown in Figure 15A with the exception that minimum wall thickness was 0.076" instead of 0.030". Also a second type liner of constant wall thickness, as shown in Figure 18 was used. This liner was made of copper and fired without a waveshaper in a larger diameter charge (2.5" instead of 1.90" for the others).

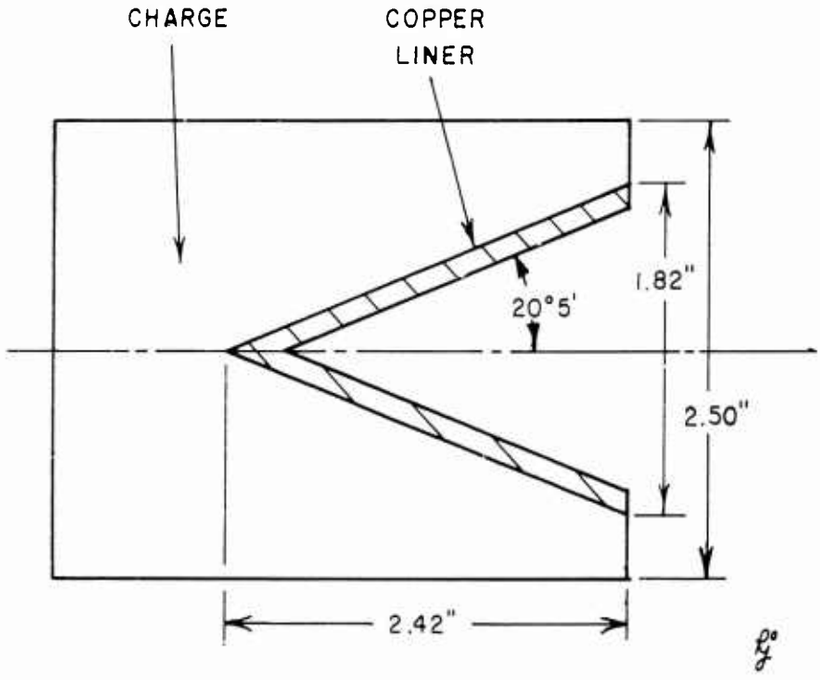

FIGURE 18. Sectional view of charge and liner used in Test E-17.

Figure 19 shows a plot of jet element velocities plotted as a function of the distance from the initial front of the jet to the position of the element in the jet corresponding to the plotted velocity. For example E-11 is shown to have a leading element velocity of 10.8 km/sec and a velocity of 5.9 km/sec for the jet element that was 4.1 cm back from the initial front of the jet. The second velocity plotted for each test was the final velocity measurable and corresponds to a ΣL_i increment

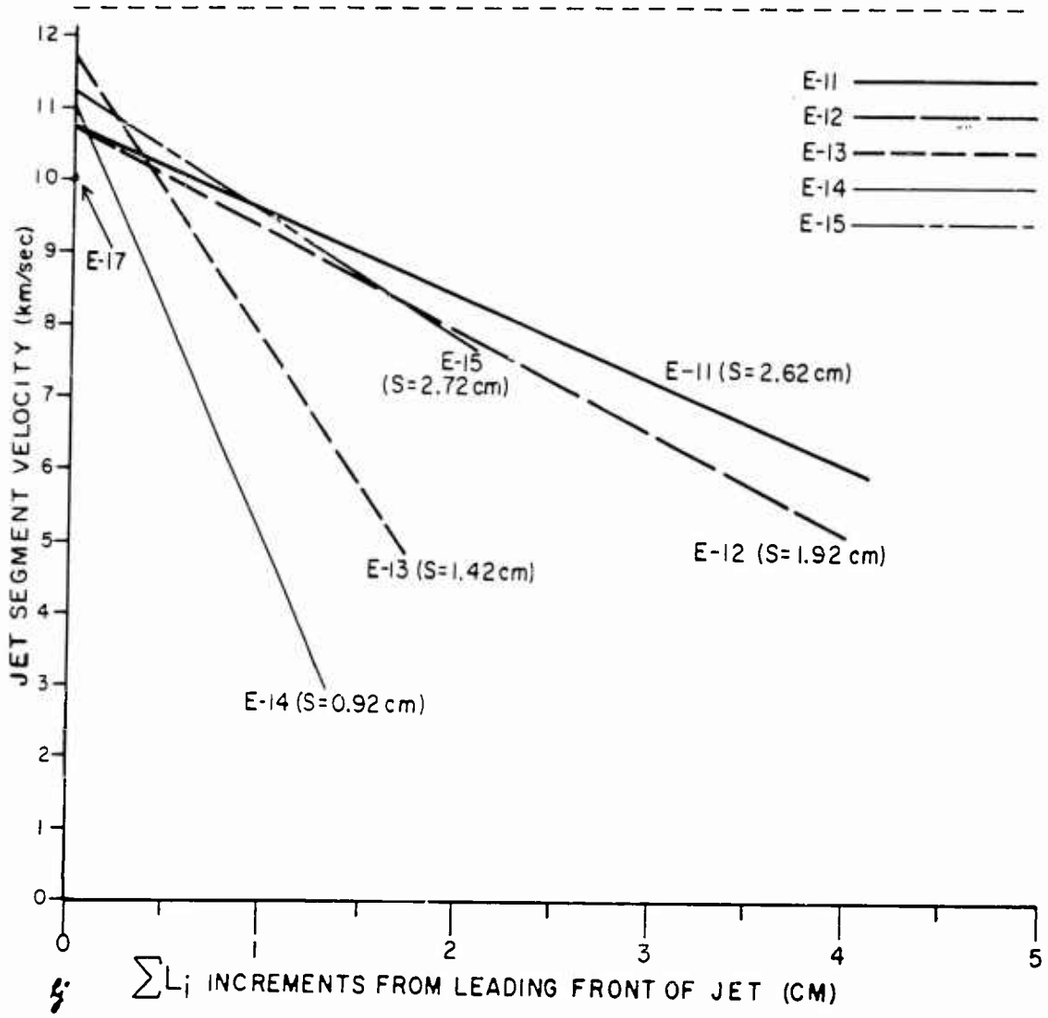

FIGURE 19. Jet segment velocities vs ΣL_i increments from front of jets for $\alpha_1 = 68°$ liners (Figure 15A).

approximately equal to the jet length. The slope of the plots in Figure 19 give an indication of the velocity gradients in the jet which are generally more pronounced with shorter S distances. However the jets with the greatest velocity gradients (E-14 and E-13) resulting from shorter S distances also have the highest initial velocities. This agrees with the principles discussed in relation to Figure 10; that is, the shorter the S distance (with a waveshaper) the more pronounced the effect of improved impulse angle, but also the greater the variation in impulse angle which increases velocity gradient.

The copper liner of E-17 had an initial velocity of 10 km/sec and a final of 2.2 km/sec at an indeterminate ΣL_i increment (and therefore couldn't be plotted). However a large velocity gradient is indicated.

The liner parameters used in the next series of tests are listed in Table 3 which refers to the general dimensions shown in Figure 20. Jet segment velocity vs ΣL_i increments for these tests are plotted in Figures 21 through 24. A cylindrical liner was used in Test E-8 and this resulted in the highest initial velocity as well as in the shortest jet length (Figure 21) as the theory predicts. The remaining plots of Figure 21 show results of the $\alpha_1 = 45°$ liners which follow pretty well the general rule of high initial velocities followed by sharp initial velocity gradients which taper off near the end of the jet. The one exception was E-19 which maintained a remarkably low velocity gradient out to nearly 5 cm jet length before the velocity started dropping sharply. This is the type of jet that would lend itself well to the use of a jet inhibitor (Figure 13) to cut off the slower trailing portion of the jet.

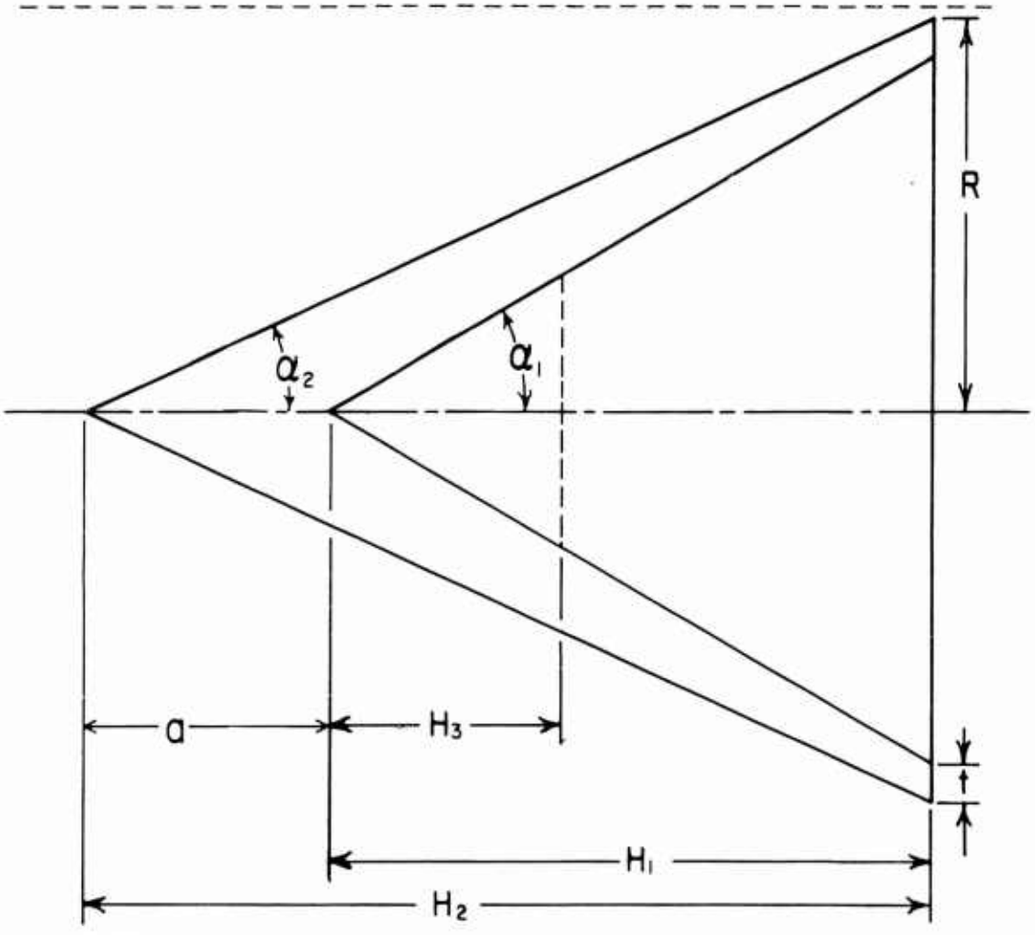

FIGURE 20: Sectional view of conic liner with generalized dimensions.

TABLE 3. Liner and charge parameters from tests shown in Figure 21 through 24. (Refer to sectional view of liner in Figure 20.)

Test No.	α_1	α_2	t	H_1	H_2	H_3	a	R	S ≠	Charge Dia.
E-8	0°	0°	.023	2.36"	--	--	--	0.875"	0.82	2.0"
E-16	68°	60°	.076	0.243	0.318	--	.075	0.875	1.15	2.0
E-19	45°	39°45'	0.03	0.750	0.902	--	.152	0.750	3.0	2.43
E-20	45°	39°45'	0.025	0.750	0.902	--	.152	0.750	3.2	"
E-21	45°	"	0.026	"	"	--	"	"	2.7	"
E-22	"	"	"	"	"	--	"	"	*	"
E-23	"	"	0.024	"	"	--	"	"	3.7	"
E-24	"	"	0.023	"	"	0.212cm	"	"	1.7	"
E-25	68°	60°	0.025	0.243	0.318	--	.075	"	1.81	"
E-26	"	"	0.025	"	"	--	"	"	2.31	"
E-27	"	"	0.023	"	"	--	"	"	3.23	"
E-28	20°	17°20'	0.032	2.402	1.970	--	0.432"	"	*	"
E-29	"	"	0.031	"	"	--	"	"	2.00	"
E-30	"	"	0.029	"	"	0.602	"	"	2.50	"
E-31	"	"	0.031	"	"	--	"	"	3.00	"
E-32	"	"	0.030	"	"	--	"	"	3.50	"
E-33	"	"	0.030	"	"	--	"	"	3.25	"
E-34	"	"	0.030	"	"	--	"	"	4.50	"
E-35	Hemispherical	Shell	0.035	--	--	--	--	0.50	2.41	"
E-36	"	"	"	--	--	--	--	"	2.91	"
E-37	"	"	"	--	--	--	--	"	3.41	"
E-38	"	"	"	--	--	--	--	"	3.91	"
E-39	68°	60°	0.030	0.243	0.318	--	.075	0.750	2.0	"
E-40	"	"	"	"	"	--	"	"	1.31	"

* No Waveshaper

≠ Distance between liner apex and top of charge.

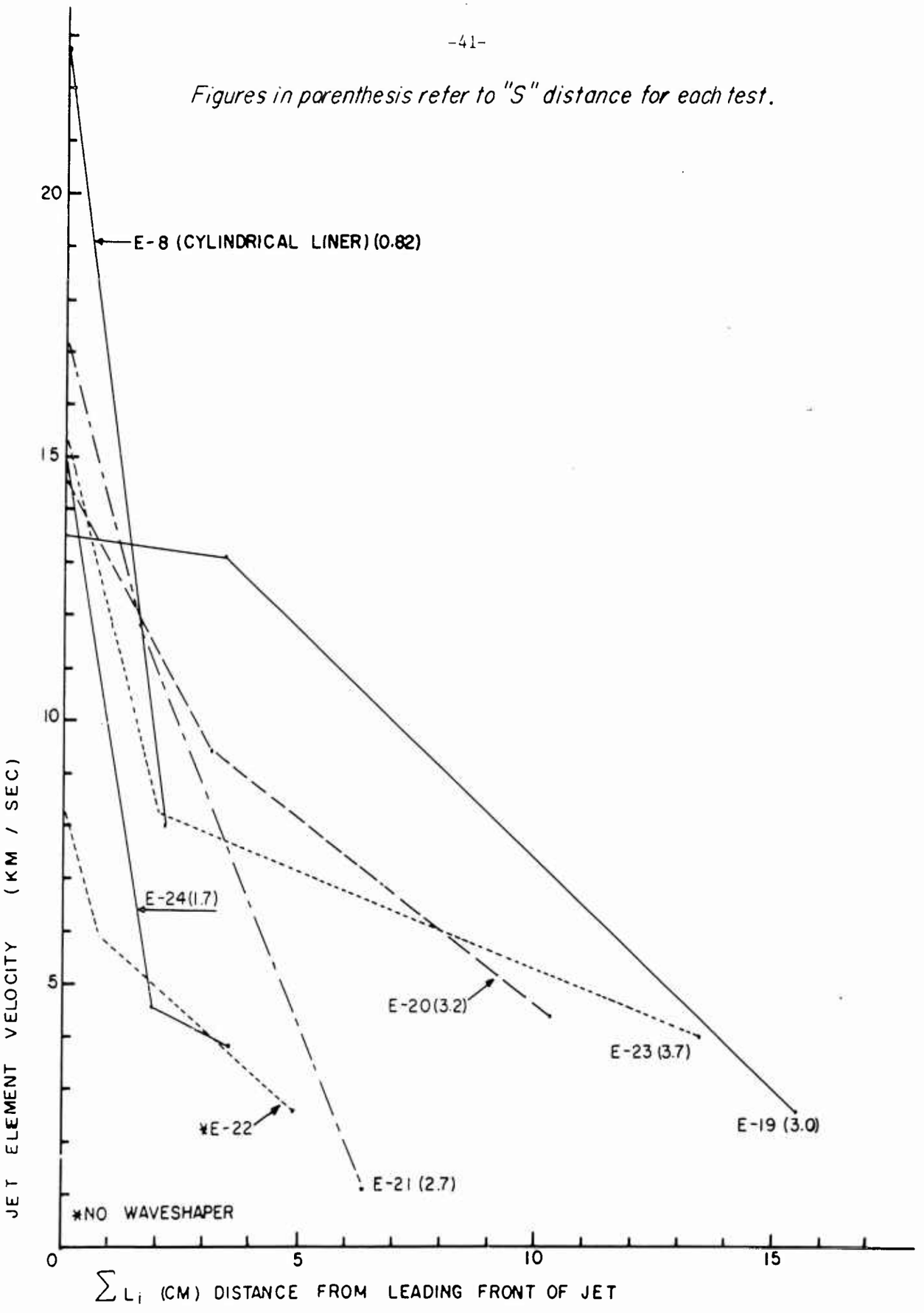

FIGURE 21. Jet segment velocities vs $\sum L_i$ increments from front of jets from $\alpha = 45°$ liners (plus jet from cylindrical liner of Test E-8).

Figure 22 indicates a fairly constant velocity gradient pattern for the $\alpha_1 = 68°$ liners. The initial high gradient made all of these large angle liners unsuitable for further consideration to produce constant velocity jets. A comparison of Figure 22 and the "S" values for these tests as listed in Table 3 shows the general trend of initial velocities and velocity gradients both being inversely proportional to "S" distances.

Results of the $\alpha_1 = 20°$ liners are shown in Figure 23 and part of Figure 24. All of the plots except the one for E-33 show a fairly regular pattern of high initial velocity gradient followed by a decrease in gradient. The reason for the departure of the E-33 jet from the normal pattern is not obvious from the one variable parameter, the "S" distance, since the latter for E-33 was intermediate between the "S" values for E-31 and E-32 and both of the jets from these liners behaved like the rest.

Figure 24 indicates that the performance of the hemispherical liners is surprisingly similar to the conic liners. The initial velocities of the hemisphere liner jets range a little below the conic liner jets, while the velocity gradients of the latter are generally a little greater than what results from using the hemispherical liners.

Figures 25 through 27 display the results of the next series of tests for the liners as defined by the parameters listed on each figure (as referred to the generalized view of Figure 20).

These plots show, in general, an appreciably smaller velocity gradient in the jets than the previous series. Also, over half of the plots in Figures 25 through 27 show a smaller gradient at first followed by a larger gradient for the trailing portion of the jet. This type of jet lends itself better to jet inhibitors to reduce the velocity gradient. Truncating the liners (E-43, E-50, E-58, E-59, and E-60) resulted in lower initial velocities since no jet could form at the liner apex which produces the highest velocities in a normal cone. However, Test No. E-60 produced a jet that showed a constant velocity over a jet length of nearly 3 cm, at least within the velocity resolution capabilities of the multiple-plate method.

For tests E-45 and E-49, two baffle plates, 3/8" apart with 0.63" diameter holes in their centers, were placed above the regular target plates (see Figure 3) in an effort to stop the slug from coming through. Figure 25 and 26 show the jet length from these two shots to be shorter than average for comparable tests. Results of these efforts made it appear advisable to use the method of Kronman and Merendino[2] to sweep the slug aside.

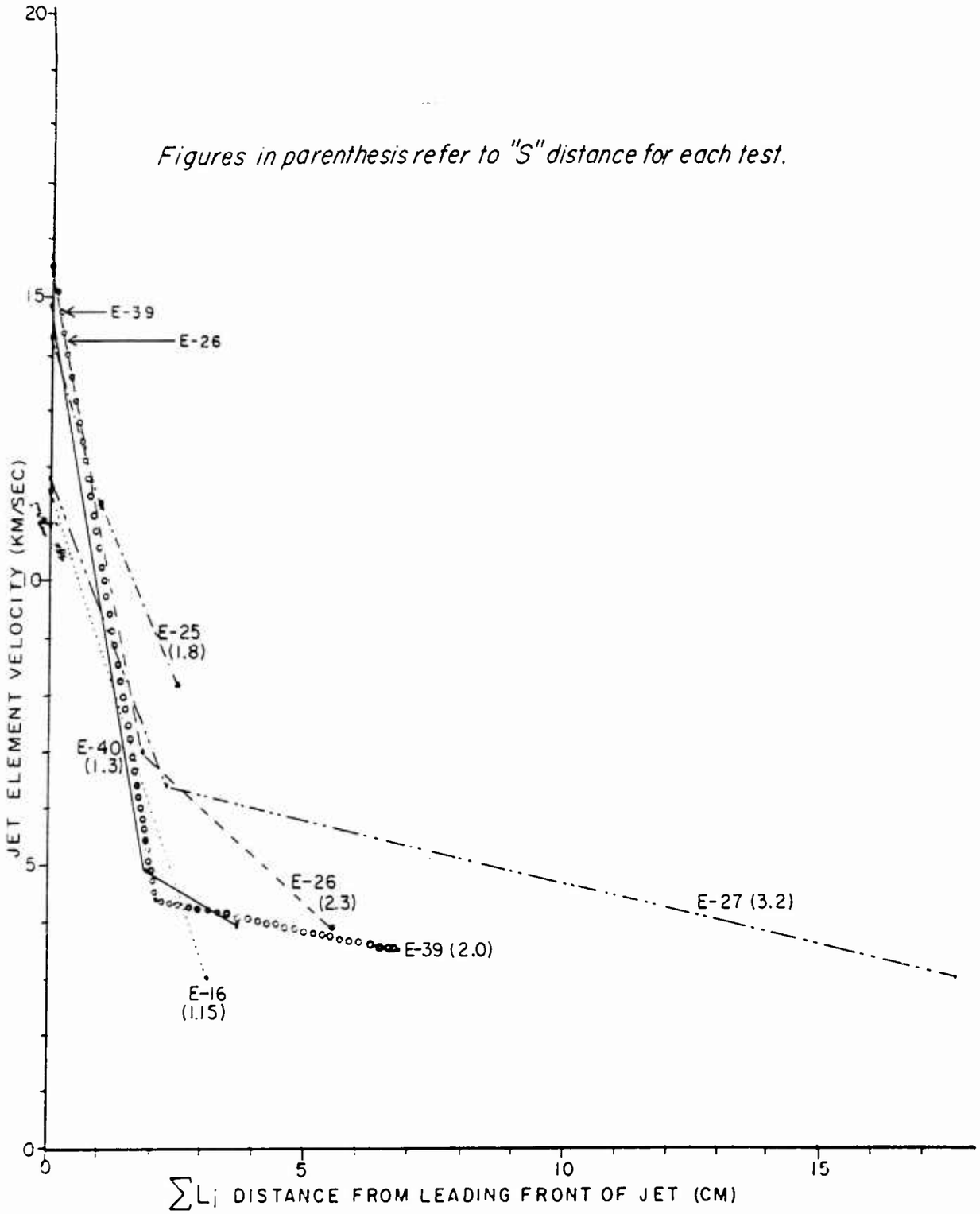

FIGURE 22. Jet segment velocities vs $\sum L_j$ increments from front of jets from $2\alpha = 68°$ liners.

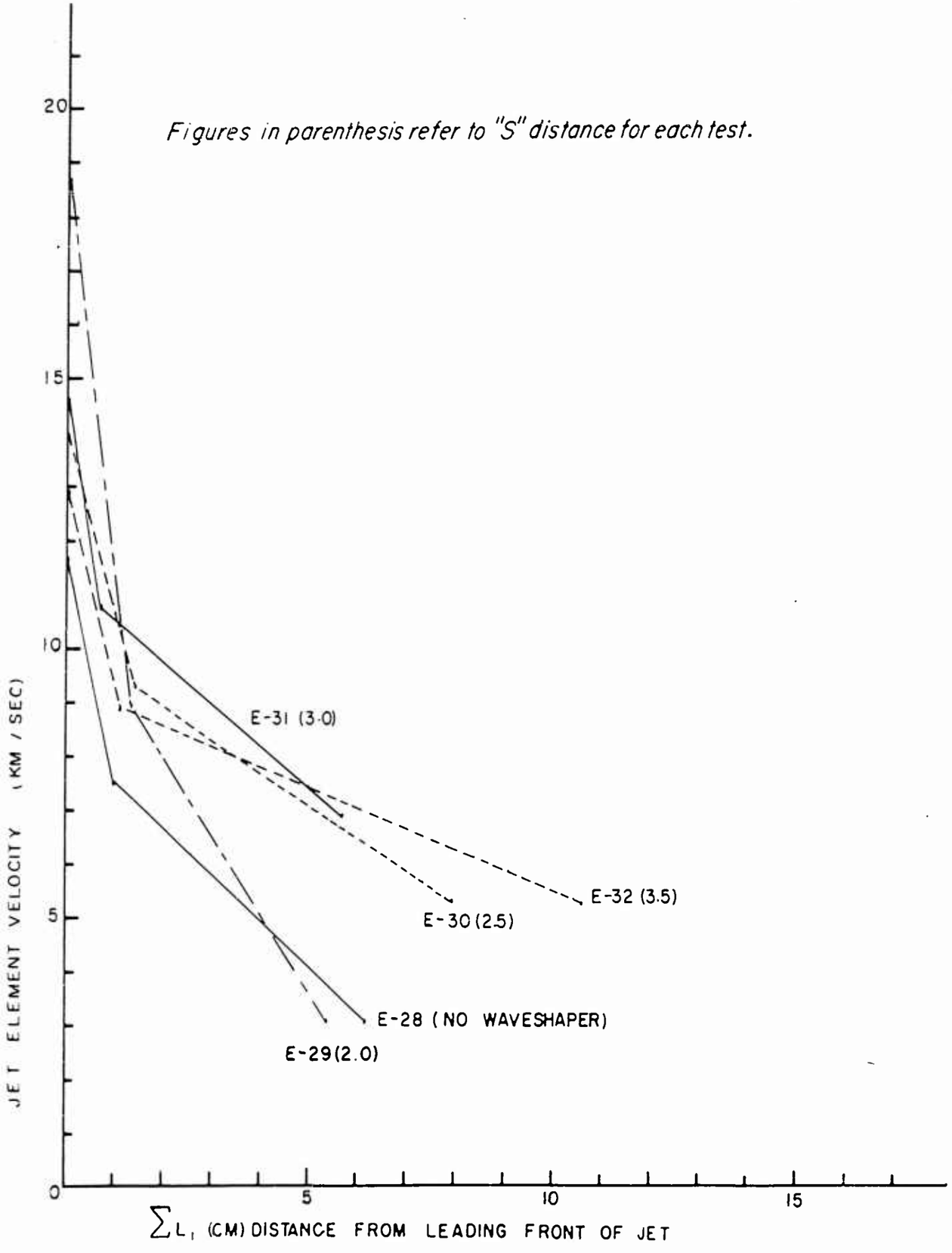

FIGURE 23. Jet segment velocities vs $\sum L_1$ increments from front of jets from $\alpha_1 = 20°$ liners.

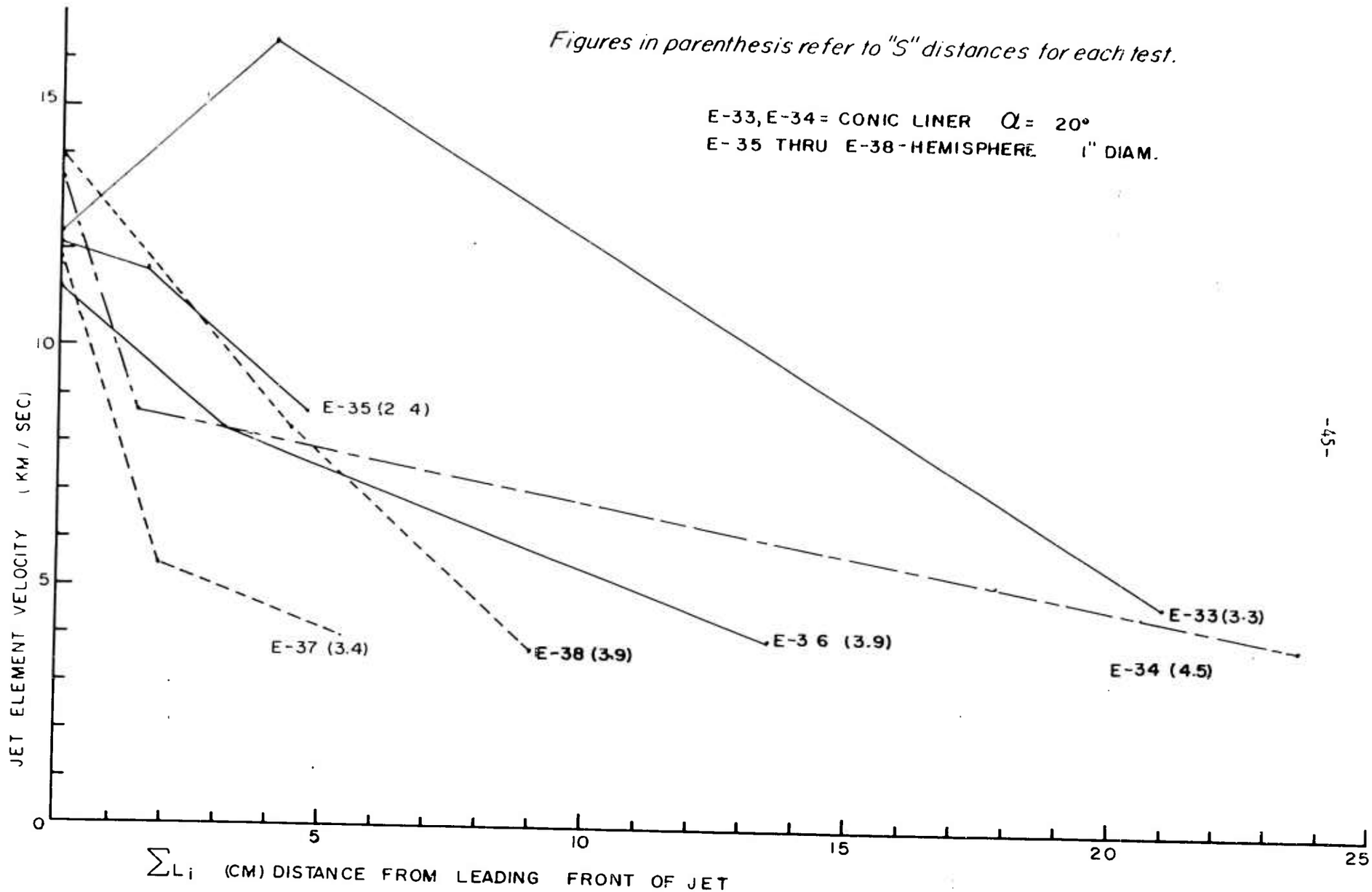

FIGURE 24. Jet segment velocities vs ΣL_i increments from front of jets from $\alpha_1 = 20°$ liners and hemispherical liners.

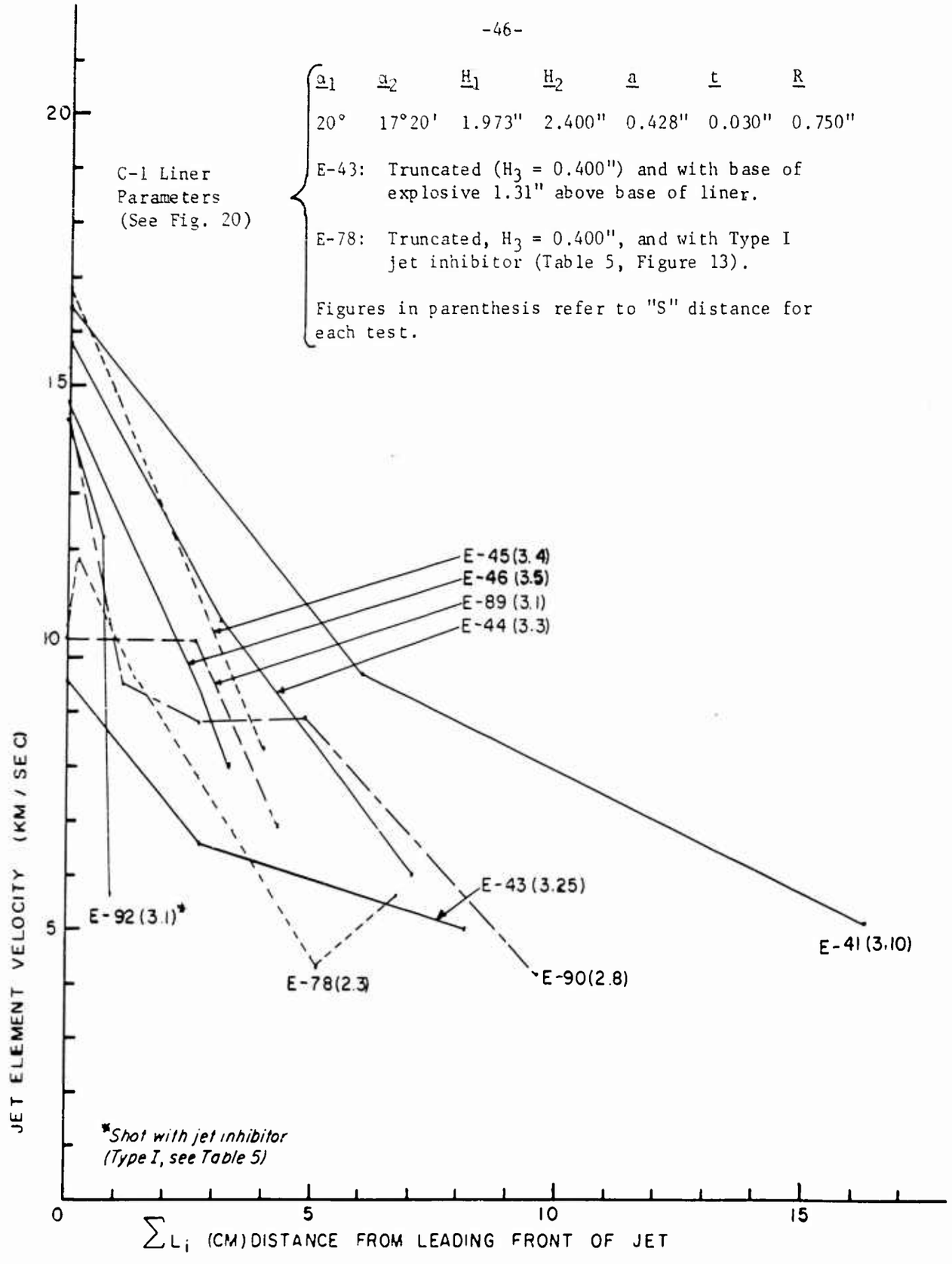

FIGURE 25. Jet segment velocities vs $\sum L_i$ increments from front of jets from type C-1 liners.

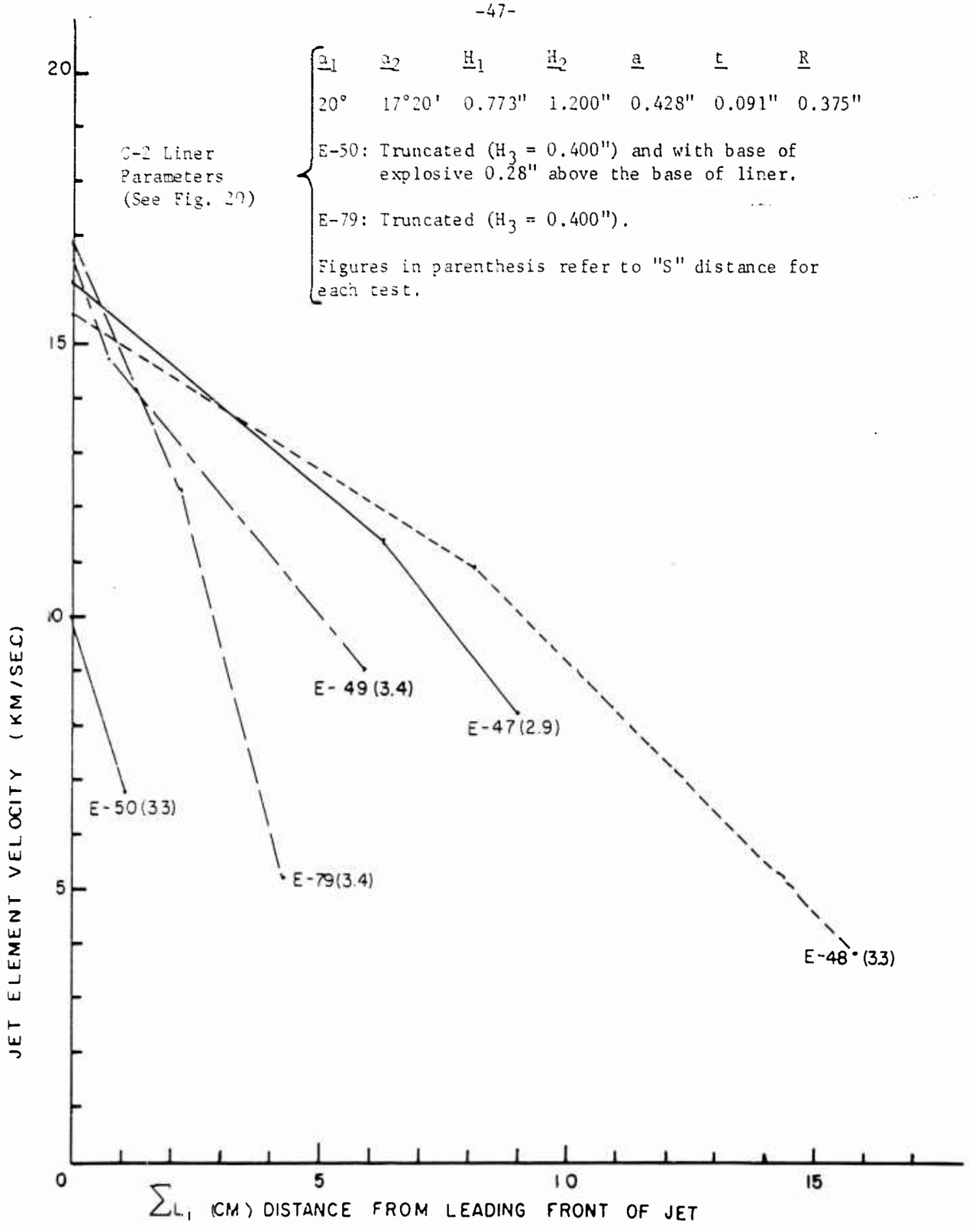

FIGURE 26. Jet segment velocities vs ΣL_i increments from front of jets from type C-2 liners.

Paraboloid Liners - The next series of tests employed paraboloid liners of the form $y^2 = 4px$ in which $p = 0.05$ and x is the axis of symmetry. Figure 28 shows a sectional view of the paraboloid with generalized dimensions which are given specific values for the five types of liners listed in Table 4. Jet segment velocities resulting from firing charges containing these liners are plotted in Figure 29.

A comparison of Figure 29 with the previous figures for conic liners shows that the latter tend to have longer jets. And of the several types of paraboloid liners tested the type C-11 generally had the lowest jet velocity gradient and the longest jets. However paraboloid liners did not show the reduction in velocity gradient expected for liners having constant cross-sectional area on all cross-sectionals normal to the liner axis. It thus became apparent that other factors were also involved in generating velocity gradients in shaped charge jets.

The paraboloid liner jets followed the same rule governing conic liners. In all cases except for test E-77, initial jet velocity was inversely proportional to "S" distance for each type liner. And, in general, the jets having the higher initial velocities also had the highest velocity gradients. Therefore a second series of paraboloid liners were tested in which the "S" distance was further decreased for the type C-11 liner, then identical "S" distances were used for the C-15 liner (see Table 5). Results are plotted in Figure 30 which shows an "S" distance of 2.90 cm for C-11 (E-80) and 2.70 cm for C-15 (E-86) to be optimum. Both of these tests produced jets having quite low velocity gradients over approximately one cm of the leading portion of the jet, but then increased rapidly thereafter. The rest of the tests resulted in high velocity gradients from the start.

Jet Inhibitors - The foregoing results made apparent the desirability of investigating the use of jet inhibitors on some of the liners previously tested. One type of conic liner, C-1 and two types of apraboloid liners, C-11 and C-15 were chosen for these tests. Table 5 lists the several types of jet inhibitors used in these and following tests. Figure 31 contains jet segment velocity vs ΣL_i segment plots for the C-1 liners, while Figure 32 contains similar plots for the C-11 and C-15 liners. The effectiveness of the inhibitors in shortening jet lengths is obvious from these two figures. However the leading portion of the jets which passed through the inhibitor have a velocity range about the same as (and sometimes even greater than) the uninhibited jets. Thus the velocity gradients of the inhibited jets of the C-1 liners were still quite pronounced and left much to be desired in realizing a constant velocity jet.

In the case of the C-11 paraboloid liner the inhibitor, in addition to shortening the jet length, appeared to have the secondary effect of increasing the velocity gradient of the uninhibited portion of the jet over that possessed by the leading portion of the corresponding

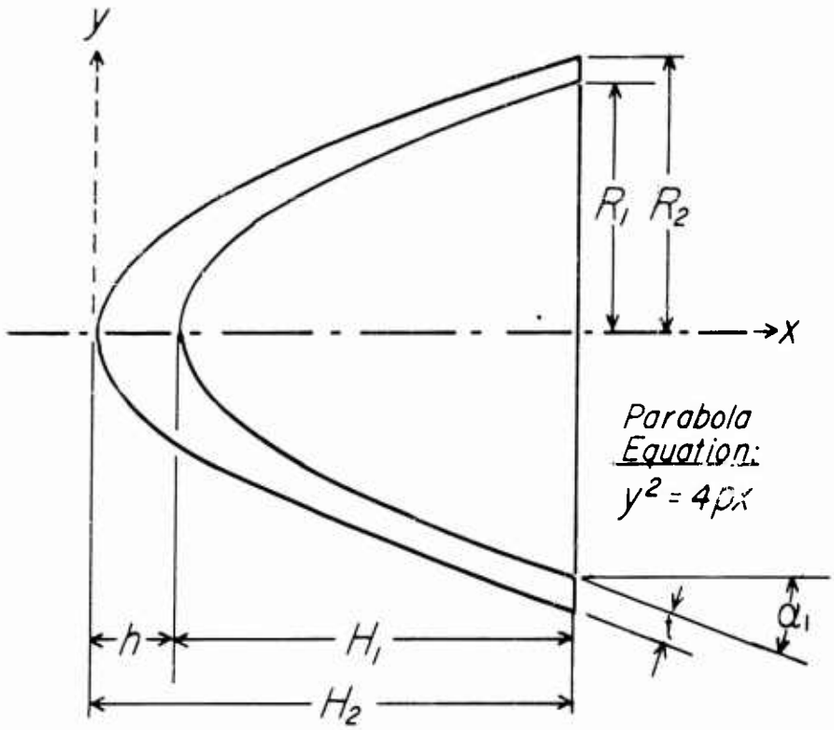

FIGURE 28. Sectional view of paraboloid liner of the form $y^2 = 4\,px$ in which p = 0.05. Specific dimensions are listed in Table 4.

TABLE 4. Paraboloid liner parameters for the generalized dimensions shown in Figure 28.

TYPE LINER	R_2	k_1	α_1	H_2	H_1	h	t
C-11	0.375	0.340	16.4°	0.703	0.579	0.124	0.034
C-12	0.375	0.285	19.3°	0.703	0.407	0.296	0.085
C-13	0.250	0.215	24.9°	0.312	0.231	0.081	0.032
C-14	0.250	0.160	32.0°	0.312	0.128	0.184	0.076
C-15	0.458	0.431	13.0°	1.050	0.926	0.124	0.026

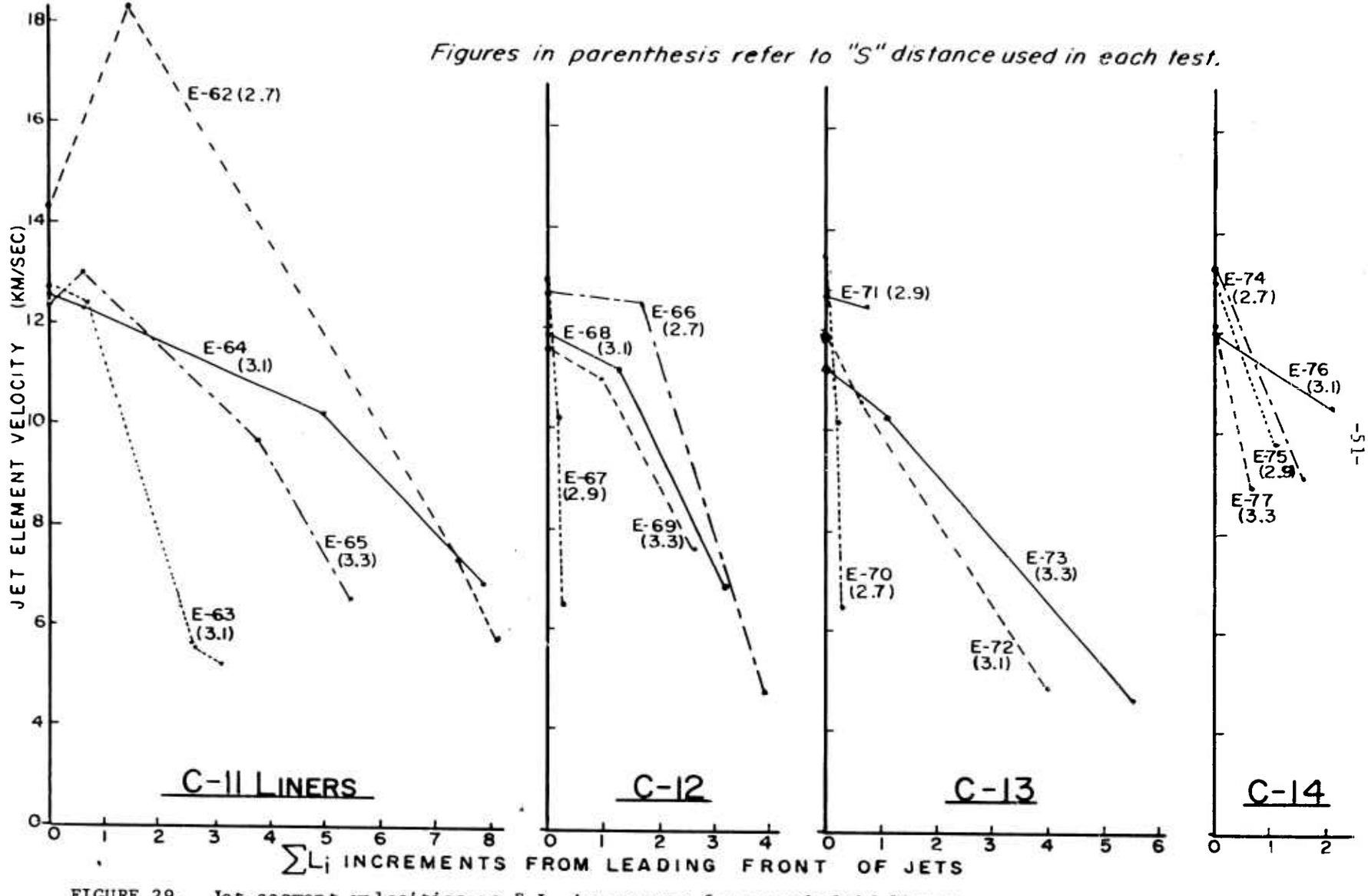

FIGURE 29. Jet segment velocities vs ΣL_i increments from paraboloid liners.

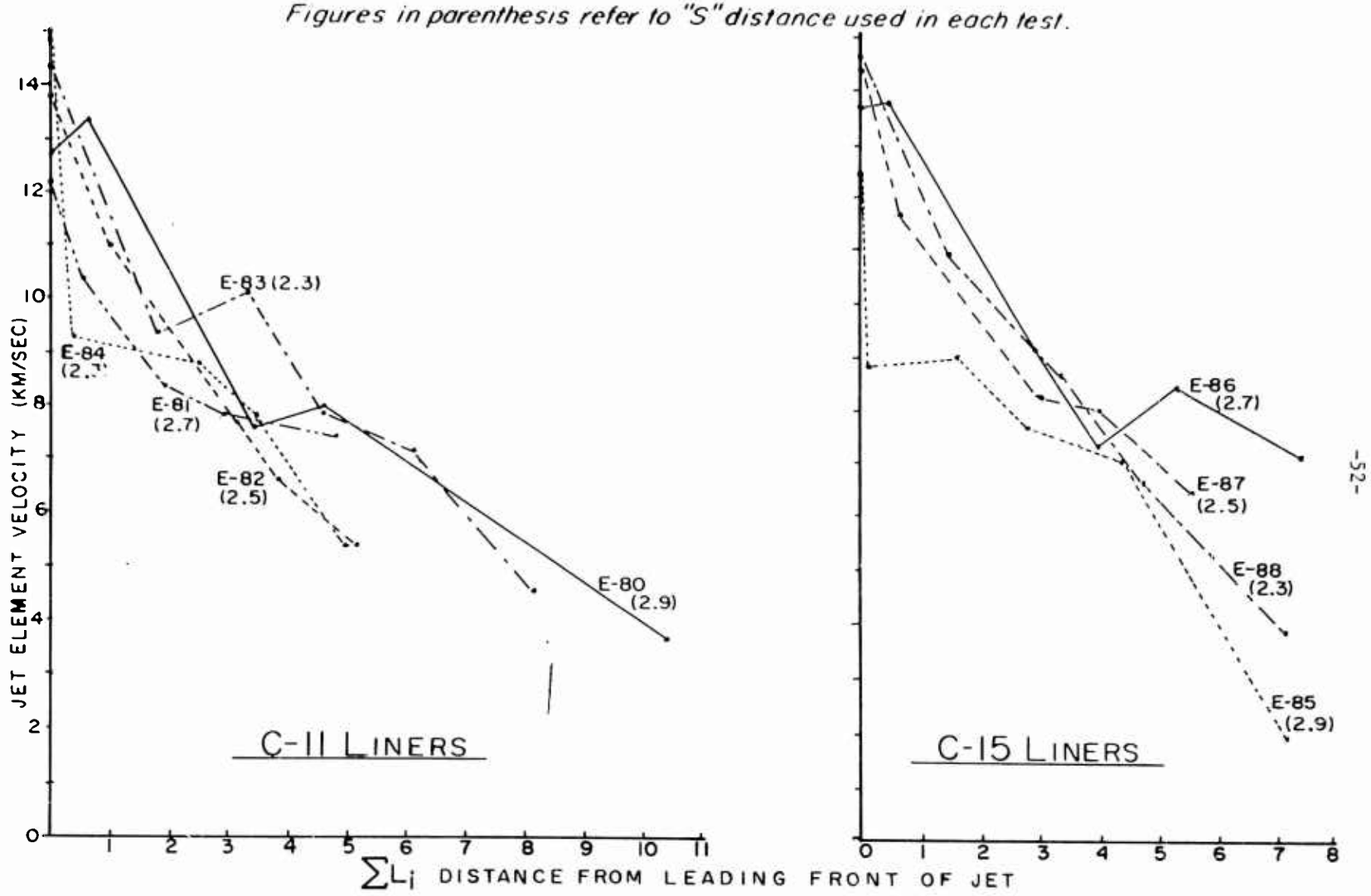

FIGURE 30. Jet segment velocities vs ΣL_i increments from C-11 and C-15 paraboloid liners.

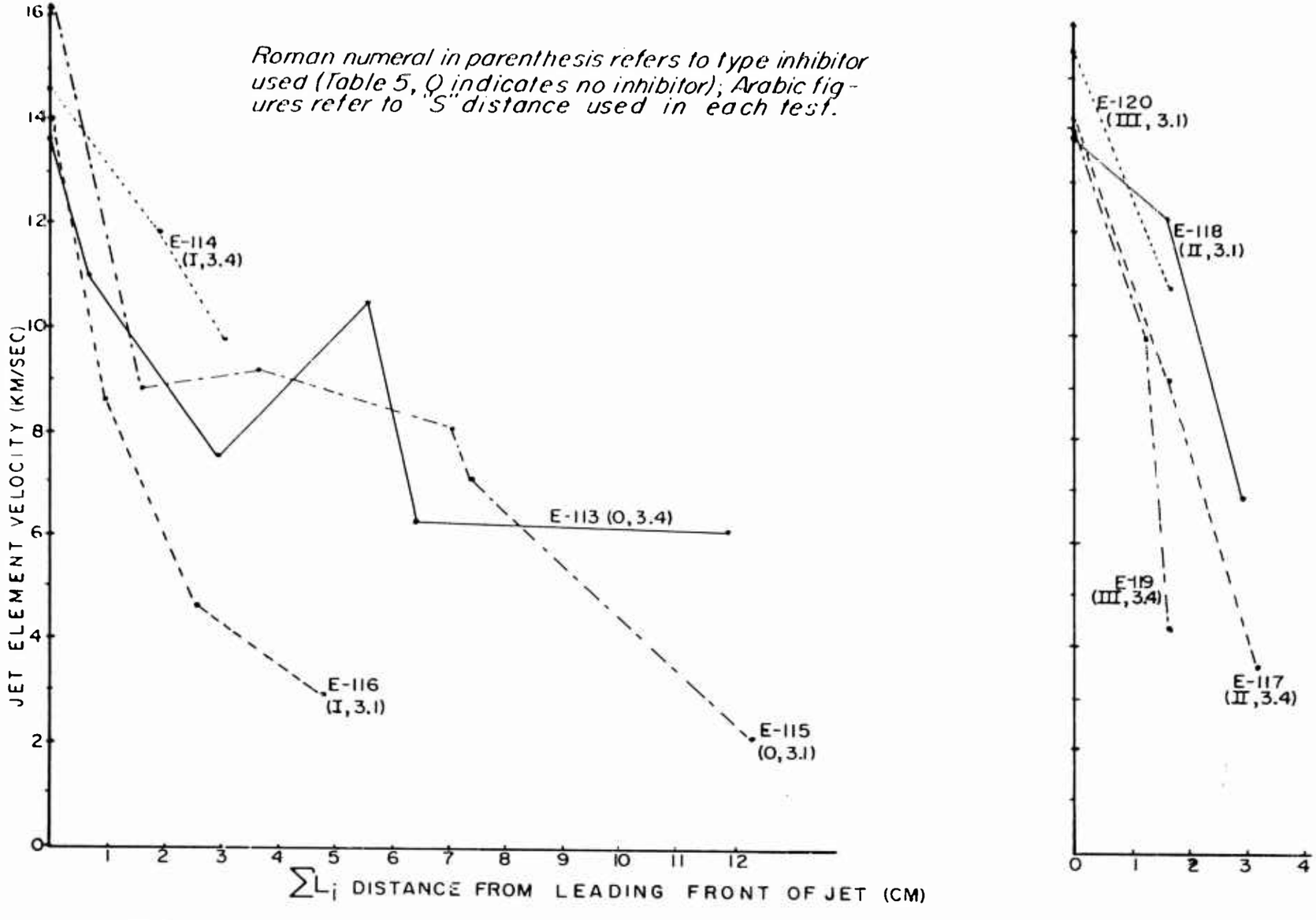

FIGURE 31. Jet segment velocities vs ΣL_i increments from C-1 conic liner to test inhibited effects.

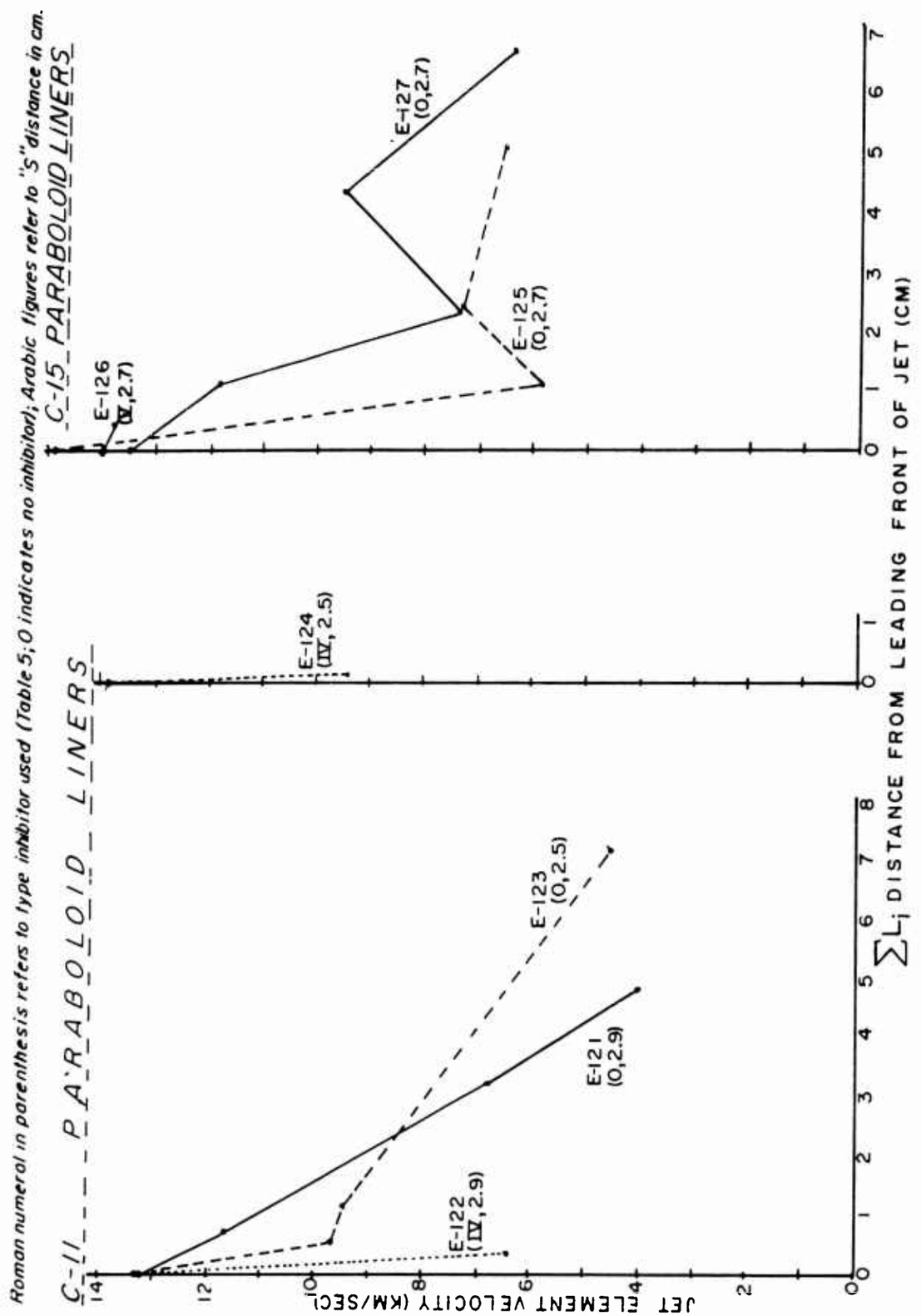

FIGURE 32. Jet segment velocities vs ΣL_i increments from C-11 and C-15 paraboloid liners to test inhibitor effects.

TABLE 5. Jet inhibitor dimensions (refer to Figure 13).

Type Inhibitor	Dimension "b" (Explosive Deficiency Thickness)	Dimension "c" (Insert Thickness)	Dimension "d" (Hole Diameter in Insert)
I	1/2"	5/8"	3/8"
II	11/16"	7/8"	3/8"
III	1"	1-1/4"	3/8"
IV	3/16"	1/4"	3/16"
V	1/4"	5/16"	1/4"
VI	1/2"	5/8"	5/8"
VII	1/4"	5/16"	3/4"
VIII	1/2"	5/8"	(Fig. 13C)
IX	1/2"	1-1/4"	(Fig. 13C)
X	1/2"	0	0

uninhibited tests. For example compare E-122 with E-121 and E-124 with E-123. This did not occur with the C-15 liner, at least the 1/2cm of jet that got through the inhibitor in Test E-126 had a very low velocity gradient compared to the uninhibited jets of tests E-125 and E-127.

Of all the shaped charge liners tested up to this point, the C-1 conic type and the C-15 paraboloid type liners performed the best. Therefore 10 each of these liners were cast into charges for tests at Eglin Air Force Base. These tests are discussed under the Eglin Air Force Base section of this report.

Extended Air Range

All tests made up to this point were conducted by shooting the jets over a relatively short air range (maximum range: about one foot). Target penetration indicated satisfactory jet formation and cohesion. However, when some of these same types of shaped charges and liners were fired over an extended vacuum range (13 feet minimum) at Eglin Air Force Base, lateral dispersion of the jet greatly reduced the jets target penetration capability. A simulated extended air range was therefore provided at the IRECO test site to test shaped charge jets over similar distances used at Eglin Air Force Base. Figure 8 contains plots of the jet velocities vs distance from target for tests made over this air range, while Figure 7 is a streak camera record of E-134, and also contains a static image of the physical setup of charge and targets for these tests. The three targets consisted of three 18" x 18" sheets of steel which were successively 1/16", 1/8", and 1/4" thick. Figure 7 shows evidence of the jet burning up in the air similar to meteorites as they come into the atmosphere. Figure 33 shows the minor target damage resulting from the C-1 liner jet

FIGURE 33. Comparative target plate damage for extended and short standoff distances from C-1 liner jet through air (see Appendix II for specific target data).

after travelling through 13-1/3 feet of air, compared to the target penetration of a jet from a similar charge and C-1 liner which was shot into the multiple plate arrangement of Figure 3 (Test E-130). In the latter the jet penetrated over 38mm of steel, while the air eroded jet of E-132 penetrated less than 2mm of considerably less cross-sectional hole area. The extended air range thus imposed a more severe requirement on the jets than did the vacuum range of Eglin Air Force Base.

Test E-135 used a pellet type liner as shown in the sectional view of Figure 34. As may be seen in Figure 8, the jet from this liner performed less well than any of the others shot over the extended air range.

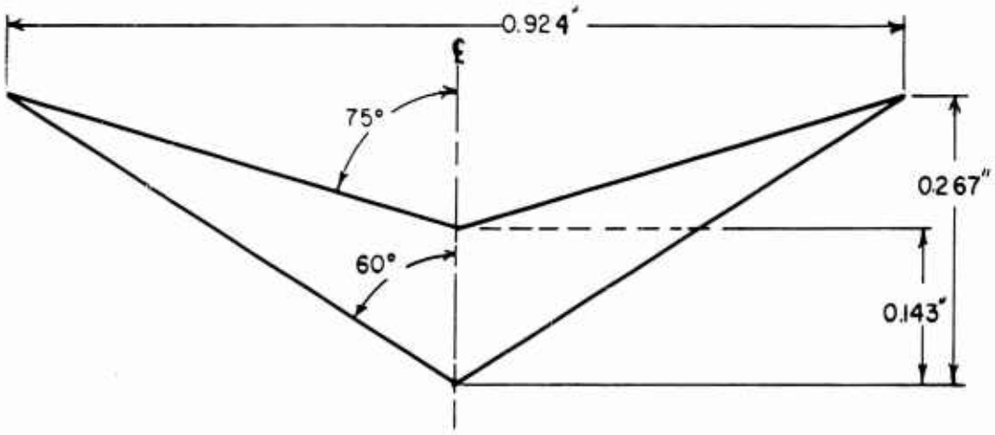

FIGURE 34. Sectional view of C-7 liner used in Test E-135 as shown in Figure 8.

Vacuum Range

The vacuum range depicted in the plan view of Figure 35 was used to more closely simulate the range used at Eglin Air Force Base. The static image of Figure 9 shows a view of the observation ports and reflected

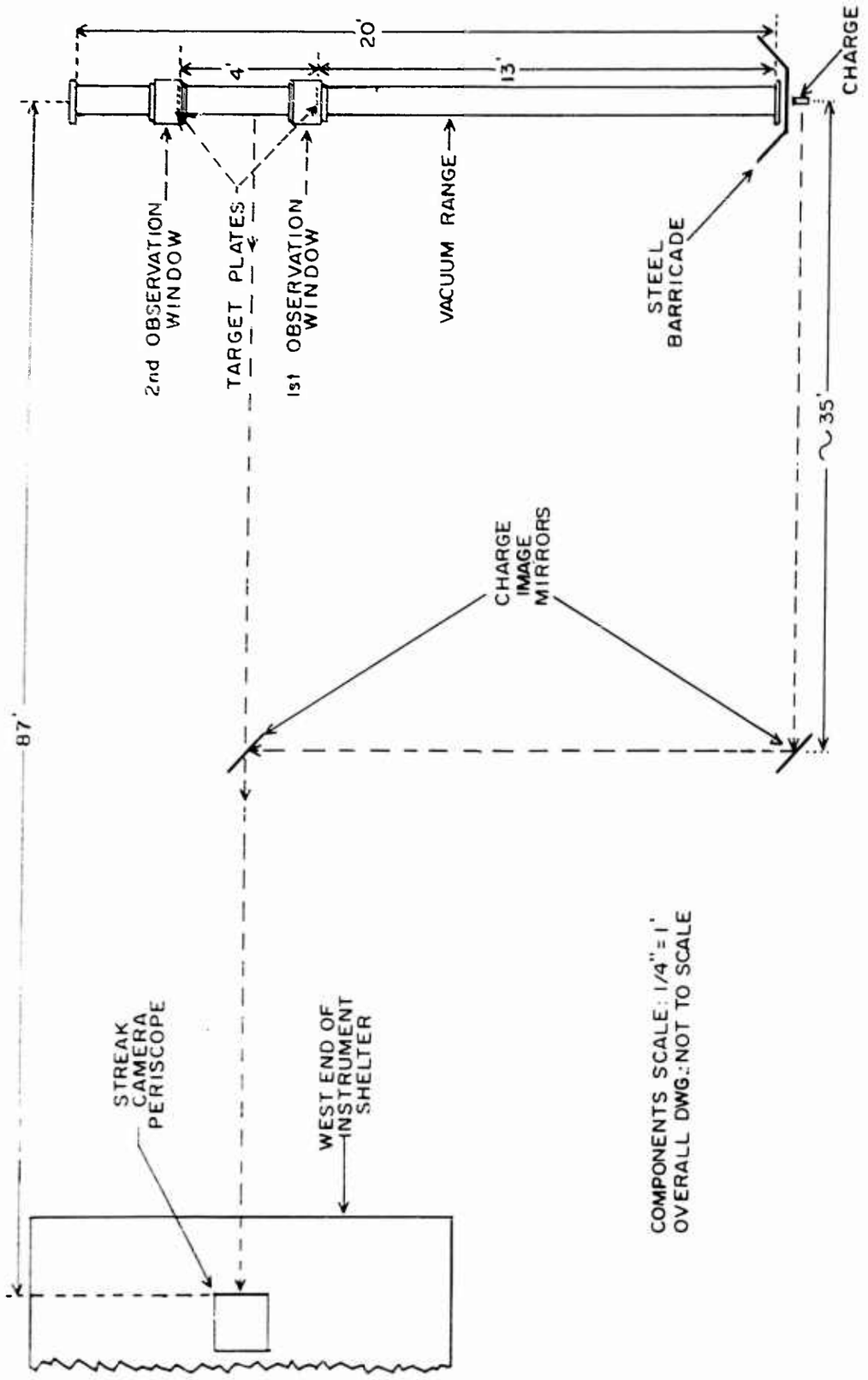

FIGURE 35. Plan view of experimental arrangement for vacuum range testing of shaped charges.

view of the charge (white object near center of mirror between ports) as seen by the streak camera. The white line across the static image is the camera slit image; all of the light forming the streak traces on the film passes through the slit.

Table 6 is a tabulation of the successful tests using the vacuum range. The 8" diameter steel target plates were placed at the leading edge of the window ports (i.e. at the right edge of the windows in the static image of Figure 9) for Tests E-138 through E-144 of Table 6. The calculated velocities were therefore a little low since the observed jet transit time from charge to first port was too long by an amount equal to the jet penetration time of the first target plate. For tests E-145 through E-197 the target plates were placed at the center of each window which resulted in streak trace records of the jet reaching, passing through, and leaving the target plates (see lower half of Figure 9).

Figures 36 through 40 show sectional views of the various type liners listed in Table 6 which have not been described previously in this report. The C-37 liner was a scaled up version of a liner developed and tested on another project[5] and was used as a reference to check the velocities and jet cohesion results of the vacuum chamber and for comparison with other liners. Tests E-138 and E-139 resulted in an average initial velocity of 10.7 km/sec for the E-37 liner which is the same as the velocity measured for the original liner from which the C-37 liner was patterned. Test E-144 was a repeat of E-138 and E-139 except the chamber was not evacuated, and this resulted in a little lower velocity. These preliminary tests provided satisfactory initial checks on the vacuum chamber and the associated velocity measuring technique.

Liner C-38 was designed to be more massive than the C-1 liner in an effort to obtain a jet that would hold together over the 13+ foot standoff range. Figure 41 shows a comparison of the C-1 liner (Test E-141) and the C-38 liner (Test E-143) when their respective jets were shot into the vacuum chamber. The C-38 jet held together much better than did the C-1 jet. Also a comparison of the E-141 target damage of Figure 41 with that of E-130 of Figure 33 shows that the latter at a 3.3" standoff penetrated 37mm of steel at a maximum hole area about half that produced by the jet of E-141 which penetrated 3.2mm of steel at a 145" standoff. Moreover, while a single clean hole resulted in E-130, Figure 41 shows the extensive particle scatter beyond the central hole of E-141. This comparison shows evidence of the lateral dispersion within the C-1 liner jet which is accentuated at extended standoff distances. And this dispersion greatly affects the penetration capabilities of the jet.

Information was also obtained from the vacuum range on the effects which jet inhibitors have on cohesion of shaped charge jets at extended standoff distances. Figure 42 displays first target plates from Tests E-159 and E-162 in which Type I and Type VI jet inhibitors were used in C-38 liners. A comparison of the shallow scattered craters of Figure 42 with the clean round hole of E-143 in Figure 41 provides good evidence of the

TABLE 6. Test shot conditions and data for test firings into the vacuum range of Figure 36.

Test No.	Liner Type	Chamber Pressure	S (cm)	TARGET Thickness (Inch) First Window	Second Window	Jet Penetration	HOLE Pattern	Area(cm^2)	JET VELOCITIES Initial (km/sec)	After 1st Plate
E-138	C-37	320μ	3.0	1/16	1/8	3/16+"	Irregular	27	10.8	--
E-139	C-37	280μ	11.0	1/8	1/8	1/4"	Round	16	10.6	5.5
E-140	C-1	140μ	2.54	1/16	0	1/16+"	Irregular	60	12.4	4.8
E-141	C-1	300μ	2.54	1/8	1/8	∿3/16"	Irregular	20	10.4	8.8
E-142	C-41	350μ	3.17	1/16	0	1/16"	Round	5mm[1]	9.7	--
E-143	C-38	450μ	4.0	1/8	1/8	<1/4"	Round	18	10.7	--
E-144	C-37	Atmos.	11.0	1/8	1/8	>1/4"	Oblong	22	10.1	3.9
E-145	C-38	4mm	7.0	0	1/16	>1/16"	Irregular	18	11.4	--
E-147	C-38	4mm	7.0	1/16	1/16	>1/8"	Irregular	30	11.6	6.6
E-149	C-1[2]	4mm	3.5	.003[3]	1/8	>.003"	--	--	12.5	5.4
E-150	C-1[2]	4mm	3.5	.003[3]	1/8	>.003"	--	--	12.5	11.3
E-159	C-38[2]	25-1/2"	7.0	1/8	1/8	∿1/16"	Craters	0	11.1	--
E-160	C-38[2]	25-1/2"	7.0	1/16	1/8	>1/16"	Circular	∿1	11.2	2.2
E-161	C-38[2]	25-1/2"	7.0	1/16	1/8	>1/16"	Scattered	1	11.4	--
E-162	C-38[4]	25-1/2"	7.0	1/8	1/8	>1/8"	Scattered	1	11.2	2.6
E-175	C-38	25-1/2"	5.0	1/8	1/8	>1/8"	Irregular	13	10.7	--
E-193	C-39[5]	25-1/2"	1.5	1/8	1/4	>1/8"	Irregular	50	10.0	--
E-194	C-42	25-1/2"	--	1/8	1/8	<1/16"	Craters	--	6.9	--
E-197	C-39-a	25-1/2"	1.4	1/8	1/8	>1/8"	Irregular	20	12.9	--

1 Hole Diameter
2 With Type I Inhibitor
3 Aluminum (all other targets were steel)
4 Type VI Inhibitor
5 Shot Without Waveshaper

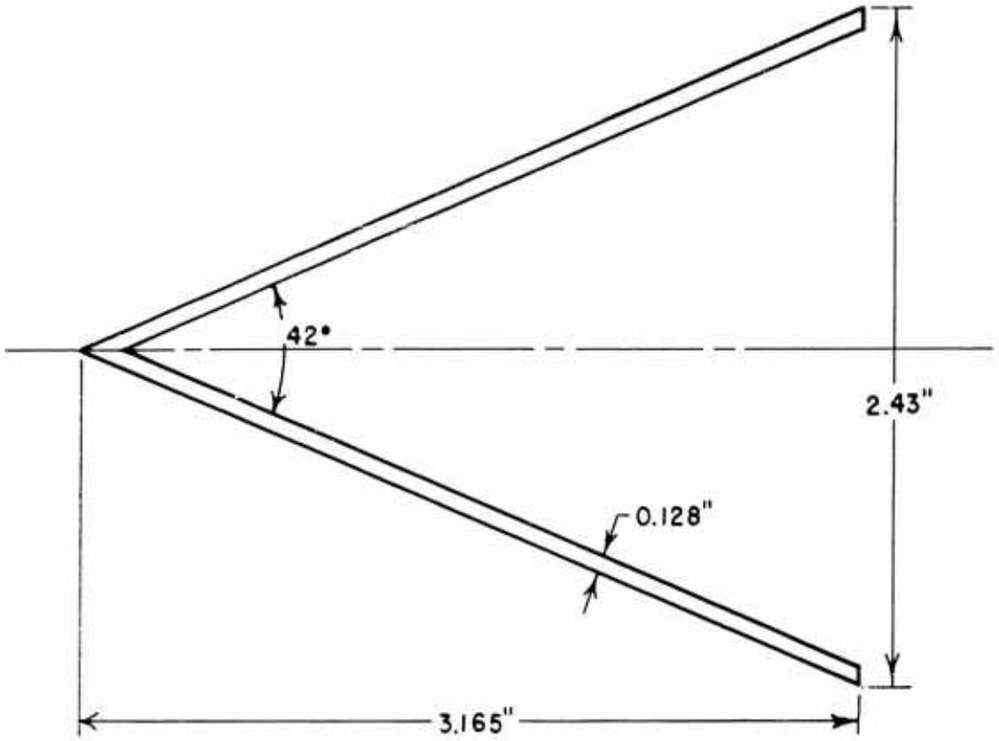

C-37 CONICAL LINER

SCALE = 1-1/2

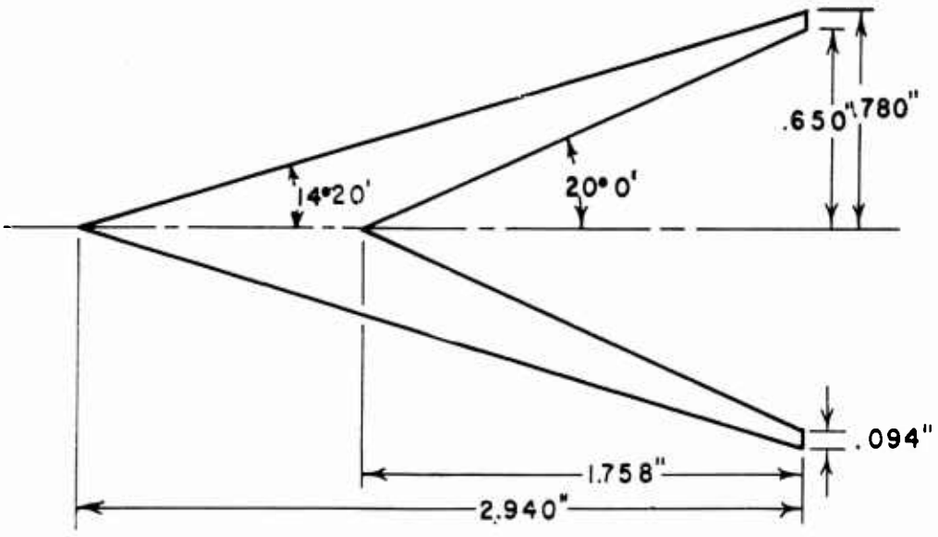

C-38 CONICAL LINER

FIGURE 36. Sectional views of C-37 and C-38 conical liners.

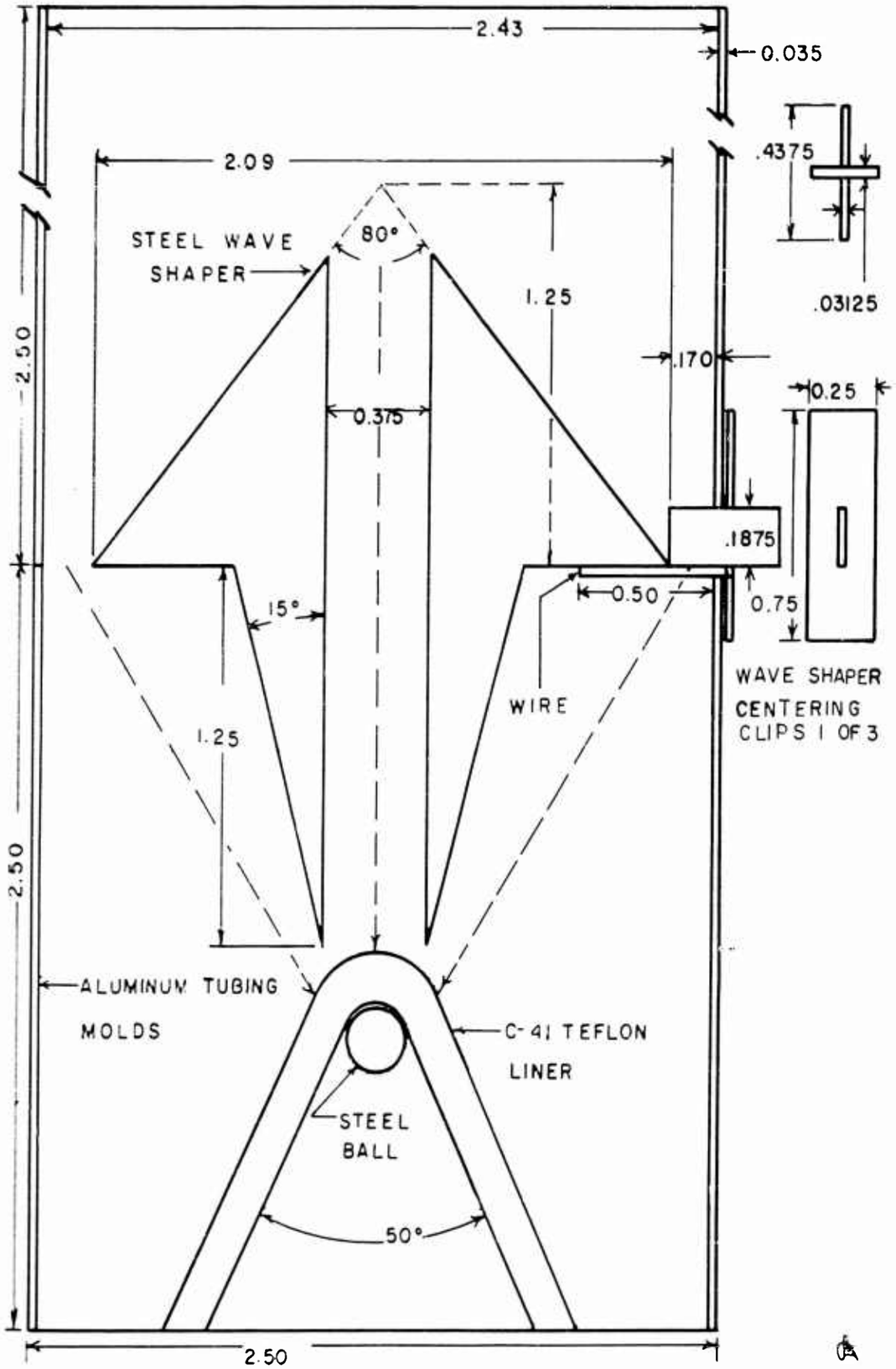

FIGURE 17. Sectional view of C-41 special liner and waveshaper.

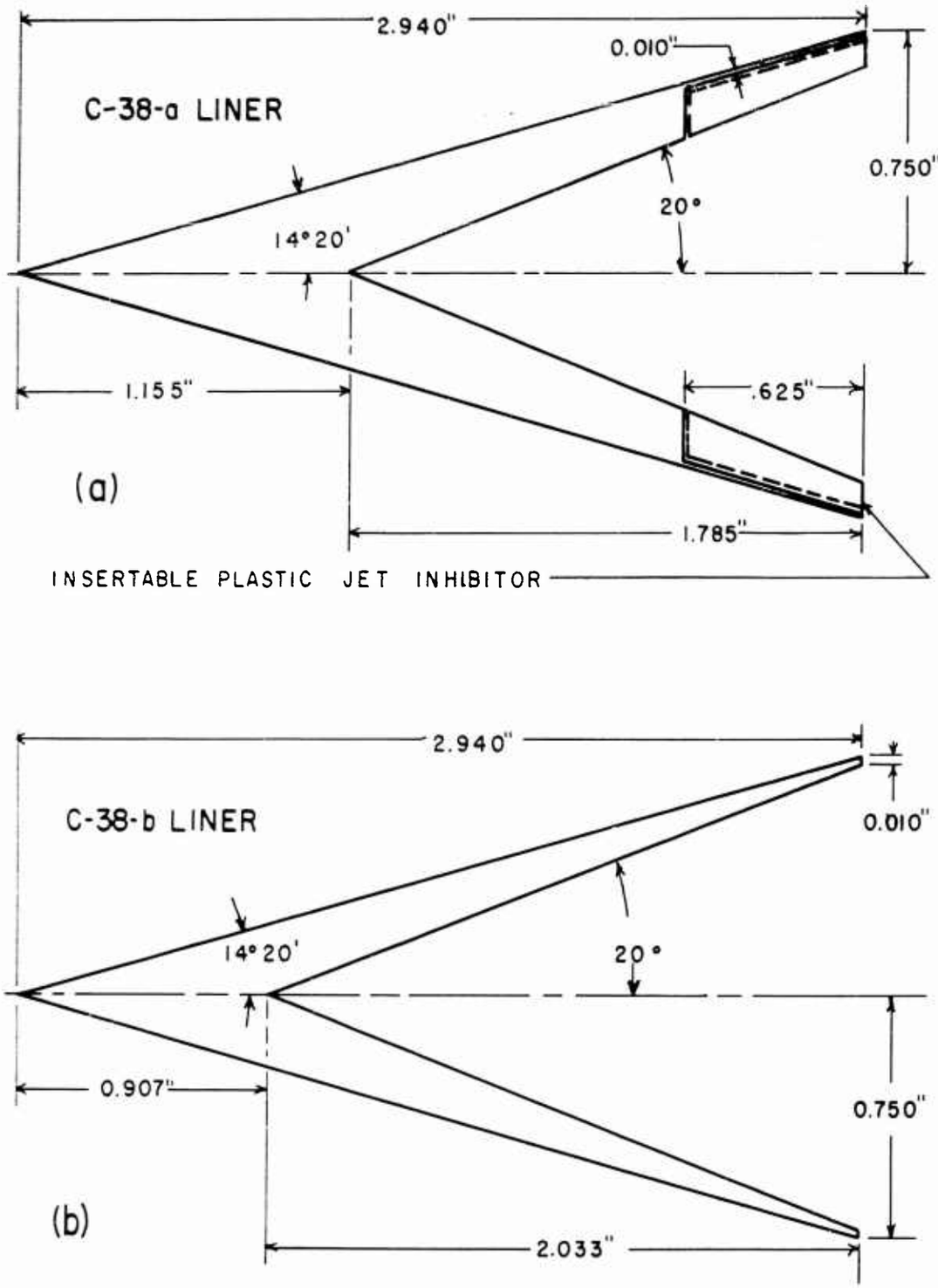

FIGURE 38. Sectional view of C-38-a and C-38-b conical liners.

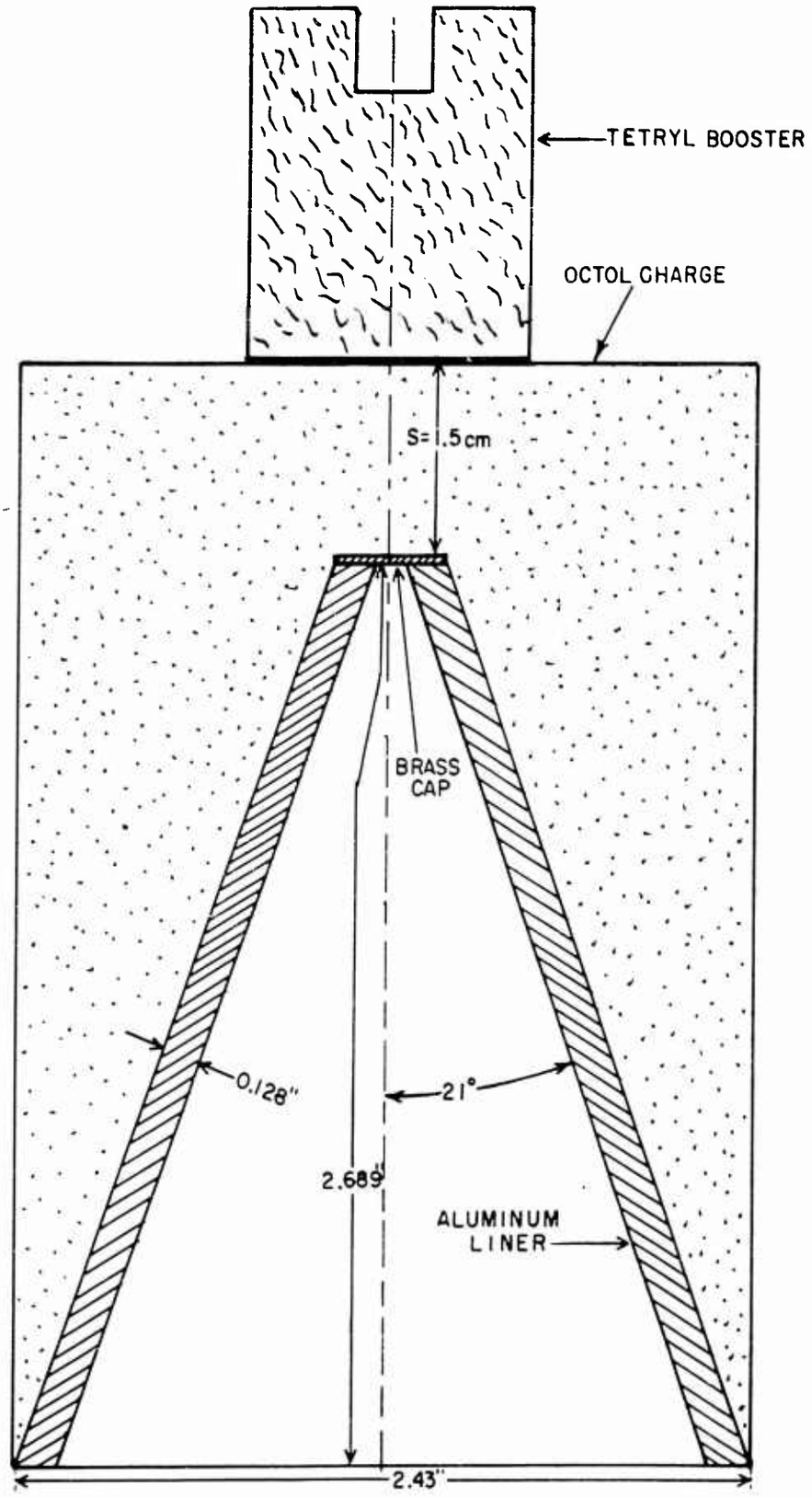

FIGURE 39. Sectional view of C-37-a liner as used in Test No. E-211.

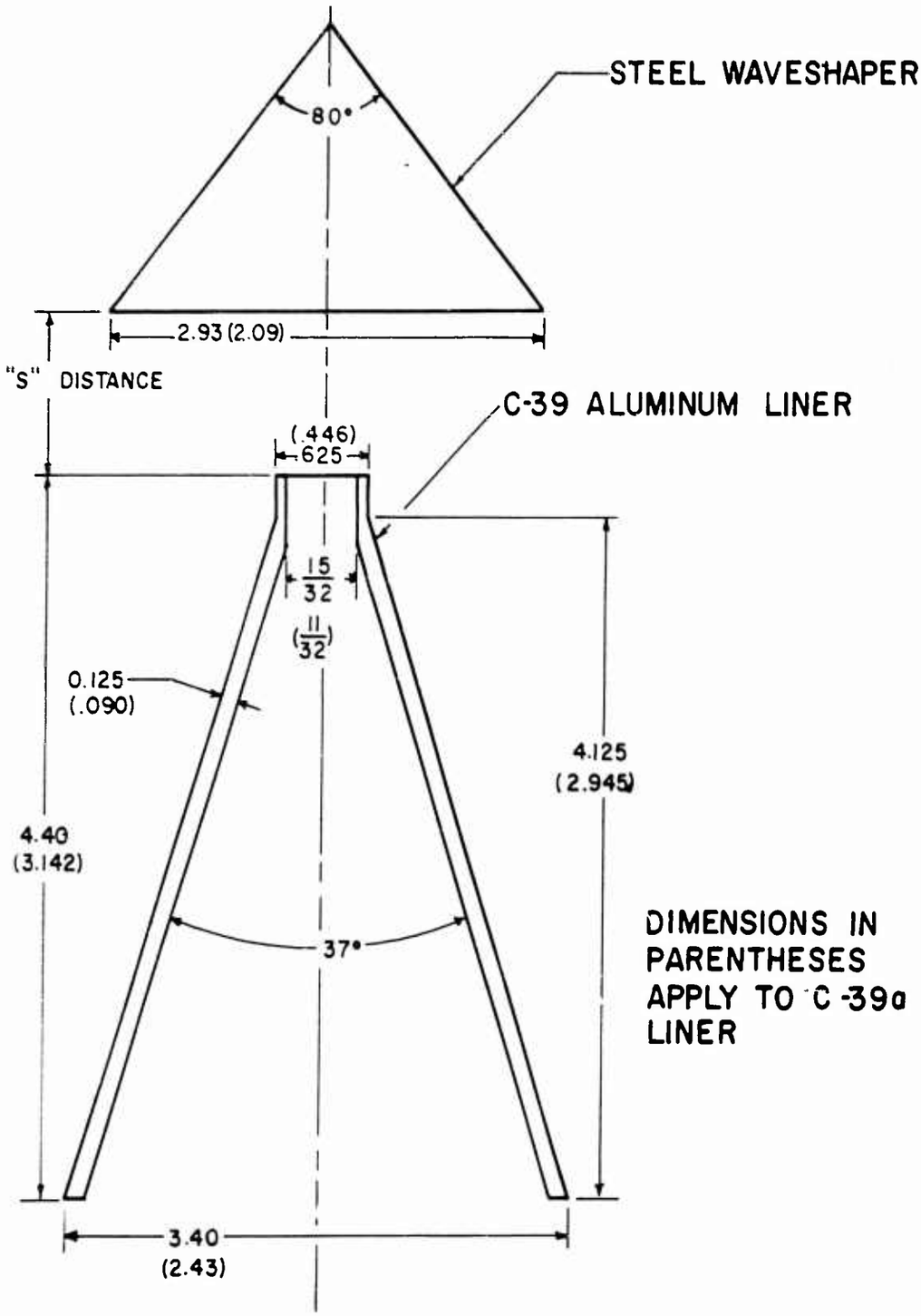

FIGURE 40. Sectional view of C-39 liner and associated waveshaper.

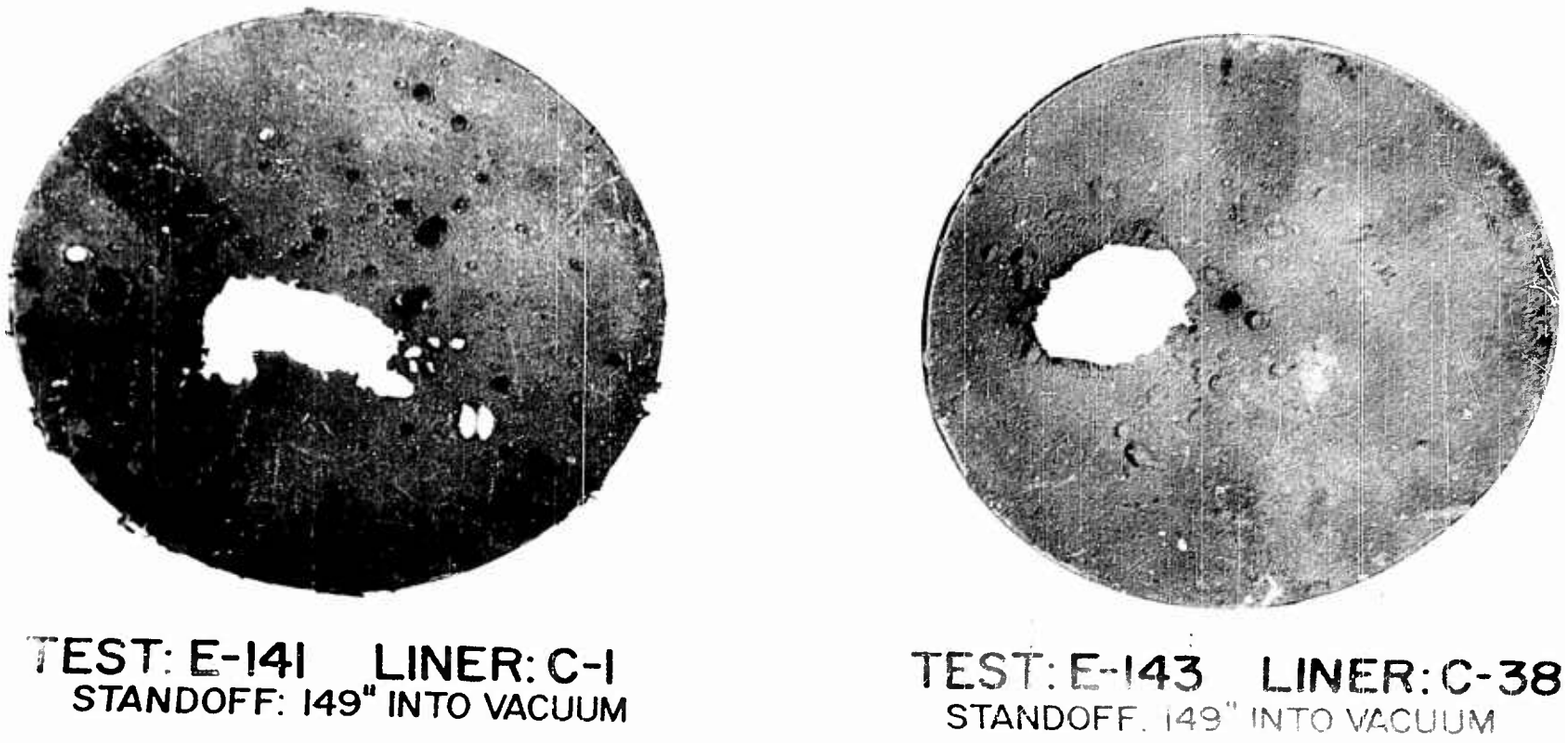

FIGURE 41. Photograph of target damage resulting from Tests E-141 and E-143 (see Table 6 for target data).

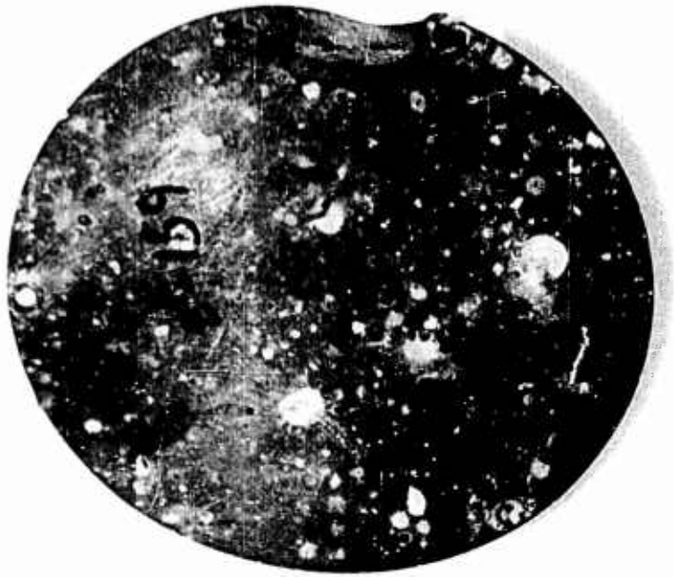

TEST: E-159 LINER: C-38
STANDOFF: 149" INTO VACUUM
INHIBITOR: TYPE I

TEST: E-162 LINER: C-38
STANDOFF: 149" INTO VACUUM
INHIBITOR: TYPE VI

FIGURE 42. Photograph of target damage resulting from Tests E-159 and E-162 (see Table 6 for target data).

disrupting effect which jet inhibitors have upon jets. The larger hole of the Type VI inhibitor helped but slightly in E-162. Target plate damage of E-160 and E-161 verifys the results of E-159, while E-145 and E-175 produced essentially the same results as E-141. A sufficient number of check shots were thus made to support the above conclusion. Also, similar results occurred with the C-1 liner which was shot uninhibited in E-140 and E-141, and with Type I inhibitor in E-149, E-150 (see "Hole" data in Table 6).

Liner C-39 was a modification of the one used by Kronman and Merendino in their jet inhibitor work. This shape of liner was chosen (Figure 40) because of the success they had experienced in obtaining radiographs of the jets from this type liner[2]. Tests E-193 and E-197 checked the jet cohesion of this type liner. The resulting target plate damage (Table 6) indicated better performance than any other liner; therefore the C-39 liner was chosen for the third series of tests at Eglin Air Force Base.

Test E-141 was made with a special "liner" and waveshaper assembly as shown in Figure 37. This was an effort to propel a 1/4" diameter steel ball directly without benefit of a collapsing liner. The waveshaper was designed to provide an impulse directly behind the ball shortly before the impulse arrived from around the sides of the waveshaper to strike the sides of the Teflon liner. Then the continuing impulse down the side of the liner was to keep the ball accelerating till it left the charge. Results were inconclusive. A single hole, apparently from an object passing through the first target plate in the wrong direction (from hole flare direction) was of a smaller size than the original bearing. Also the velocity streak record may have been from the charge plasma instead of from the ball, since an object having even a fraction the mass of the ball bearing traveling at 9.7 km/sec would have resulted in a lot more plate damage.

The vacuum range proved to be very useful in resolving the discrepancy between results obtained with jet performance over short range air shots at IRECO and extended range vacuum shots at Eglin Air Force Base≠. In addition the vacuum range helped select the type of liner most suited for proposed tests at Eglin Air Force Base.

Figure 43 contains jet velocity vs ΣL_i jet segment plots of tests with C-38 liners (Figure 36) under varying conditions of jet inhibition as indicated on each plot. E-154 and E-158 were uninhibited and had the longest jets of this group. The inhibiting condition for E-153 consisted of explosive deficiency only (no plastic insert); that is, jet elements could form, but were swept aside by the configuration of the explosive at the base of the charge. This shortened the jet, compared to E-154, but it was longer than the jet from E-155 which had both plastic insert and explosive deficiency inhibition.

≠ Page 55.

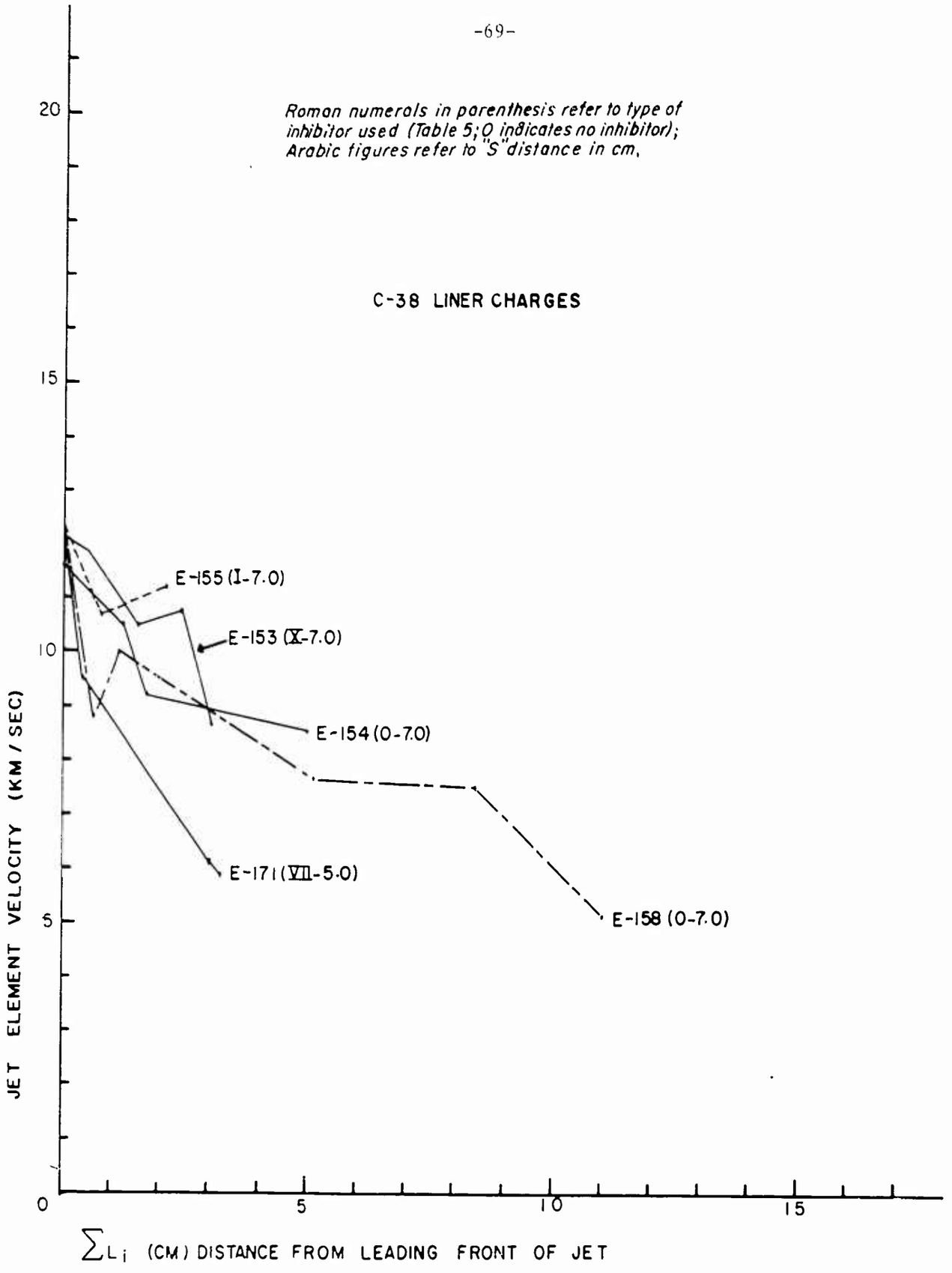

FIGURE 43. Jet segment velocities vs $\sum L_i$ increments from C-38 liners under varying conditions of inhibiting jet.

The jet from E-155 is a good example of the effectiveness of a jet inhibitor in reducing the overall velocity gradient and providing a leading jet segment with a low gradient. Figure 43 shows that E-155 had a jet length of 2.1 cm with a velocity gradient of only $\pm$ 7% of the mean velocity of 11.5 km/sec.

Figure 44 contains jet velocity vs ΣL_i jet segment plots of several variations of the basic C-38 liner of Figure 36. Liner C-38-a was designed with a thinwall skirt, as pictured in Figure 38, to check the effectiveness of this configuration in shortening the jet. Test E-182, using C-38-a without a plastic insert, produced a longer jet than the basic C-38 liner did (see Figure 43). Therefore in Test E-187 a plastic insert was used, and this shortened the jet to about 2/3 the length of E-182, but still practically as long as E-158 (Figure 43). Apparently the thinwall skirt produced the trailing segment of the jet in E-182, and it would appear that the plastic insert of E-187 succeeded in cutting off the jet from the thinwall skirt. Further shortening of the jet by this method could be accomplished by increasing the height of the skirt. Liner C-38-b (Figure 38) retained the same outside dimensions and apex angles as C-38, but had a shorter "a" dimension (0.907" instead of 1.155") to accentuate the taper of the liner wall. The other tapered liners have generally been designed to give the liner a constant cross-sectional area normal to the axis at all points. C-38-b had sufficient taper to give the liner a decreasing cross-sectional area from inner apex to base to decrease the mass to be accelerated, as the detonation progressed towards the base, in hopes that this would increase the velocity of the trailing elements of the jet. Results of Test E-186, in which this liner was used, are shown in Figure 44. When compared to E-158 of Figure 43, accentuated tapering had the reverse effect of that anticipated.

A further modification, within the basic outline of the C-38 liner, was made as shown in Figure 45 and designated as the C-38-c and C-38-d liners. The latter were truncated to permit a more nearly optimum impulse angle between the waveshaper initiating locus at the top of the charge and the upper portion of the liner as indicated by the dashed lines in Figure 45. Also two heights of thinwall skirts were used with these two liners. The increase in initial velocity due to truncating the liners was quite spectacular, ranging up to over twice the initial velocity from the basic C-38 liners of Figure 43.* However, the initial velocity gradient was just as spectacular, following the principles depicted in Figure 10 and described in the associated discussion.

The thinwall skirts of these liners weren't noticably effective in shortening jet lengths, at least when compared with jet lengths of the basic C-38 liners of Figure 43. Both E-188 and E-189 were shot without plastic inserts which would have cut off the trailing portions of their jets as occurred in E-187. However the C-38-c liner with the 1-1/4" high skirt did have a jet only 52% as long as the jet from the C-38-d

*compare with E-188 and E-199 of Fig. 44.

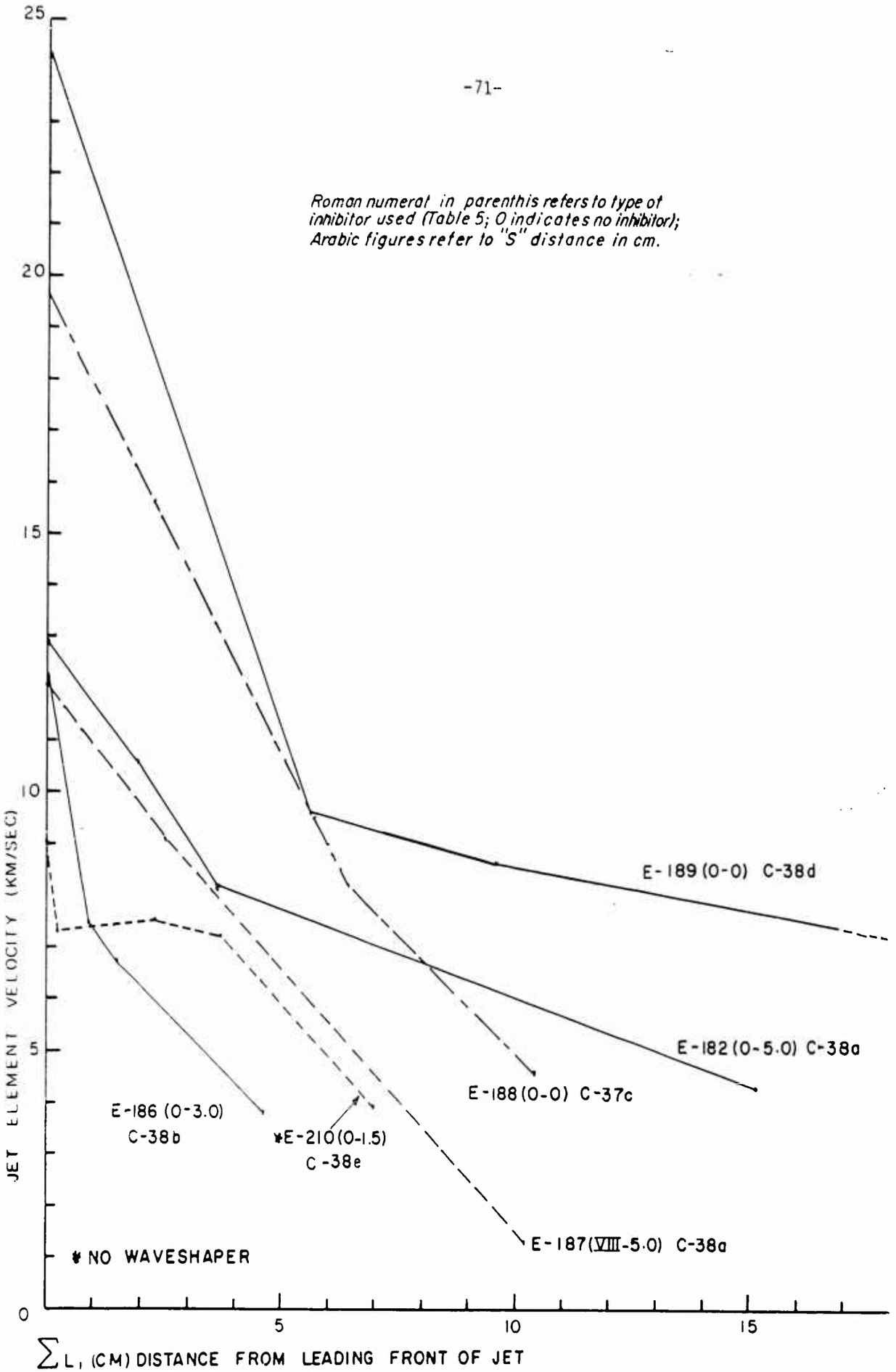

FIGURE 44. Jet segment velocities vs $\sum L_i$ increments from basic C-37 and C-38 liners.

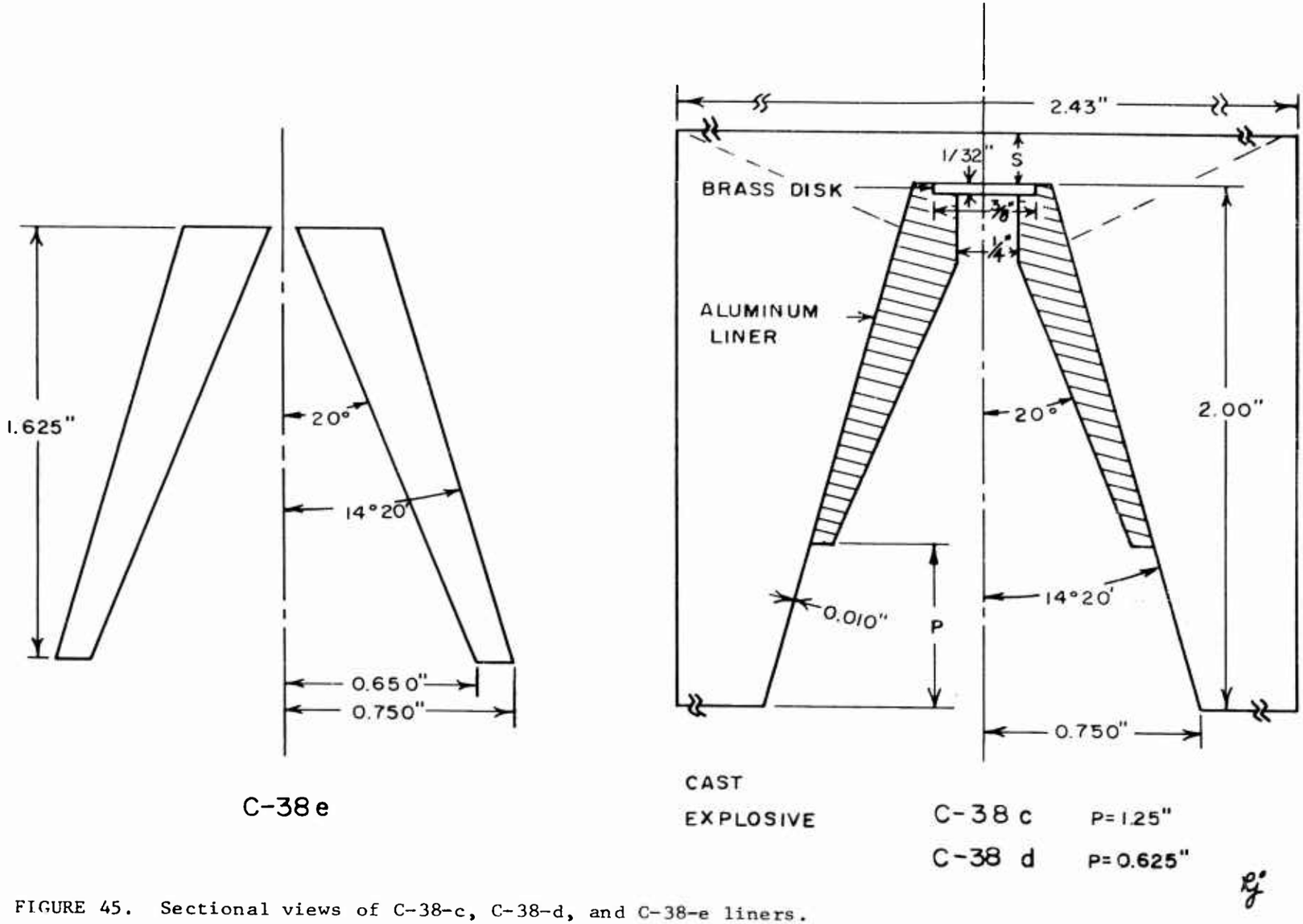

FIGURE 45. Sectional views of C-38-c, C-38-d, and C-38-e liners.

liner with the lower 5/8" skirt. Actually there does not exist a one to one correlation between any two of these different variations of the C-38 liner for comparing jet lengths, because of the different impulse angles throughout the entire lengths of the liners which also markedly affects the trailing segments of the jets.

Figure 45 also shows the configuration of the C-38-e liner which is simply the basic C-38 liner truncated. E-210 was fired without a waveshaper which resulted in a much lower initial velocity. Then, after a very sharp but short initial velocity gradient, an exceptionally low velocity-gradient segment of 3-1/2 cm length occurred in which there was a gradient of only $\pm$ 2% above and below a mean of 7.35 km/sec. This follows from the effects shown in Figure 10-a in which the impulse angle was far from optimum, but was more constant, than in Figure 10-b, as it progressed down the liner. Hence the great difference between the velocity structure of E-210 and E-180. A further check on the effect of truncating conic liners and firing without waveshapers was made in Test E-211. A basic C-37 liner was truncated as shown in Figure 39. The resulting C-37-a liner was fired without a waveshaper. Figure 46 shows a lower initial velocity (compare E-138 and E-139 of Table 6) followed by a moderate velocity gradient after which a 3-1/2 cm segment of fairly low gradient occurred.

Figure 46 also shows comparative results of firing the C-39 truncated liner with and without a waveshaper. In agreement with theory E-196 with waveshaper had a high initial velocity and high initial velocity gradient, while E-192 without waveshaper had a considerably lower initial velocity but with a leading 2.9 cm jet segment of low velocity gradient.

Figure 47 shows cross-sectional views of the C-43 and C-43-a liners which were used to determine the effect of confining shaped charges. Results are displayed in Figure 48 for which all charges were fired without waveshapers. A comparison of E-190 and E-199 shows quite a remarkable improvement in decreasing velocity gradient as a result of charge confinement. The unconfined charge of E-190 had a higher initial velocity, but this was followed by a continually decreasing velocity all the way to the end of the jet. On the other hand, the confined charge of E-199 had a lower initial velocity and then, after a momentary decrease in velocity, it recovered, climbed higher than initial velocity, and then maintained a low gradient to the end of the jet which had a velocity equal to 87.5% of initial velocity. Velocity gradient for E-199 was $\pm$ 10.5% of its mean 8.6 km/sec velocity, compared to $\pm$ 30.6% of a mean 7.35 km/sec velocity for the unconfined control charge E-190. E-199 had a larger velocity gradient than did E-155*, but the latter achieved its low gradient by inhibiting the slow trailing segment of its jet; therefore the jet of E-155 was only 27% as long as the jet of E-190. And when E-158, the uninhibited control charge for E-155 was compared with E-199 out to

---

* Page 70.

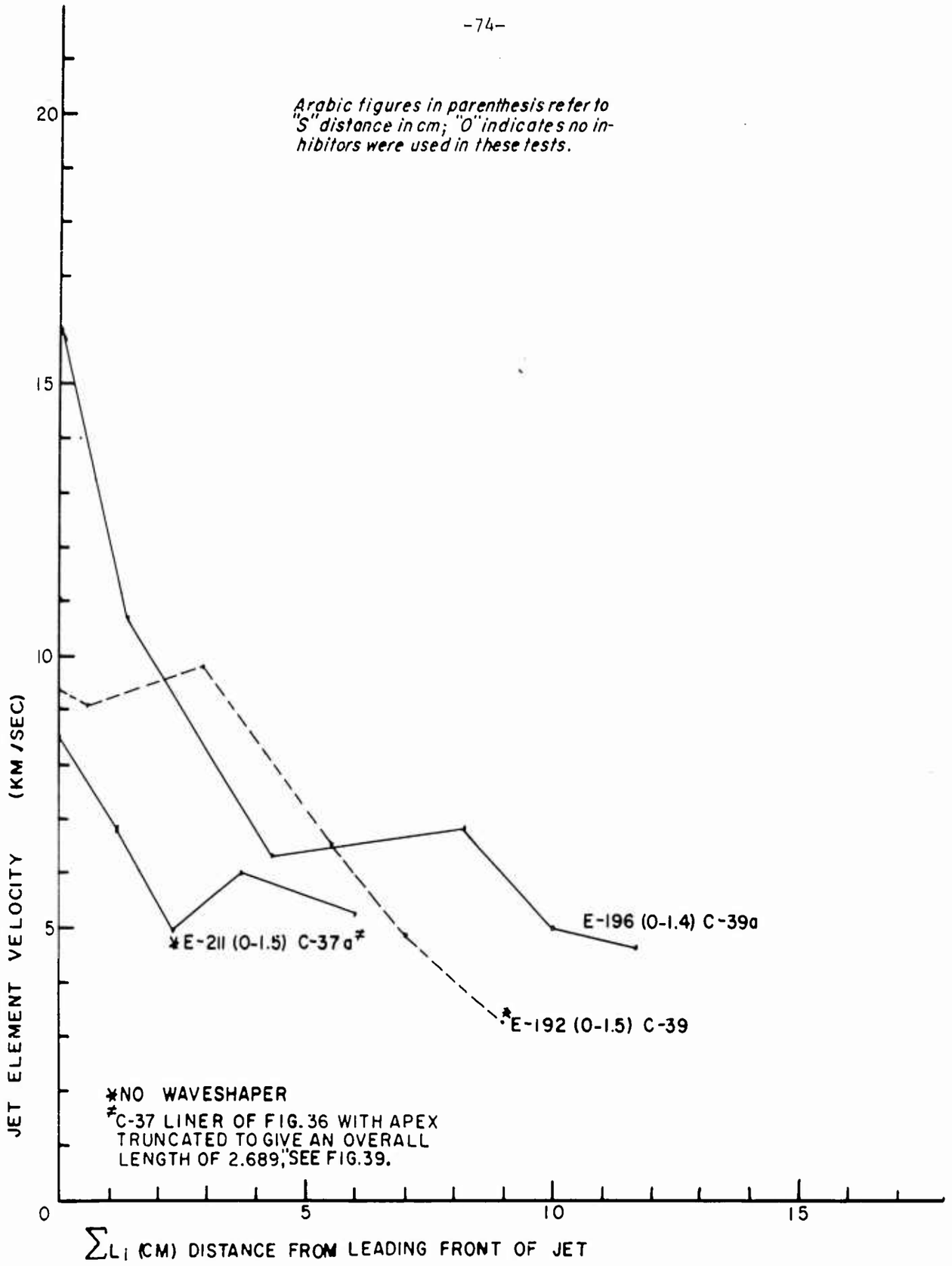

FIGURE 46. Jet segment velocities vs $\sum L_i$ increments from C-38 liners under varying conditions of inhibiting jet.

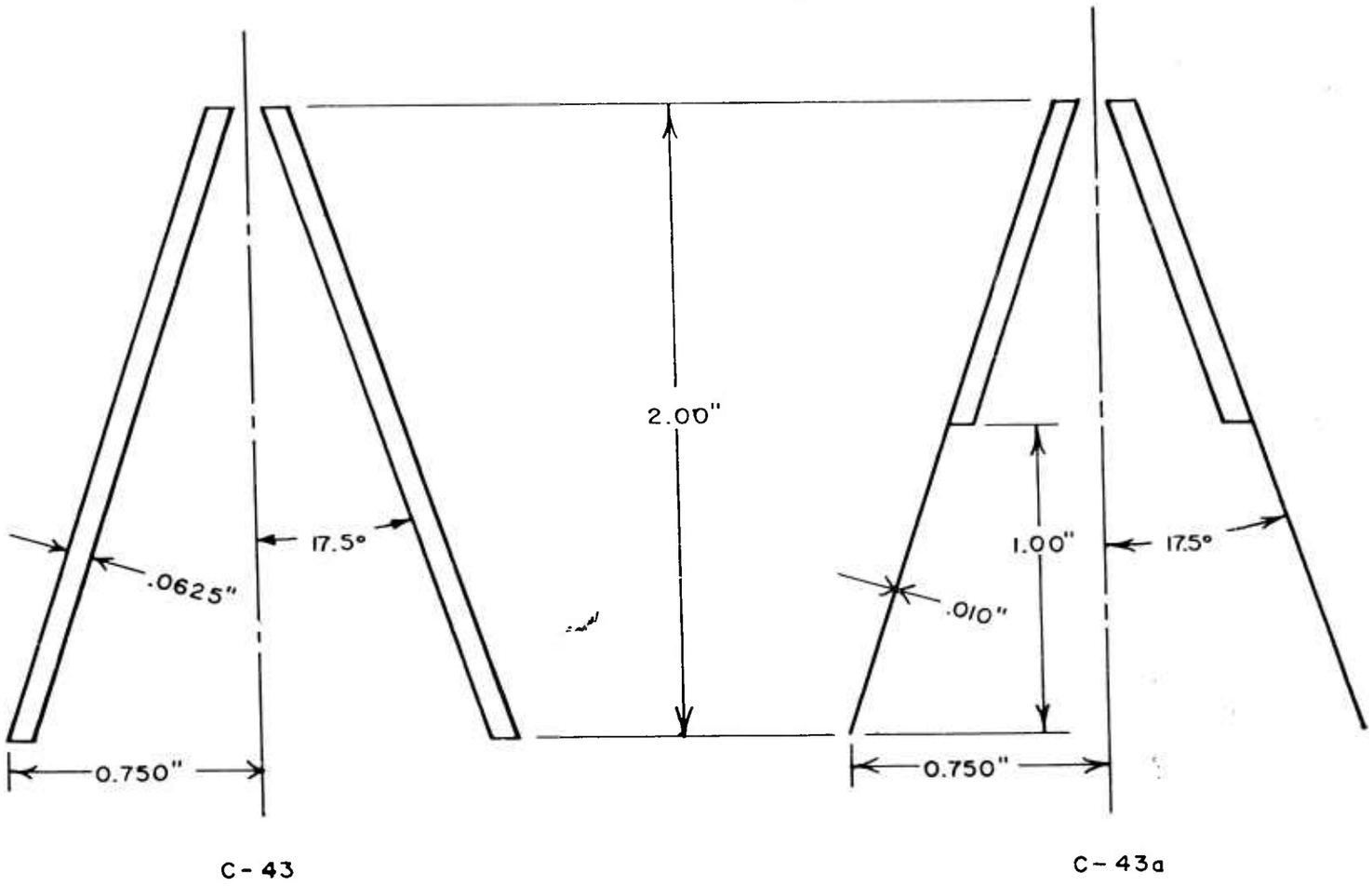

FIGURE 47. Sectional views of C-43 and C-43-a liners used in confined charge tests (see Figure 11).

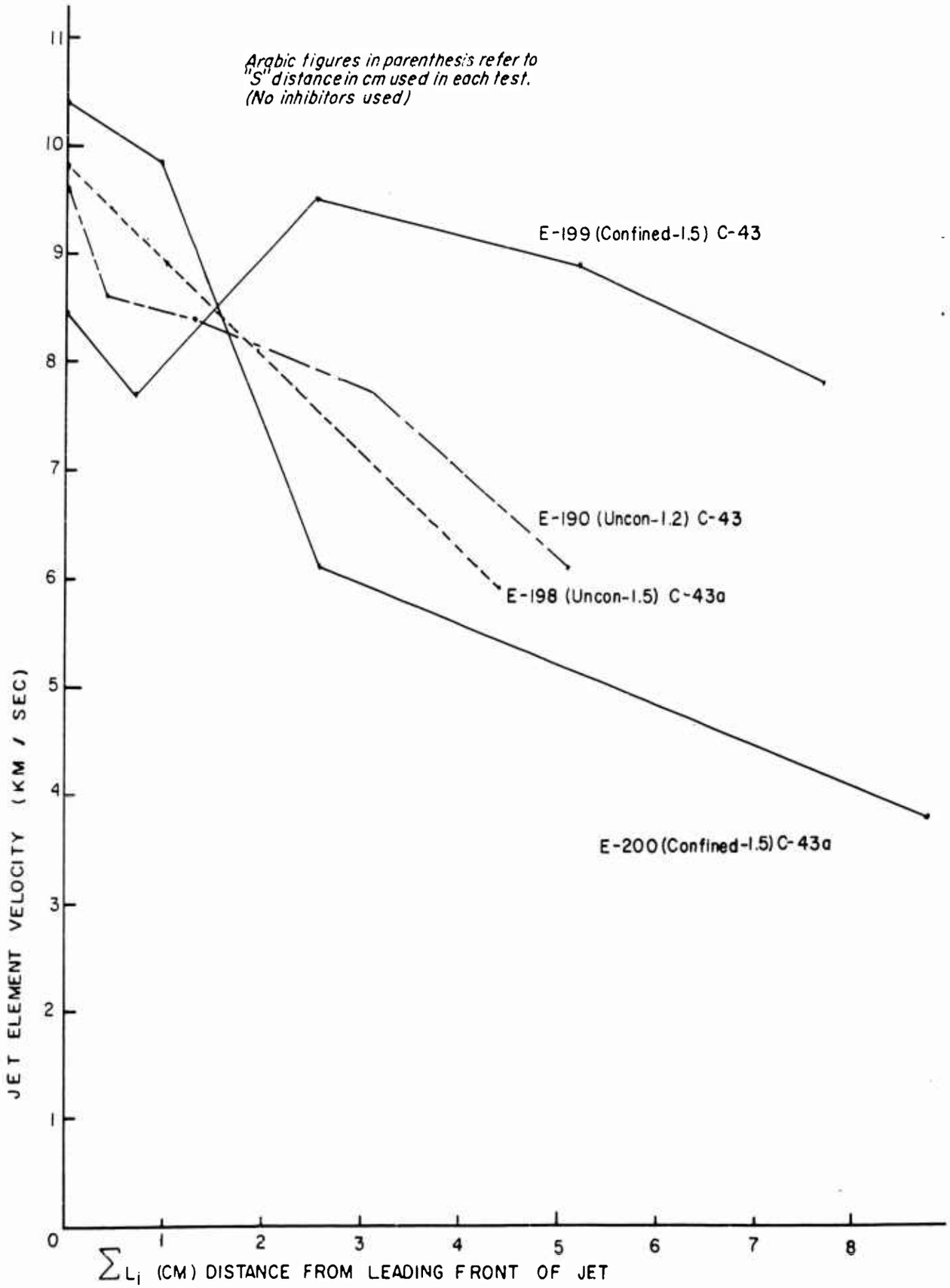

FIGURE 48. Jet segment velocities vs $\sum L_i$ increments from C-43 and C-43-a liners in confinement tests.

equivalent jet lengths (7.7 cm), E-158 was found to have a velocity gradient of ± 23.5% of a 10 km/sec mean velocity.

As a final check on the mechanism by which charge confinement enhances the trailing segment of shaped charge jets, Test E-198 and E-200 were made. These tests used the type C-43-a liner which had a thinwall skirt for half the liner height (Figure 47). According to results obtained by Gainer[6], confining a charge has the effect of increasing the target penetration of the jet elements originating near the base of the liner. This was interpreted as being equivalent to increasing the velocity of the trailing jet elements. Therefore use of the C-43-a liners, with minimum material around the base from which jet elements could be formed, served as control tests to show the effectiveness of confinement.

The unconfined charge test, E-198, produced a jet quite similar to E-190 except that it was about 14% shorter. The confined charge of E-200 produced a jet having the highest initial velocity, lowest final velocity, and greatest jet length of any in this series. If the trailing segment of the jet was formed from the thinwall skirt of the C-43-a liner, confinement of the charge should have maintained its velocity at a higher level. At least Gainer found that charge confinement was most effective for approximately the lower 3/8" of the liner[6]. It might thus appear that the trailing segment of E-200 was formed from higher up in the liner where the effects of confinement is not so pronounced. Further experimental work is needed to more fully resolve the factors and effects involved in charge confinement.

Disc-Shaped Charges

Prior to making any experimental charges in this category, tests were conducted on the peripheral initiator as discussed earlier in this report*. After the detonation symmetry of these initiators was found to be satisfactory the tests listed in Table 7 were made. All of the disc-shaped charges were of the shape and size shown in Figure 12, having been cast in the same special mold. And all of the charges listed in Table 7 (with the exception of E-237 which was shot without a liner) used the C-42 liner shown in Figure 49 which also displays the geometrical construction used to analyze the results of Test E-184 later in this section.

Figure 50 is the streak camera record of Test E-151 in which multiple plates were used as targets. The streak trace of the jet may be seen to curve from the time it became visible just below the charge-centering block until it reached the second target plate. This trace represents a continually decreasing velocity as the jet eroded in the air, but the decrease in velocity due to erosion of leading jet elements and the decrease due to air drag is indeterminate. If the jet were as long as

---

* Pages 34 to 36.

TABLE 7. Experimental parameters and calculated results of disc-shaped charge investigation.

Test No.	Type[1] Charge	Charge Explosive	S (cm)	Initial V_o	1		2		3		4		5		6	
					V_2	ΣL_i	V_4	ΣL_i	V_6	ΣL_i	V_8	ΣL_i	V_{10}	ΣL_i	V_{12}	ΣL_i
E-151	Disc	Octol	--	32.7 to 18.2	18.9 to 12.1	0.5										
E-152	Disc	Octol	--	23.7 16.1	—	--										
E-156	Cylinder	Octol	2.50	15.5	10.0	1.4	10.7	4.9	3.3	7.5						
E-157	Cylinder	Octol	3.35	13.7	10.6	0.8	9.6	3.3								
E-181	Disc	Baratol[2]	--	Failed												
E-183	Disc	Baratol[3]	--	Failed												
E-184	Disc	Octol	—	24.6												
E-185	Cylinder	Baratol[3]	0	10.0	10.0	0.6	8.0	2.3	9.4	3.0	10.2	4.7	6.6	5.9	3.8	7.8
E-194[4]	Disc	Octol	--	?												
E-195	Disc	Baratol[3]	--	Failed												
E-207	Disc	TNT	--	Failed												
E-208	Disc	Octol	--	31.6												
E-209[5]	Cylinder	Octol	0	25.4	8.6	3.4										
E-235[6]	Disc	Octol	--	8 to 11												
E-236	Disc	Octol	--	8.3 to 29.3												

1 All charges used C-42 liners except as noted
2 $Ba(NO_3)_2$/TNT = 70/30
3 $Ba(NO_3)_2$/TNT = 60/40
4 Vacuum shot (all others, air shots)
5 Shot without waveshaper
6 Shot without liner (all others had C-42 liner)

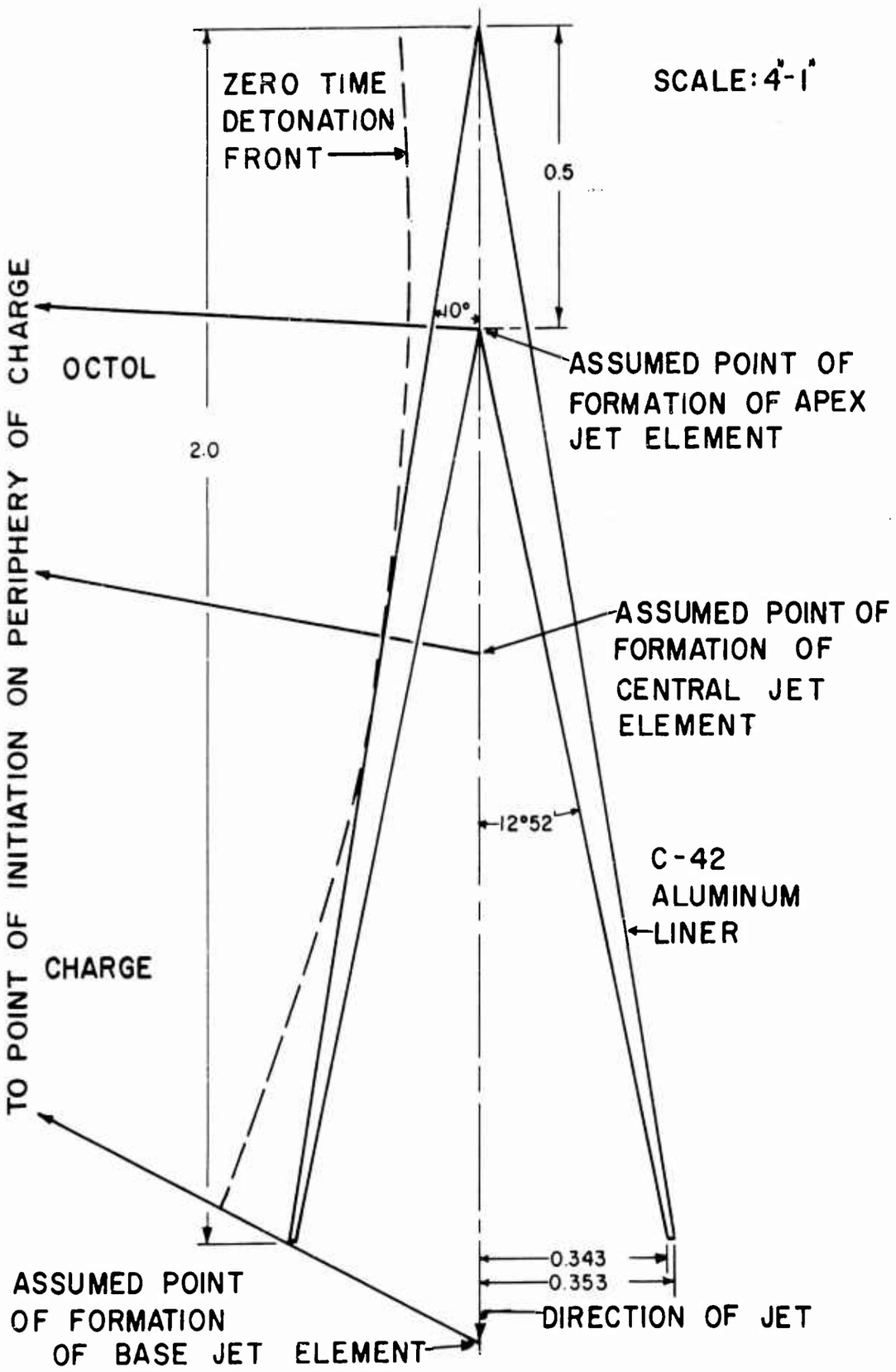

FIGURE 49. Sectional view of Type C-42 liner showing geometrical construction of theoretical jet formation.

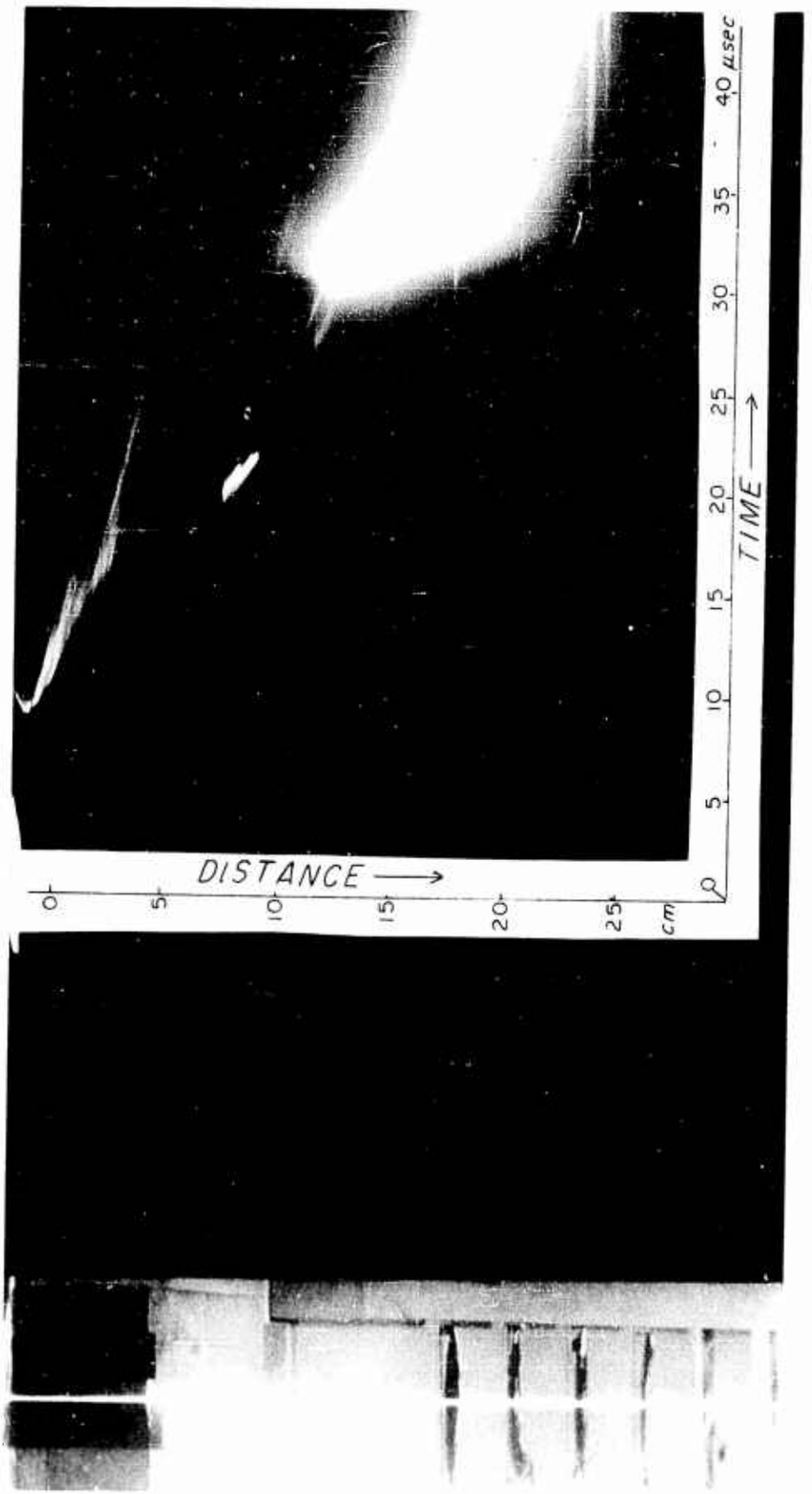

FIGURE 50. Photographic reproduction of streak camera record from disc-shaped charge Test No. E-151.

jets from cylindrical charges, air erosion could account for a large percentage of the decrease in velocity. However there is some evidence that the jet was considerably shorter than conventional jets and that at least some of the jet elements were travelling along at virtually the same velocity. The jet velocity just prior to entering the first plate was slightly less than the emergent velocity out of that plate. The L_i jet length dissipated in the first plate was 5mm and therefore a jet element 5mm further back in the jet was travelling with about the same velocity. Also the jet's energy was dissipated before getting through the second 1/16" thick plate; this could result from a jet having a shorter structure than conventional elongated jets from cylindrical charges.

For comparison, Tests E-156, E-157, and E-185 were made with the same type C-42 liner as used in E-152 and E-156, but in standard cylindrical charges. The jets of these tests all penetrated at least four 1/16" plates in addition to a 1/8" plate for E-156, and a 1/8" plate plus a 1/4" plate for E-185. Thus the long jets are efficient in penetrating a deep relatively small diameter hole. On the other hand, a more compact jet would tend to dissipate its energy over a larger diameter area and therefore be unable to penetrate as deeply. No trace was ever found of the upper target plates from any of the octol disc-charge shots listed in Table 7, except the more massive plates of the last four tests.

Another evidence of the higher energy in the leading segment of jets from disc-charges is the amount of light generated by interaction between the jets and the air. A comparison of the streak trace intensities of Figure 5, which were produced at a camera speed of 300 rps, with the trace intensity of Figure 50 produced at 400 rps (25% less exposure time) shows the latter to have several times as much light intensity (the film from E-211 of Figure 5 had about the same trace intensity as E-156 which used the same C-42 liner in octol as E-151, but in a cylindrical charge).

One further consideration in comparing the streak traces from typical disc-charge jets with traces from typical cylindrical charge jets is the trace shape. As may be noted from Figure 50 the upper trace, between its initial point and the point where it struck the first plate curved sufficiently to indicate a velocity decrease from 32.7 to 18.2 km/sec. When this is conpared with the corresponding trace of Figure 5 (second trace from the left) it may be noted that the latter trace is virtually straight, as were practically all velocity traces from cylindrical charge jets over the short air range into and through multiple-plate targets. Thus no change-of-velocity evidence of jet erosion norair drag occurred with the cylindrical charge jets.

The pronounced change in velocity of the disc-charge jets, in addition to the corroborating evidence of greater light intensity, indicated the presence of considerably more erosion of these jets' leading elements. Jet erosion of a hypervelocity particle may be expressed by the differential mass equation developed by Opik[7]:

$$\frac{dm}{df} = -\frac{\Lambda A}{2\zeta}\left(\frac{m}{\rho m}\right)^{2/3}\rho_a V^3$$

in which m is particle mass, ρ_m particle density, ζ the heat of ablation of the particle material, Λ the heat-transfer coefficient, A the effective cross-sectional area of the particle, ρ_a the air density, and V the particle velocity[8]. From this and the air drag equation* it is evident that both erosion and air drag are proportional to the third power of velocity for a given cross-sectional area, A. If the jets of the several disc-charge tests listed in Table 7 were compact structures of low velocity gradient elements, then the velocity decrease evident in Figure 50 would be mainly due to air drag since erosion of front particles would expose to air erosion ensuing particles of near-equal velocity. At least this was apparently the case at the first target plate where adjacent jet elements had velocities of 18.2 and 18.9 km/sec, and it may have been true for other segments of the jet.

In an effort to obtain more information on the characteristics of disc-charge jets, Tests E-208 and E-209 were made. Instead of using thin (1/16" thick) initial target plates as previously, two massive (1/2" thick) plates were used in each test to insure recovery of the plates as well as to provide a target that would permit a better cratering analysis. The jet from the disc-charge of E-208 created in the first target plate a shallow crater of relatively large diameter, having a diameter to depth ratio of 35mm/3.5mm = 10. In comparison, the cylindrical charge jet of E-209 produced through both target plates deep cratering of relatively small diameter, having a diameter to depth ratio of 17mm/25.4mm = 0.67.

Figure 51 shows photographs of the target plates with the first plate in each case at the top of the figure. In Test E-208 the first plate was severly deformed and eroded to 90% of its initial thickness, 130% of its original length, and 74% of its prior weight. In contrast to this the first plate of E-209 was undistorted, suffering only a central crater hole which reduced the plates weight to 90% of its prior weight.

To determine whether the plate deformation of E-208 was due to effects of the jet or of the blast pressure, Tests E-235 and E-236 were conducted. The C-42 liner of E-235 was removed after the charge was cast thereby leaving only a C-42 shaped cavity where the liner would normally be located. The first plate suffered approximately the same deformation as the first plate in 208, and so it was concluded that blast pressure was responsible for all of the plate damage in E-208 except the crater, as no crater was evident in E-235. Even a Munroe effect[9] depression was not evident in the first plate of E-235 because of a 3-1/2" standoff between charge base and target. However it was of

---

* Page 17.

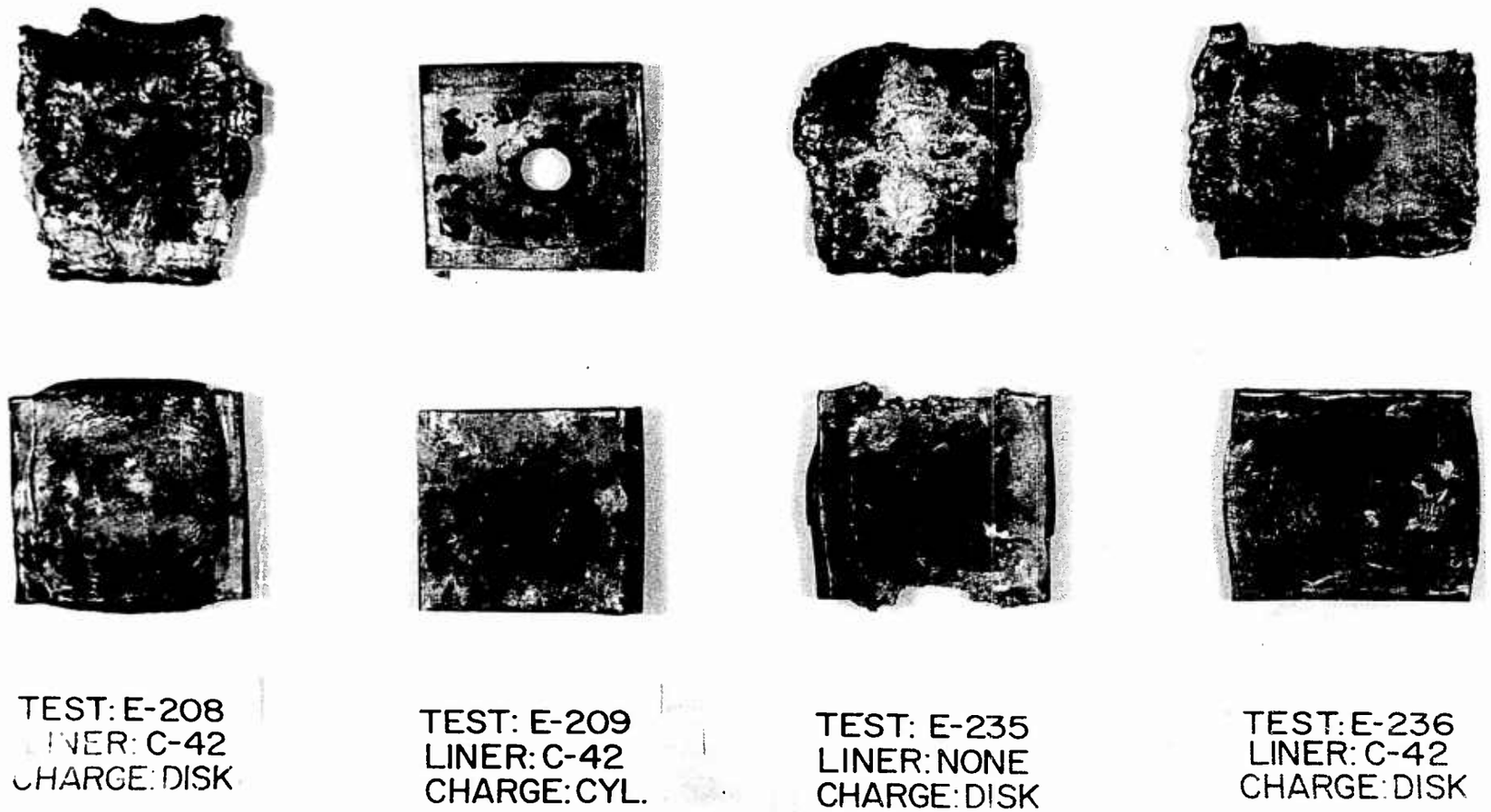

FIGURE 51. Comparative target plate damage from cylindrical and disc charges.

interest to note the luminous gases emitted by the cavity of E-235 since their velocities were up in the range of many of the shaped charge jets from cylindrical charges listed earlier in this report.

Test E-236 was a repeat shot of E-208. Target plate deformation was similar to E-208 except that the first plate split in half and left a sharp-ridge imprint of the split on the second plate (Figure 51). The crater in the first plate was smaller in diameter (15mm), but about the same depth (3.5mm) as the crater of E-208. A study of Table 7 shows other variations in the performance of similar disc-charges. For example initial velocities, V_o, have a sizeable range for the various octol disc charges. These variations are perhaps somewhat greater than corresponding variations of cylindrical charges, and this may be attributed to the critical requirements of symmetrically initiating the disc-charges. A slight difference in arrival times of the detonation front on different sides of the liner (Figure 12) would result in an appreciable variation in the performance of the jet, which could account for the difference in craters for E-208 and E-236, as well as for varying initial velocities, etc. Imperfect casting of the explosive, resulting in air cavities, could also account for unsymmetrical liner wall collapse.

Figure 52 shows the streak camera record of Test E-184, one of the octol disc-charges listed in Table 7. Results of this test are of particular interest because of the further possibilities it suggests on the jet structure from disc-charges. Due to the way in which the detonation wave progresses from liner apex to base in a cylindrical charge, as well as the increasing wall to axis wall-collapse time from apex to base, the jet elements from such a charge are emitted in successive segments which originate progressively in order from apex to base. And since the general velocity trend of these various elements is decreasing velocity of elements from apex to base, faster elements generally do not pass slower elements in cylindrical charge shots.

In the case of the disc-charge, however, the detonation wave reached the central section of the liner first and progressed to apex and base in less than a half microsecond (Figure 49) compared to 6 μsec for apex to base detonation wave travel time for the same liner in a cylindrical charge. The start of liner wall collapse from apex to base was therefore virtually coincident. Results of this action are shown in Figure 52. Since wall collapse time at the inner apex was practically zero, jet elements from the apex got started first and appear in Figure 52 as the left trace. The liner wall at its central portion was accelerated to a higher jet segment velocity when it reached the liner axis, but since wall collapse velocity at this point of the liner was only 8% of the jet segment velocity from the apex, the higher velocity jet segment from the central portion didn't form at the axis and travel to appear as the center trace in Figure 52 until 1.3 μsec after the appearance of the apex jet segment. But since the central jet segment was travelling over twice as fast as the apex jet segment, the former overtook the latter at the "X" junction of Figure 52.

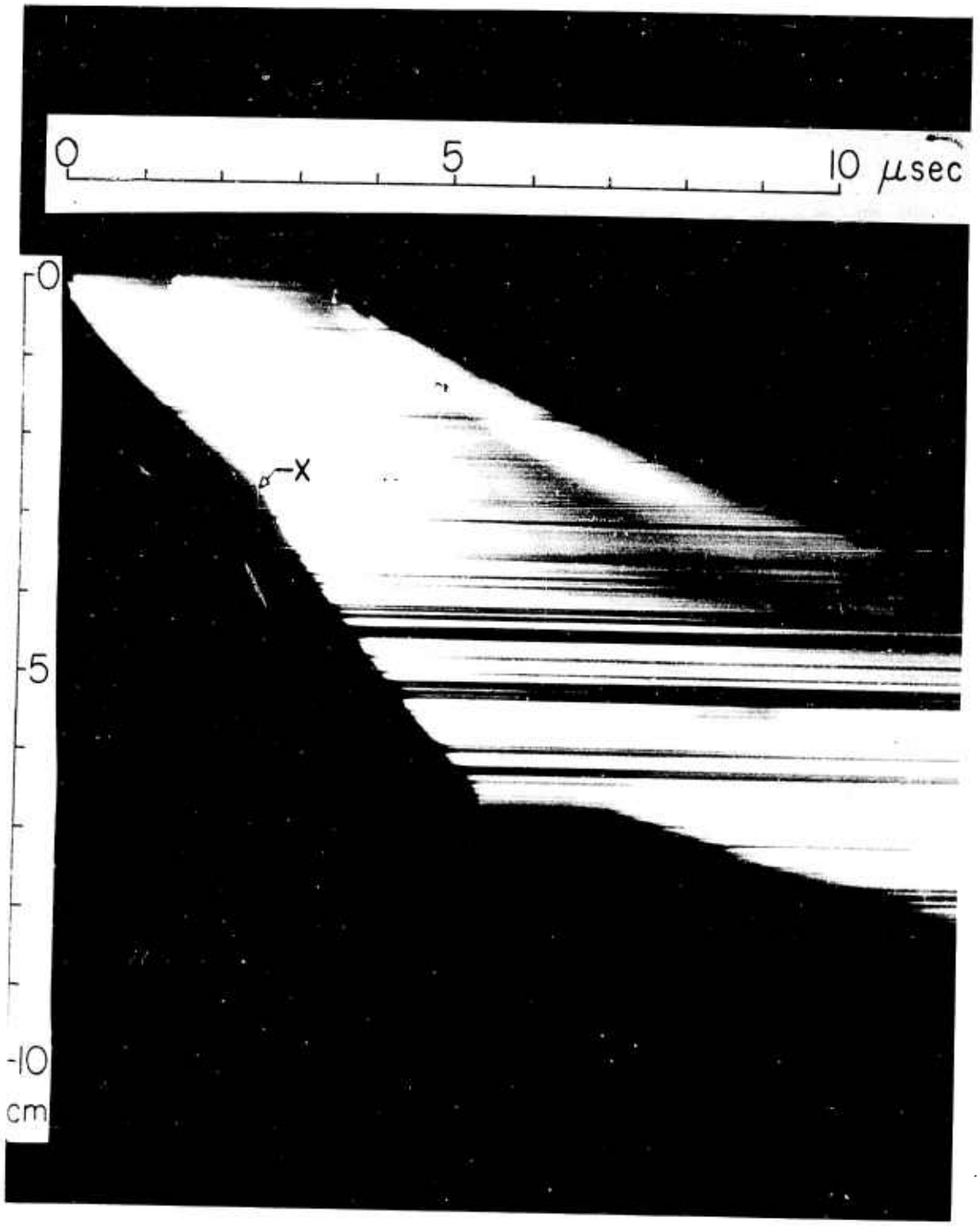

FIGURE 52. Photographic reproduction of streak camera from disc-shaped charge Test No. E-184.

A third trace is also visible in this streak record, appearing to the right of the other two traces. This jet segment was assumed to have originated from the base section of the liner, and due to its lower velocity and the greater wall collapse time it appeared 3.4 μsec after the appearance of the apex jet segment. If this trace is extrapolated up to 0 cm where the other two traces first appear it would have appeared at about 3 μsec. The fact that it appeared below the visible point of the charge holding block would indicate that this jet segment was not sufficiently well formed to produce a trace on the film until it reached the point where it is visible in Figure 52. This could be considered as evidence that this third jet segment originated at the base of the liner.

Various assumptions were made concerning the points of origin of the three jets, but the only set of conditions that would fit the geometry and velocities involved was that described above (see Figure 49). Table 7 lists only the maximum velocity for E-184, but the following tabulation lists maximum and minimum velocities as measured from each of the three traces of Figure 52. In addition, an extrapolated velocity at the assumed

TABLE 8. Measured and calculated velocities from Test E-184.

Velocity	Left Trace (1st)	Center Trace (2nd)	Right Trace (3rd)
Maximum	11.5 km/sec	24.6 km/sec	7.0 km/sec
Minimum	7.5	12.8	5.7
Extrapolated	18.8	35.0	7.5
Average	15.7	30.0	7.3

point of formation of each jet segment was made, based upon the velocity gradient visible in Figure 52 for each trace and the construction shown in Figure 49. And finally, an average jet segment velocity from assumed point of jet element formation to point of visibility, was calculated for each trace. Using these average velocities and the time relationships of jet appearances in Figure 52 resulted in calculated wall collapse velocities of 0.90 km/sec at the central portion of the liner and 1.93 km/sec at the base. The reason for the latter being higher may have been due to the thinner liner wall at the base than at the center thus resulting in greater acceleration for a given detonation pressure.

An approximation of jet length of E-184 may also be gained from Figure 52. From the appearance of the first trace to the appearance of the third trace was 3.5 μsec. And at a camera speed of 500 rps the image writing rate was 3.75 mm/μs. Therefore the distance between the leading elements of the first and third traces was:

$$L_i = 3.75 \text{ mm}/\mu\text{s} \ (3.5 \ \mu\text{s}) = 13 \text{ mm}$$

Now if it may be assumed that the trailing segment of the jet that formed the third trace was from the very bottom of the liner, then very little jet length existed beyond the appearance of the third trace (which would have been obscured from making a trace on the film because of the third trace), and the above jet length L_i would be a fairly close approximation of the true jet length. However L_i would be the length of the jet as formed. What happened to the jet length beyond the juncture "X" may be another matter. If the faster moving central jet segment of the record trace gradually swept up the slower-moving apex jet segment, resulting in a composite aggregate traveling faster than the apex segment and slower than the central segment, then the final jet length as it reached the first target plate would be approximately:

$$L_i = 3.75 \text{ mm}/\mu\text{s} \ (1.0 \ \mu\text{s}) = 3.75 \text{ mm}$$

where 1.0 μsec is the time between the juncture "X" and the appearance of the third trace. If the jet diameter from the C-42 liner may be scaled according to the method of Kronman and Merendino[2], a jet diameter of about 1.5 mm came from the C-42 liner, although this would undoubtedly increase somewhat if there was a sweeping-up action by the faster central jet segment. So perhaps a jet having approximate dimensions of 4mm length and 2mm diameter may be visualized. But even without sweeping action considerations the first calculated jet length above of 13mm is relatively short when compared with uninhibited jets from cylindrical charges which range from about 50 to 150 mm in length (see preceding graph figures).

A close inspection of the E-208 test picture of the first target plate (Figure 51) reveals two adjacent sub-craters, in the bottom of the main crater, each having a depth of 1.7mm and a diameter of 7mm. These smaller craters could very well have been formed from a trailing segment jet of Test 208 (corresponding to the base segment jet of Figure 52) after the main crater had been formed several microseconds previously by the higher velocity main jet. The volume of the large crater is about 30 times as great as the sum of the volumes of the two sub-craters which gives some idea of the ratio of energies involved. So if the third trace of Figure 52 may be disregarded because of its minor target damage effect, then the approximate jet length for E-208 would be:

$$L_i = 3.75 \text{ mm}/\mu\text{s} \ (1.3 \ \mu\text{s}) = 5 \text{ mm}$$

without assuming any jet shortening due to possible sweeping-up action.

If the foregoing assumptions are valid, then the higher-velocity segments of disc-charge jets have a relatively small length/diameter ratio and account for virtually all the target damage. Moreover, as may be seen in Figure 51, a disc-charge jet forms a crater having a large diameter/depth ratio, compared to cylindrical charge jets, which is a characteristic trend of cratering effects as particle velocity increases and jet length shortens. The crater of E-208 in Figure 51 resembles the diameter/depth ratios of the larger craters of the moon.

Another possible explanation of the multiple traces visible in Figure 52 is that one or more of the "extra" traces were due to plasma or luminous gases. Supporting evidence of this possibility is Test E-235 which produced streak traces without benefit of a liner and therefore could only be due to plasma. Moreover the measured velocity of the plasma in E-235 ranged between 8 and 11 km/sec (Table 7), the latter velocity being practically equal to the initial velocity of the left trace in Figure 52 (see Table 8). In fact when the overall trace pattern of E-235 (Figure 53) is compared with that of E-208 (Figure 52), a striking resemblance may be noted even though traces in the latter are considerably sharper than in Figure 53. It is quite evident that luminous gases made the trace pattern in Figure 53 since no liner was present.

However the question that must be answered, if the assumption is to be made that gases were responsible for any of the traces in Figure 52, is how the gases got past the barricade provided to prevent such an occurrence. The static image of Figure 50 shows the same type of wooden charge holder that was used with all disc-charge tests. These wooden discs were turned to fit the bottom contour of the disc-charges (Figure 12) and extended an inch beyond the outer rim of the charge. Since the bottom of the disc was flat, the wood thickness between the charge and the flat bottom varied from 3/8" at the center to over 1-1/2" at the charge periphery. A hole, with diameter equal to the base diameter of the liner, was provided at the center of the wooden disc to permit an unobstructed passageway for the jet leaving the bottom of the liner. Now in order for gas traces to show up in the film record of E-184, the gas would have had to escape from around the outside of the liner base and through the hole in the bottom of the wooden disc. And this gas would have originated from straight blast pressure on the outside of the charge and not from a "shaped" or directed gas jet from within a cavity as was the case in E-235. An example of how ineffective straight blast pressure is in even interfering with much slower jets is shown for Test #-190 in Figure 54 in which maximum jet velocity was 9.6 km/sec (see Figure 48). As may be seen in the static image in this figure, a slot was cut through the wooden charge-holding block to permit a view of the jet formation as it left the liner, instead of after it became visible below the block as in other tests (e.g., Test E-211 in Figure 5). This slot left an exposed area of explosive on the bottom of the charge free to expel straight blast pressure gases downward into the area of the streak traces. This certainly occurred, but obviously not in sufficient time or luminous intensity to obscure any of the jet traces or to even appear as an

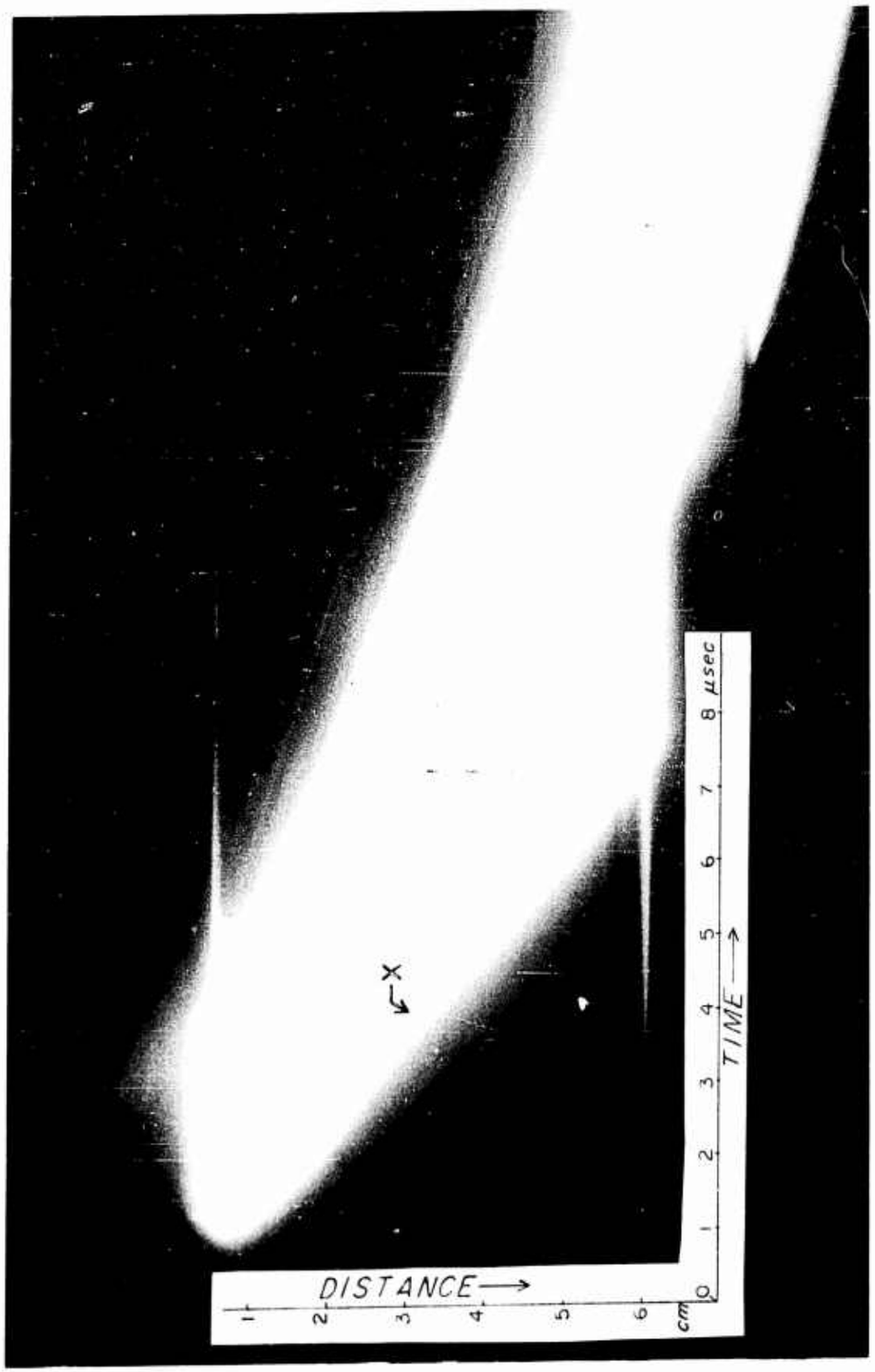

FIGURE 53. Photographic reproduction of streak camera record of disc-shaped charge Test No. E-235 shot without liner.

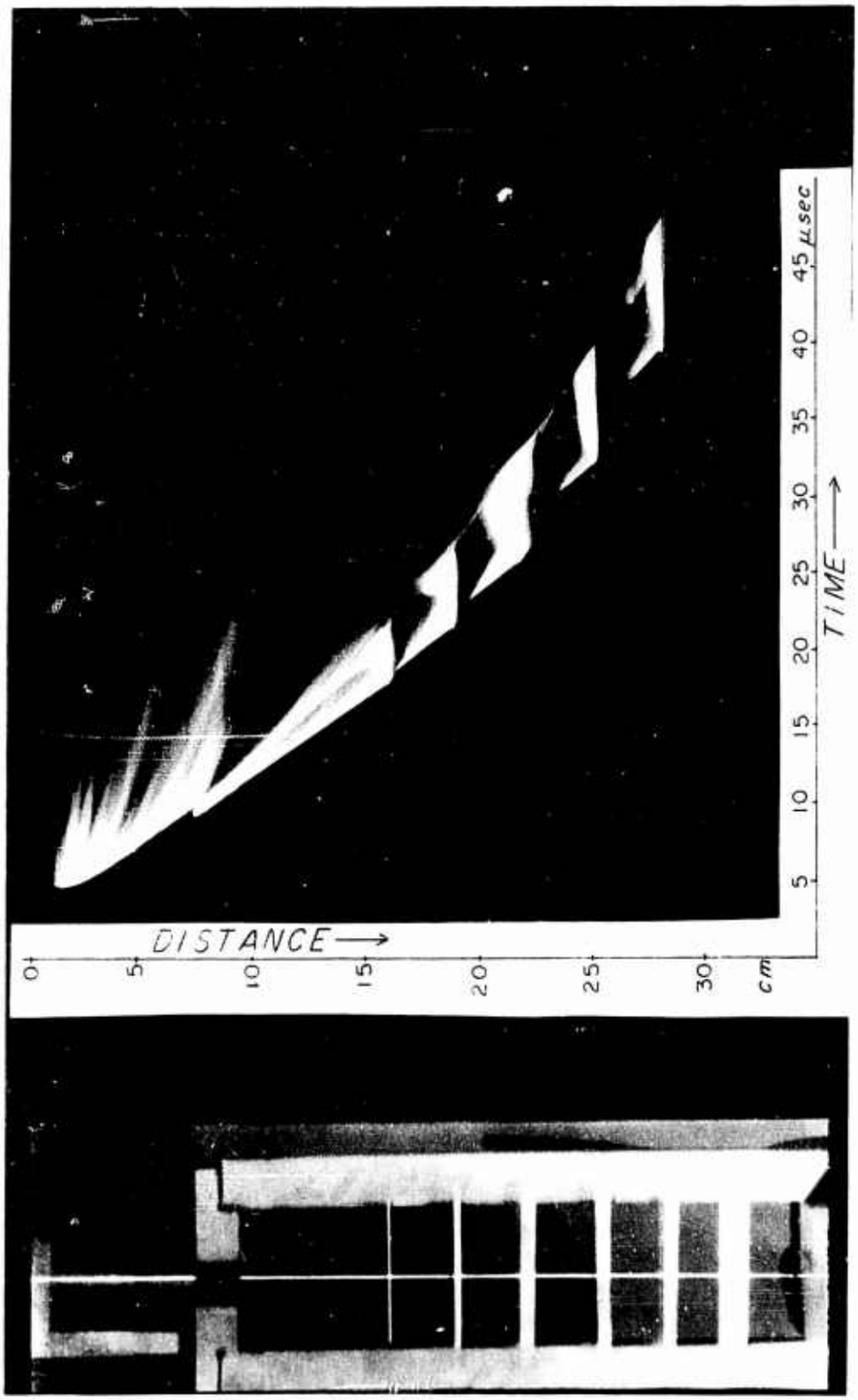

FIGURE 54. Photographic reproduction of streak camera velocity traces through multiple plates of Test E-190.

ambiguous jet trace. Close inspection of Figure 54 will reveal an extremely faint trace to the left of the upper 1/4" of the top jet trace. An accurate gauge of the incidence, quantity, intensity, location, and duration of light from straight blast pressure is shown in the uppermost trace which resulted from the detonating charge. This light faded completely out even before the jet had traversed the multiple plates in 30 μsec.

It may thus seem unrealistic to assume that any of the bright traces of Figure 52 resulted from luminous gases when the latter appear relatively faint in Figure 54 at a camera speed of 300 rps which provided 2/3 more exposure time than was available in Test E-184 as the camera speed was 500 rps in the latter. Gases from straight blast pressures have been known to approach 10 or 11 km/sec in vacuum, but that velocity would appear somewhat high in the air environment of Test E-184. The right trace of Figure 52, with a maximum velocity of 7.0 km/sec, conceivably could have been produced by luminous gases as far as realistic velocities are concerned; but in view of trace brilliance comparison with Figure 54, even this appears doubtful. If the right trace of Figure 52 was due to gases, then the overall jet length as previously calculated would be even shorter.

The trace pattern of Figure 53 may have been produced in somewhat the same manner as the suggested mechanism outlined for Test E-184*. Since gases have some of the same tendencies to form high velocity "jets" as liners do (e.g., the Munroe effect), the two-velocity pattern of Figure 53 may have resulted from gas "jets" from two different segments of the liner cavity. But in this case wall collapse velocity, as well as differential wall-to-axis collapse time from apex to base of cavity was not involved. Instead, the lower velocity trace forming the upper portion of the pattern in Figure 53 may have originated from the base portion of the cavity and arrived first due to shorter travel distance than that required of the higher-velocity "jet" originating at the mid-section or apex of the cavity. And the higher-velocity "jet" finally overtook the slower-velocity jet at the "X" juncture of the trace pattern in Figure 53.

In order to conclusively resolve what is occurring in disc-shaped charges, further tests using modified configurations and special devices to provide additional data will be necessary. Adequate time was not available to conduct further investigation under this contract.

The foregoing improvements in jet velocity, and apparent improvement in reducing velocity gradient and jet length, resulted from a first trial effort in departing from the progressive wall collapse action of cylindrical charges to employ virtual simultaneous initiation of wall collapse of disc-charges. And the results were sufficiently encouraging to consider modifying the configuration of the disc-charge shown in Figure 12 to one

---

* Page 84.

that would further improve jet performance by optimizing the time relationship of detonation wave arrival along the various segments of the liner wall. For example, it may be advantageous to have the detonation wave reach the liner base segment first and then progressively reach segments towards the apex with the latter being reached last (i.e., just opposite to the action in conventional cylindrical charges). This would result in a more favorable time relationship of wall-segment arrival at the axis, with optimum conditions existing when the segment leaving the apex would be successively joined by wall segments arriving at the axis throughout the length of the liner to produce a "spherical" jet of constant velocity.

One approach towards accomplishing this, while also maintaining optimum detonation-wave impulse angles throughout the length of the liner to produce maximum jet velocity, consists of using a two-component shaped charge comprised of two explosives having different detonation velocities. An outer shell of explosive would have the higher velocity, while the main body of the charge surrounding the liner would have the lower velocity. Since "Detasheet" would form a convenient outer shell, several disc-charges were cast of explosives having lower detonation velocities than "Detasheet". These charges consisted of baratol and TNT as listed in Table 7. However in each case the initiation sensitivities of the explosives were below the level required to create symmetrical initiation by the "Detasheet" of the peripheral initiator (see Figure 12). The charges detonated, but not sufficiently well to form a jet from the C-42 liners. It was therefore concluded that a better approach would consist of casting a two-component charge using octol as the higher-velocity outer shell and perhaps TNT as the main charge. Then the octol, which initiates satisfactorily from "Detasheet" would act as booster to initiate the TNT. Time limitation prevented this from being pursued further.

Tests Conducted at Eglin Air Force Base

Test Facilities Available

Figure 55 shows the general layout of equipment at the Terminal Effects Division of Eglin Air Force Base that was used during the four field trips conducted under this contract. The fore and back chambers could be evacuated to simulate high altitudes which minimized jet erosion by air, as occurred in such IRECO tests as E-134 (Figure 7). The three orthogonal x-ray stations had film cassettes centered at the distances indicated in Figure 55. These were exposed with x-rays from a Fexitron Model 730-4-C/231 system. The Kerr cell framing camera was a Model KFC-600/B (Electro-optic Instruments, Inc.). Timing impulses were supplied with three two-channel time delay units (Model 200, Abtronics, Inc.). A Cordin Co. Model 60-010A delay firing unit was used to fire the charges. In addition there were several type 551 and type 535 Techtronic oscilloscopes equipped with type C-12 cameras. Kinney vacuum pumps were used to evacuate the forechamber to a simulated altitude of up to 196,000 ft. while the back chamber could be evacuated to about 60,000 ft. Tests utilizing the fore chamber resulted in relatively long standoff distances of 13.5' to the

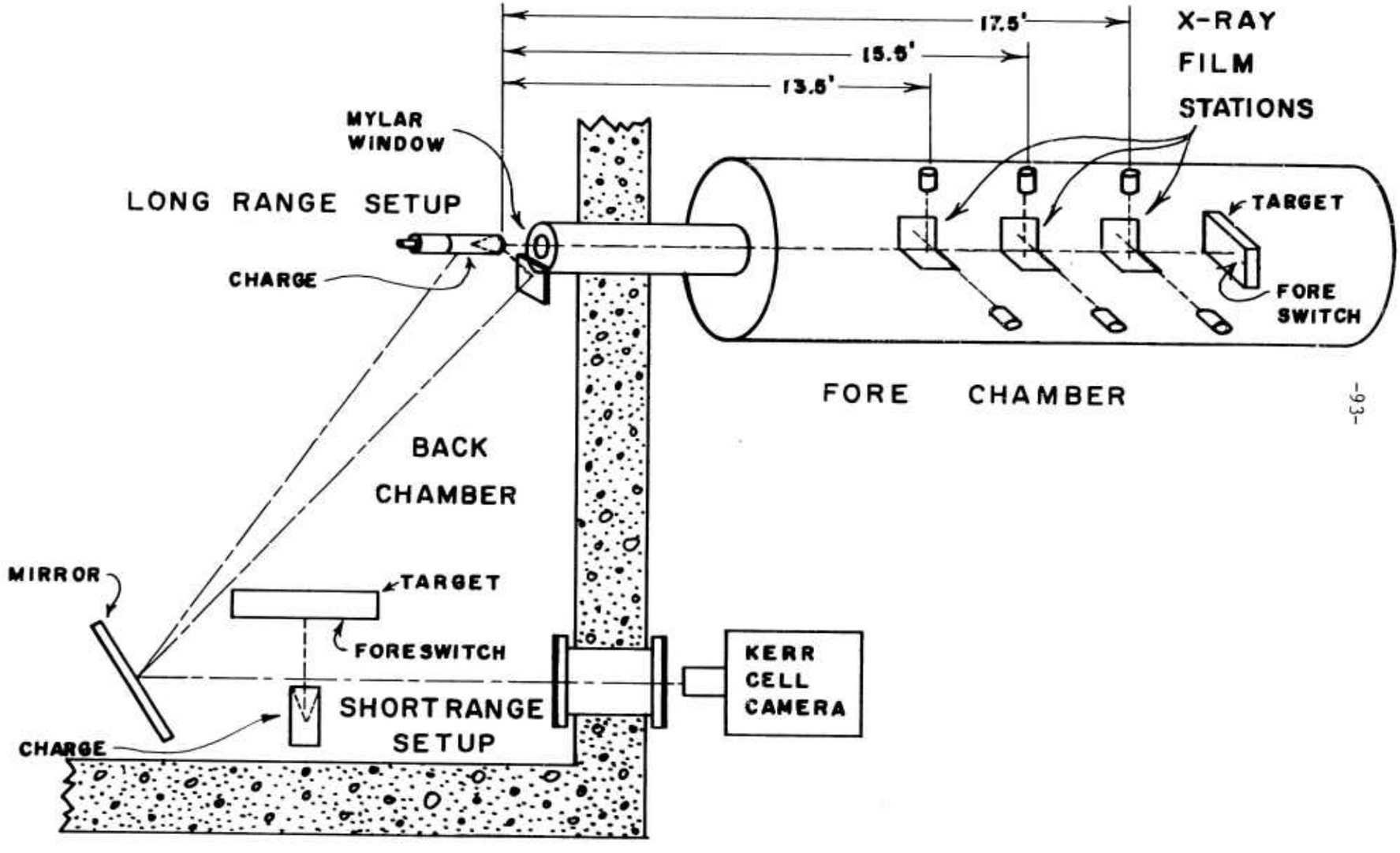

FIGURE 55. Test facilities at Hypervelocity Laboratory, Terminal Effects Division, Eglin Air Force Base, Florida.

nearest x-ray film and about 20 ft to the final target. Tests using the short range setup only (without x-ray coverage) had shorter standoff distances ranging from several inches to several feet. The Kerr cell camera was used on all short range tests and, with the aid of a mirror or two, on some of the long range tests.

January 1964 Test Series at Eglin Air Force Base

Ten each shaped charges with C-1 conic liners (Figure 25) and "S" distances of 3.40 cm, and C-11 paraboloid liners (Figure 28 and Table 4) and "S" distances of 2.90 cm, were prepared and shipped to Eglin Air Force Base. Eight of the C-1 charges were equipped with Type I inhibitors, and eight of the C-11 charges were equipped with Type IV inhibitors. Several inhibitor and non-inhibitor type charges in both charge categories were fired over the long standoff vacuum range of Figure 55. Target distances ranged from 17.7 to 19 feet. Leading jet-element velocities ranged up to 16.5 km/sec for C-1 charges and to 13.1 km/sec for the C-11 charges. These values confirm the velocities obtained with the multiple plate method for these two types of liners (see Figures 25 and 29).

Negative results were experienced in attempting to obtain radiographic pictures of jet particles in flight for any of these tests. And the reason for this was evident from target plate damage. No holes resulted in the targets at the 17.7+' standoff distances that remotely resembled the clean large holes of the multiple plate tests (see, e.g., Test E-130 of Figure 33). Maximum target damage consisted of scattered small holes and craters.

These results were attributed to the existance of lateral dispersion of the jet elements, which wasn't too evident in the close standoff distances used in the multiple plate tests, but which increases to serious proportions as the standoff distance is increased to values required by the geometry of the fore-chamber in Figure 55. Due to these results, further testing of the remaining charges would have contributed no added information, so the tests were discontinued.

August 1964 Test Series at Eglin Air Force Base

Development of the vacuum range at the IRECO test site (Figure 35) permitted an appraisal of jet cohesion of the various liners tested in a facility which simulated the standoff distances of the Eglin Air Force Base fore chamber (Figure 55). And the liner which exhibited the best cohension was the C-38 tapered-wall conic liner (Figure 36). A comparison of the C-38 liner's performance with that of the C-1 liner (used in the January 1964 test series) is shown in Figure 41. The C-38 liners jet had less scatter and made a more symmetrical hole than did the C-1 liner, although there was still lateral dispersion present. The diameter of a circular hole, having the area of the one in Test E-143 of Figure 41, is 4.8 cm,

which is twice as great as the diameter of the largest hole in the short standoff (3-1/2") multiple plate test E-158 (see Appendix II in the last section).

Ten charges having the following specifications were prepared and shipped to Eglin Air Force Base:

> Liner: Aluminum, Type C-38 conic as per Figure 38-a;
> Explosive: Octol (HMX/TNT = 75/25); Length = 3.75";
> Diameter = 2.43"; "S" distance = 5.0 cm;
> Waveshaper: as per Figure 10-b; Jet Inhibitor: 5 charges without, 5 charges with type shown in Figure 13-b.

Six of these charges (5 without inhibitor and 1 with) were fired over the long range setup of Figure 55, while a seventh was fired over the short range setup. The Kerr cell camera was used on all the tests, and all except the seventh test had x-ray coverage. Timing of the x-ray system was adjusted to cover as large a range of velocities as practical. In some of the tests three timing intervals were set up, one for each orthogonal pair of x-ray channels which provided coverage of three jet velocity ranges. For the other tests all six x-ray channels were programed to fire at different times, and this resulted in the coverage of six velocity ranges (but eliminated orthogonal coverage). The latter provided continuous coverage of velocities from 6.3 to 11.6 km/sec which would include virtually all the jet segment velocities of the C-38 liners as measured at the IRECO test site (Figure 43). An example of how the calculations were made to arrive at the proper time delay settings for the six x-ray channels is shown in Appendix I.

Table 9 lists target specifications, target damage, and velocity range covered by the x-ray station for the charges fired. No particles of significant size were discernable on any of the x-ray plates. Static calibration checks of the x-ray system indicated that particles having diameters of 1/16" or greater could be resolved. It must therefore be concluded that the target holes were made by particles having diameters <1/16", but if this were the case it must also be concluded that a fairly large swarm of small particles were present in some of the tests to cause the target hole sizes indicated in Table 9 (e.g. Tests E-164 and E-165). Therefore, even though the C-38 liner produced target damage far superior to the C-1 liner used in the January 1964 tests*, apparently lateral dispersion of the C-38 liner jets was still of sufficient magnitude to prevent obtaining in-flight radiographic pictures of the jets.

Kerr cell camera coverage of these tests is shown in Figure 56 and varied from views of the detonating charge to views of the liner collapse. Difficulties were experienced in obtaining proper exposure and timing and the resulting photographs added no significant data. Exposed areas of the film were attributed to plasma and no evidence of pictures of jets could be identified.

---

* Page 94.

TABLE 9. Target and velocity information for August 1964 tests at Eglin Air Force Base.

Charge No.	Thickness (inches)	Distance (Feet)	Large Holes		Medium Holes		Approx. Hole Area		Velocity Range Covered (km/sec)
			Dia. (in.)	Approx. No.	Dia. (in.)	Approx. No.	Large & Medium Holes (dia.)	Pin Holes (dia.)	
E-163	0.1	18.1	0.4	14	0.2	14	4"	12"	36-39
E-164	0.1	18.1	3	1	0.2	20	4	14	30-43
E-165	0.1	18.1	3	1	0.2	30	4	14	21-38
E-166	0.1	18.1	--	--	--	--	--	--	21-38
E-167	2.0	18.1	0.4 Deep				2	12	21-38
E-168	2.0	18.1	0.3 Deep ($7/in^2$)					12	21-38
E-169	--			(Kerr cell framing camera only)					

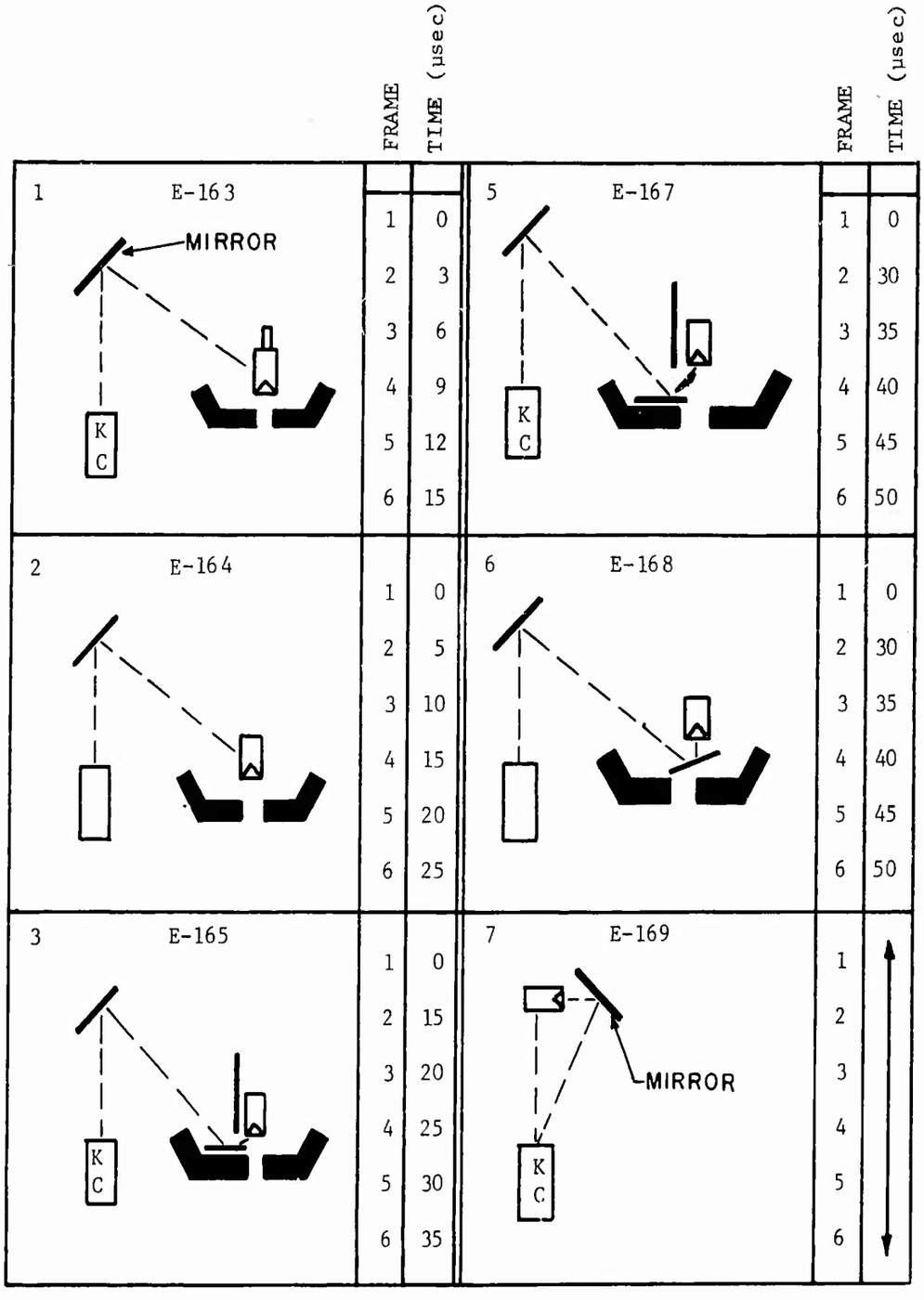

FIGURE 56. Plan views of Kerr cell framing camera arrangements for August 1964 tests at Eglin Air Force Base.

A study of the six pictures from each of the tests indicated an unexplained 15 to 25 μsec delay from the firing pulse zero time until the charge started to initiate.

September-October 1964 Test Series at Eglin Air Force Base

After testing several types of new liner designs at the IRECO test site in efforts to reduce jet velocity gradients and lateral dispersion in jets, a decision was made to test at Eglin Air Force Base a type liner that produced jets that had been successfully photographed with x-rays. The liner chosen was a scaled modification of the type used by Kronman and Merendino[2] in their jet inhibitor work which produced excellent radiographs at a standoff of 42". This liner was designated as type C-39 and is shown in Figure 40. Results of Test E-192 multiple target plate damage at close range in air (3-1/2" to first plate) is shown in Figure 57, which also shows extended standoff (149" in vacuum) target damage of Test E-193. Both of these charges were shot without a waveshaper, resulting in lower velocities, but Test E-192 showed that this liner, without waveshaper, to have nearly 3 cm of initial jet length with low velocity gradient (Figure 46). The jet of E-193 struck its target plate off center and caved it in; the view in Figure 57 was taken after the plate was straightened which gives the illusion of a larger hole than the approximate hole diameter of 50mm measured prior to straightening. And since the largest hole diameter for the short range test of E-192 was about 42mm, this C-39 liner exhibited less lateral jet dispersion than any other liner tested. Therefore six 3.40" diameter charges of various lengths containing C-39 liners (see Table 10), and five waveshapers of the type shown in Figure 10-c, but also of various lengths, were prepared and shipped to Eglin Air Force Base for the third series of tests there.

The first two tests, E-201 and E-203 were shot over the short air range, shown in Figure 55, at atmospheric pressure to provide reference tests for comparison with long range vacuum tests. A foreswitch on the face of the target plate (similar to the foil-film type shown in Figure 2) of each test was designed to provide time intervals from the zero time cap firing pulse to the time of arrival of the first jet element at the target plate. From the elapsed time recorded with the foreswitch had to be subtracted the time delay from zero time until the jet left the apex of the liner in order to obtain jet velocity over the known standoff distance. This time delay was determined by assuming E-201 had the same initial velocity as Test E-193 in which an identical charge setup was used. The resulting 19.2 μsec was then subtracted from ensuing foreswitch time intervals in determining jet velocities, as well as for setting up the Kerr cell camera and x-ray timing sequences for the ensuing tests.

Table 10 data shows impressive target damage for tests E-201 and E-202 which indicated good jet cohesion at the relatively short standoff distance used. The larger target hole of E-202 was probably due to a

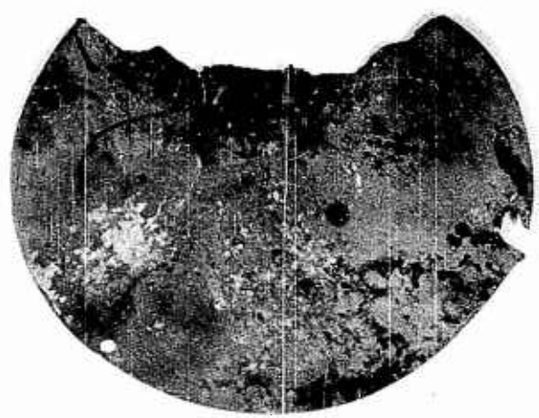

FIGURE 57. Photograph of close and extended standoff target damage from C-39 liners.

TABLE 10. Shaped charge tests results for September-October 1964 Eglin Air Force Base tests.

Test≠ No.	Charge Length (in.)	"S" Dis. (in)	TARGET DATA				Wave-shaper Length (in.)	CHAMBER ALTITUDE (ft.)		Max. Jet Velocity (km/sec)
			Standoff (in.)	Thickness (in.)	HOLE DIMENSIONS Size & Shape	Depth		Fore	Back	
E-201	5.00	0.60	8.5	4	∿1-1/4" dia. +7" dia. Back Spall	4"	0	0	56,000	10*
E-202	5.00	0.60	8.5	4	∿1-1/2" dia. + 5" dia Back Spall	4"	2.16	0	50,500	**
E-203	4.88	0.48	216	0.5	Scattered Craters	1/4	0	176,600	50,500	10.34
E-204	4.40	0	216	0.5	1-3/4 x 2 (irregular)	1/2	2.11	196,500	56,500	17.0
E-205	5.00	0.6	216	0.5	∿1/2" dia. & Random Craters	1/2	0	174,500	49.000	**
E-206	4.50	0.1	216	0.5	2 x 5 (irregular)	1/2	3.36	193,000	55,750	**

* Assumed to be the same as E-193, Table 6. ≠All Charges contained C-39 liners.

** Foreswitch failure prevented obtaining velocity data.

higher jet velocity that would be expected from using a waveshaper with E-202 and not with E-201 (foreswitch failure prevented obtaining velocity data for E-202).

The remaining four tests were made over the extended standoff vacuum range shown in Figure 55, using the three pairs of orthogonal x-ray stations in each of the tests. E-203, without waveshaper, had a velocity very close to that resulting from the similar charge setup of E-201. The target damage, however, from the relatively slow jet at the 216" standoff distance was very minor.

Test E-204 had a much higher velocity than E-203 which was to be expected from using a waveshaper and zero "S" distance with E-204. Resulting target damage was also much more impressive for E-204 because of higher velocity and perhaps from better jet cohesion.

Test E-205 used an identical charge setup as E-201 and would therefore be expected to have about the same lower velocity as E-201 (foreswitch failure prevented obtaining velocity data). Target damage was somewhat better than E-203, but much less than for E-204.

Test E-206 used a slightly longer "S" distance and a longer waveshaper than was used in E-204 and produced the greatest target damage of any of the extended standoff tests. Again no velocity data was available, but was assumed to be equal to or a little higher than for E-204.

A comparison of the velocity and target damage data of Table 10 shows very consistent results as the "S" distance and waveshaper parameters were varied. However none of the x-ray plates from the last four tests showed any identifiable jet element images. So apparently even the C-39 liner, which produced cohesive jets out to at least 42", had sufficient lateral dispersion to reduce jet element particle sizes to less than the 1/16" diameter size which the x-ray system was capable of resolving. This conclusion, of course, was based upon the assumption that the x-ray timing and exposure were at optimum settings.

Also, due to improper exposure or inaccurate timing, or both, the Kerr cell camera gave negative results as far as coverage of detonating charges or jet elements in flight were concerned. However good static images of charge setups were obtained when exposure time was carefully controlled. And the same precautions would probably result in useful dynamic shot pictures.

November-December 1964 Test Series at Eglin Air Force Base

Results of the three previous test series at Eglin Air Force Base indicated that it would be better to forego further attempts to x-ray shaped-charge jets in flight, at the standoff distances involved (Figure 55), in favor of attempting to obtain Kerr cell camera pictures of the jets. The

latter would permit inspection of the jet at much closer standoff distances than possible with the x-ray system (compare short and long range setups in Figure 55). Experience to this point indicated that it would be simpler to barricade targets under study from blast pressure effects of shaped-charge explosives than to reduce lateral dispersion within the jets to acceptable levels at the standoff distances involved in Figure 55. Therefore several of the liners which have shown good performance in the short range multiple plate tests were chosen to make up the charges listed in Table 11. A sufficient number of each type charge was included to allow for preliminary calibration shots to provide for equipment adjustments.

When jets are shot in air a brilliant light results (see, e.g., Figures 7 and 50) that can be interpreted to give jet velocity magnitude, but which yields no quantitative data on jet shape or size. To obtain the latter with the Kerr cell camera it was necessary to shoot the shaped charges in a chamber having sufficiently low air pressure to prevent generation of light by the jet. Then a backlighting explosive light bomb was required to enable the Kerr cell camera to take a silhouette picture of the jet in flight as shown in Figure 58. However when the chamber is evacuated to a

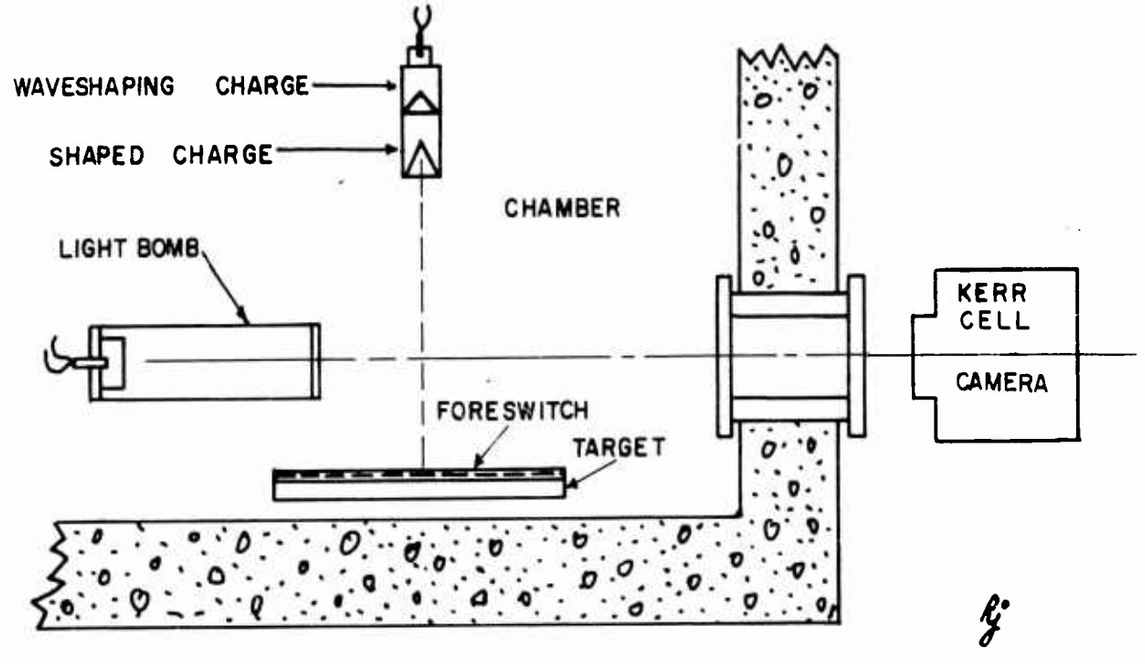

FIGURE 58. Plan view of experimental arrangement for November-December 1964 tests at Eglin Air Force Base.

TABLE 11. Shaped charges which were prepared for November-December 1964 tests at Eglin Air Force Base.

Charge No.##	Liner Type	Liner Ref.	Charge Shape	Liner Length	S Distance	Charge** Confinement
E-212	C-37-a	Fig.36*	Cylinder	2.660	1.50cm	None
E-213	C-37-a	Fig.36*	Cylinder	2.660	1.50	"
E-214	C-42-a	Fig.49*	Disc	1.501	--	"
E-215	C-42-a	Fig.49*	Disc	1.449	--	"
E-216	C-1	Fig.25	Cylinder	2.400	2.41cm	"
E-217	C-1	Fig.25	Cylinder	2.400	2.41	"
E-218	C-1-a	Fig.25*	Cylinder	1.572	1.50	"
E-219	C-1	Fig.25	Cylinder	2.400	1.50	"
E-220	C-1-a≠	Fig.25	Cylinder	1.777	1.50	"
E-221	C-1-a≠	Fig.25	Cylinder	1.658	1.50	"
E-222	C-38-e	Fig.46	Cylinder	1.635	1.50	"
E-223	C-38-e	Fig.46	Cylinder	1.603	1.50	"
E-224	C-38-a	Fig.38*	Cylinder	1.702	1.50	"
E-225	C-43	Fig.47	Cylinde:	2.004	1.50	3/8" Steel
E-226	C-43	Fig.47	Cylinder	2.003	1.5	None
E-227	C-43	Fig.47	Cylinder	2.010	1.5	"
E-228	C-43	Fig.47	Cylinder	2.003	1.5	"
E-229	C-43	Fig.47	Cylinder	2.003	1.5	"
E-230	C-43	Fig.47	Cylinder	2.004	1.5	3/8" Steel
E-231	C-43-a	Fig.47	Cylinder	2.0	1.5	None
E-232	C-43-a	Fig.47	Cylinder	2.0	1.5	"
E-233	C-43-a	Fig.47	Cylinder	2.0	1.5	"
E-234	C-43-a	Fig.47	Cylinder	2.0	1.5	3/8" Steel

* Basic liner shape in figure shown, but truncated to length shown under "Liner Length" column above.

≠ Copper liners, all other aluminum

** See Figure 47 for confinement details

All charges cast of octol (HMX/TNT = 75/25); in addition two "Detasheet" peripheral initiators (Figure 12) were sent with E-214 and E-215. Also octol waveshapers as per Figure 10-b were shipped.

pressure that eliminates jet light streaks it also prevents adequate light from the light bomb for silhouette pictures. Therefore 22 light bombs of the type shown in Figure 59 were made and shipped for these tests. They were assembled at Eglin Air Force Base by cementing the charge and cap in place, then the front and back plates were cemented in place so that atmospheric pressure would be maintained within the light bomb assembly when the latter was placed in the evacuated back chamber of Figure 58. This, then, would provide air to produce adequate backlighting within the chamber which was evacuated sufficiently to prevent the jet from producing light. The light bombs were made sufficiently long to provide about 30 microseconds of event time before plasma from the charge reached the front plate and rendered it opaque.

Table 12 lists the 30 test shots made during this series, but most of these tests consisted of efforts to adjust the Kerr cell timing and backlighting intensity to properly silhouette shaped-charge jets in flight. This was accomplished by using the arrangement shown in Figure 58, except a static array of ball bearings cemented on Mylar film was substituted for a jet from a shaped charge in order to establish proper backlighting intensities. For example, Test 2 was set up as shown in Figure 60 with four ball bearings of the sizes shown. For both Test Nos. 1 and 2, a fair amount of light appeared on the first frame with the two largest ball bearings just discernable in Test No. 2. In both tests it appeared that the light intensity was on its way down already on the first frame, even though the frame delays were adjusted to cover an earlier event in Test 2 (Table 12). Test 3 failed to show any light from a cap in a 0-10 μsec interval, from which it would appear that the light intensity was too low or the timing was off. Frontlighting of ball bearings on black paper was tried in Test 4, but only the block of wood, which shielded the direct light from the camera, could be faintly seen as a silhouette on the first frame.

Test No. 5 was a full scale test using a shaped charge with a plastic tube lightbomb as shown in Figure 58. A 3/32" ball was placed on the face of the lightbomb (see Test 5 static image, Figure 61 which also shows charge at right) to provide a reference for any jet particles that might have been photographed. However only the first frame was exposed as shown in Figure 61. The light pattern appears to be the late stages of the jet path and target strike flare.

Results of Test 5 appeared as if the event was practically over by the time the first frame was exposed. Test 6 was an attempt to check on relative timing of charge detonation and camera framing sequence. An 8-foot length of primacord was arranged in a spiral to provide a continuous source of light for about 380 μsec, but none of the 6 frames were exposed.

At this point it was assumed that insufficient light intensity was responsible for the negative results, so a number of aerial M112 A1 photoflash cartridges were obtained for light intensity tests. Various arrangements of front and back lighting were used in Tests 7 through 12,

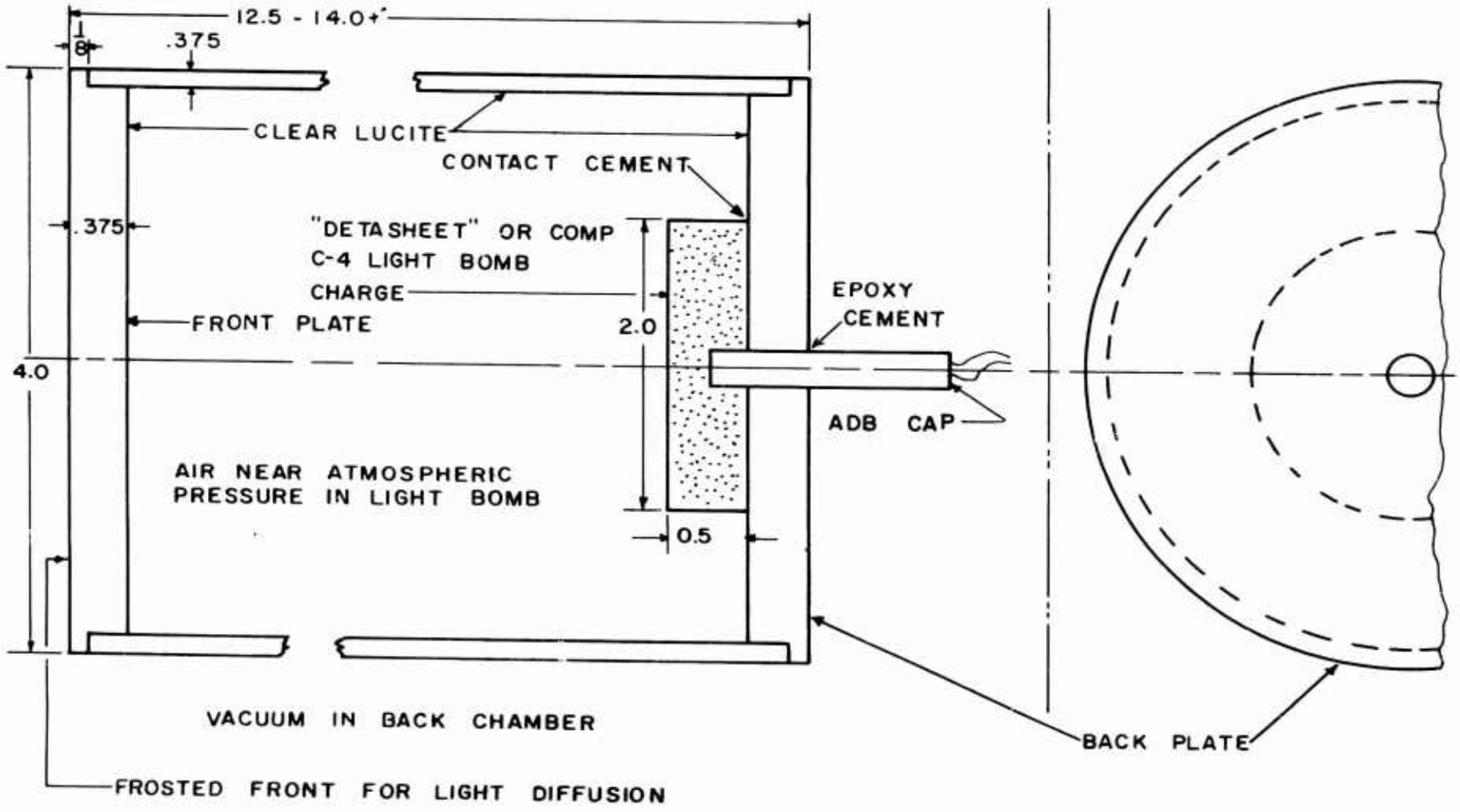

FIGURE 59. Plastic light bomb used for backlighting December 1964 test shots at Eglin Air Force Base.

TABLE 12. Experimental conditions and results of November-December 1964 tests at Eglin Air Force Base.

Test No.	Backlight Source Size (in.)	Explosive	Camera Object (in. dia. of Steel Balls)	Kerr Cell[2] Frame Delay (μsec)	Chamber Altitude (feet)	Results	Delay (μsec)
1	1/8x2-1/2x10	Detasheet	*1/16,3/32,1/8,3/16	10,15,20,25,30,35	59,600	Light on 1st Frame only	0
2	1/2x2-1/2dia.	"	* " "	0,3,6,9,12,15	0	Ditto	0
3	ADB Cap	--	Cap Light	0,2,4,5,8,10	0	No light visible	0
4	1/2x2-1/2dia.	Detasheet	1/16,3/32,1/8,3/16	0,2,4,5,8,10	0	1st frame faint silhouette	0
5	1/2x2x2	Comp.C-4	*E-212 Jet	0,5,10,20,30,40	59,600	1st frame blob of light	0
6	Spiral	Primacord	Primacord light	0,2.5,5,10,25,50	0	No light visible	0
7	M112 A1[1]		*Cartridge light	0,50,100,150,200,250	0	6 frames overexposed	0
8	"		3/16"	0,5,10,25,35,50	0	Sporadic	0
9	"		3/16"	0,5,10,25,35,50	0	Too much light	0
10	"		3/16	0,5,10,25,35,50	57,600	Ditto	0
11	"		3/16	0,5,10,25,35,50	57,600	Ditto	0
12	"		3/16	0,5,10,25,35,50	55,400	Sporadic	0
13	1/2x3x3	Comp.C-4	3/16 & 1/4	0,2.5,5,10,20,30	0	1st frame: far light	0
14	1/2x2x2	"	*1/4	0,5,10,20,30	0	Good lighting	10
15	(1/2x2x2)≠	"	*E-225 Jet + 1/4	0,10,20,30,40,50	54,500	1st frame: blob of light	10
16	1.5x3.75dia	"	#1/4	0,10,20,30,40,50	55,00	Mostly overexposed	10
17	(1/2x2x2)≠	"	*Lightbomb face	0,10,20,30,40,50	0	Charge failure	10
18	1/2x2x2	"	*1/4	0,10,20,30,40,50	54,500	Fairly good lighting	10
19	2/3x2x5.4	"	*E-226 jet	0,20,40,60,80,100	55,500	Overexposure	10
20	No backlight source used		E-118 Jet	0,50,100,150,175,200	54,000	Overexposure	50
21	1/2x2x2	Comp.C-4	Charge light	0,50,100,150,200,250	0	Light on 1st frame	300
22	1/2x2x2	"	Charge light	0,50,100,150,200,250	0	Ditto	1000
23	1/2x2x2	"	Charge light	0,0,50,100,150,200	0	Ditto	75
24	1/2x2x2	"	Charge light	0,25,50,75,100,125	0	Inadvertently exposed	10
25	1/2x2x2	"	Charge light	0,25,50,75,100,125	0	Improved exposure	10
26	1/2x2x2[3]	"	Charge light	0,25,50,75,100,125	0	About same as #26	10
27	1x2x2	"	Charge light	0,25,50,75,100,125	0	Erratic lighting	0
28	1x2x2	"	Charge light	5,10,15,20,25,30	0	Early light transmission	75
29	1x2x2	"	Charge light	20,20,20,20,20,20	0	Apparent light leakage	
30	1x2x2	"	Charge light	30,25,20,15,10,5	0	light leakage only	

1 Air Force photo flash cartridge

2 Underlined delays indicate no pulsing voltage applied

3 With 1/2 x 1/2 tetryl booster

4 Microseconds delay of cap initiation time relative to zero time of camera framing sequence.

* Indicates backlighted, others front lighted.

≠ Charge inside of lightbomb tube (Figure 59).

but in all cases the light intensity was too high except Test 8 in which it ranged from too high to too low. Results of these tests indicated that the cartirdges can be set off (with primacord wrapped around the outside) fast enough for precision timing, and that excess light is available. In order to be practical for this use, however, some means of controlling the light intensity must be devised, such as controlling the quantity of material used.

A larger composition C-4 charge was used in Test 13 than was used in Test 1 through 7. A faint light appeared on Frame 1 which silhouetted the larger ball bearing; but the remaining frames were unexposed which made it appear as if the event was practically over before even the first frame was exposed, presumably at 0 μsec, even though it should require about 7 μsec for the charge to start detonating (because of cap and booster delay). To check the accuracy of the relative timing sequence between cap initiation pulse and zero time of the camera sequence a delay was introduced in Test 14 to cause the cap to be fired 10 μsec after the zero time of the first frame setting on the camera. Test 14 gave better lighting results than any previous tests. All of the frames

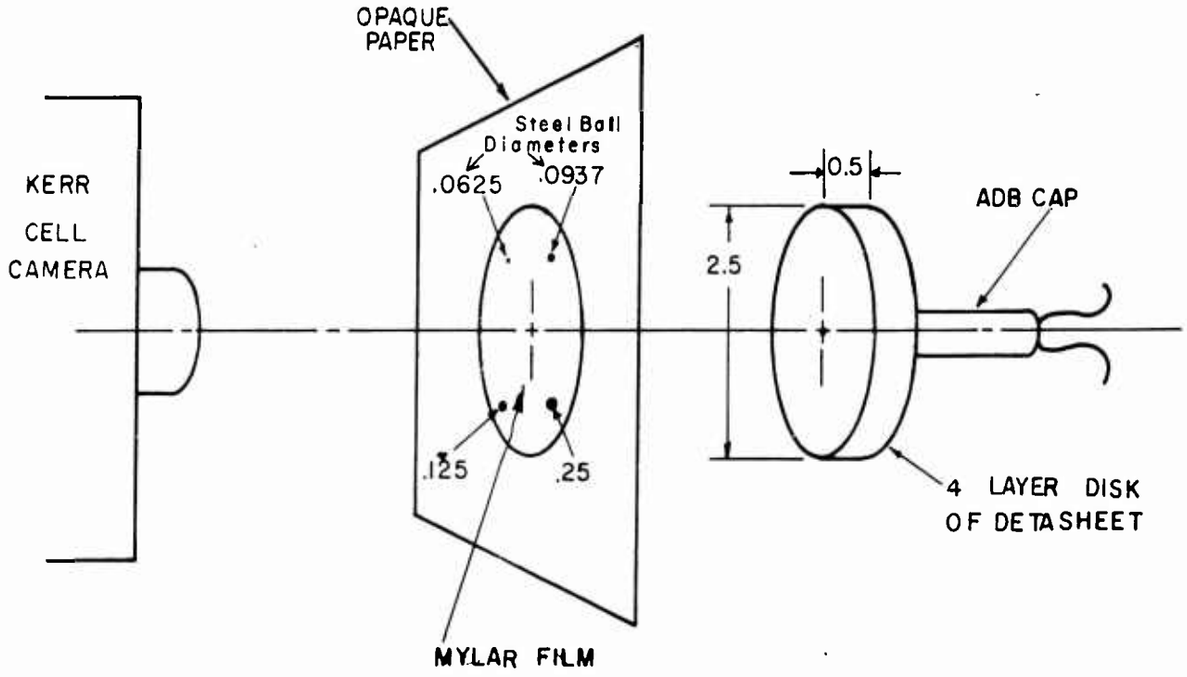

FIGURE 60. Physical arrangement of components used in Test 2 of Table 12.

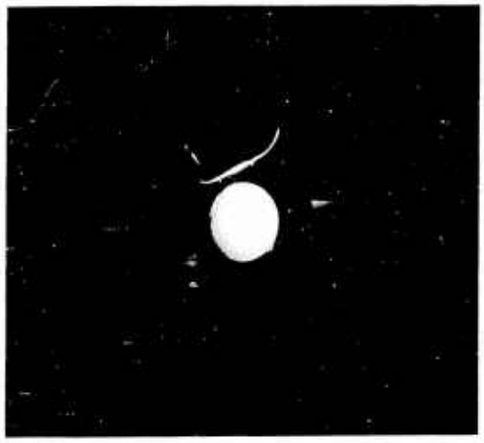

TEST 5: STATIC IMAGE

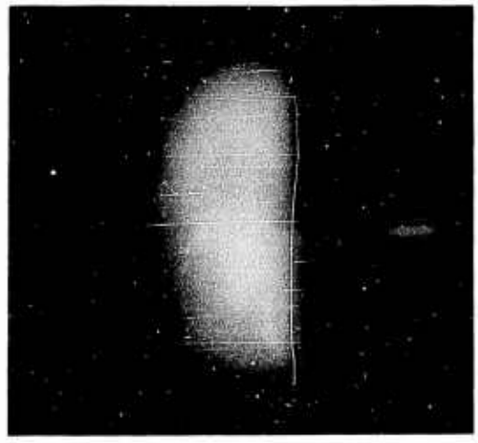

TEST 5: FRAME 1

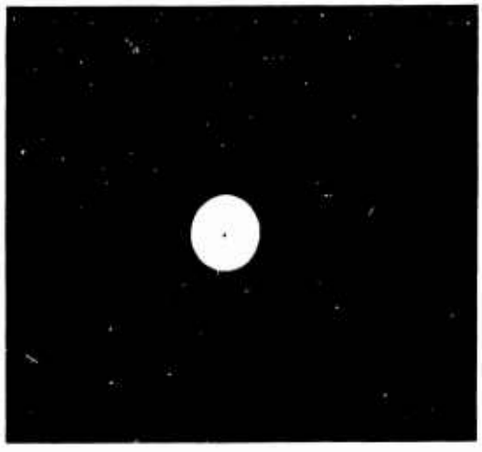

TEST 14: FRAME 5

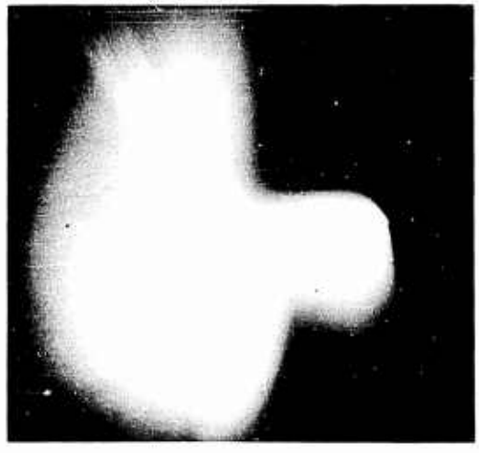

TEST 15: FRAME 1

TEST 18: FRAME 1

TEST 25: FRAME 5.

FIGURE 61. Sample Kerr cell camera photographs taken during November-December 1964 Eglin Air Force Base tests.

had about the same contrast as Frame 5 of Figure 61 which shows an excellent silhouette of a 1/4" ball. From these results it was concluded that an internal delay in the timing networks was delaying the start of the camera's framing sequence by an unknown interval. The latter was still in doubt because the introduction of 10 μsec delay on the cap extended the light duration from near zero (Test 13) to over 30 μsec (Test 14).

A full scale setup was used in Test 15 which utilized the same lightbomb charge as Test 14 except it was in a plastic tube (Figure 59) to permit evacuation of the test chamber. In Figure 61 may be seen Frame 1 of Test 15 which is overexposed and indicated that light, from either the in-flight jet or the jets' impact with the target, was so brilliant that it obscured the backlighting. The remaining frames had undecipherable ghost images of low intensities. A 9cm^2 hole through the 1" thick aluminum target plate indicated that a good jet was formed.

Test 16 was made to determine whether or not the frosted front plate of the lightbomb was obscuring the backlighting since there was no evidence of the latter in any of the frames of Test 15. Use of a larger light-bomb charge in Test 16 overexposed Frame 1 so that it appeared to have a shape and light intensity somewhere between the first frames of Test 5 and 15 in Figure 61. The remaining frames were also overexposed but the Mylar circle (Figure 60) could be seen in most of them, and even the steel ball in Frame 2.

The size of the lightbomb charge was reduced in Test 17 and the plastic tube face was left clear to check light intensity; however the charge failed to detonate.

Since some of the previous tests indicated a fair amount of light from lightbomb charges in the partial vacuum of the back chamber (e.g., Test 1), Test 18 was conducted in the same environment. Results were almost equivalent to Test 14 with steel ball silhouettes comparable to Frame 5 of Figure 61, but with slightly less backlight intensity. In view of this performance, Test 19 was made with the same thickness and width of backlighting charge as for Test 18 but the length was increased to cover more event time and distance. Results were similar to the previous full scale setup and several of the frames compared closely with Frame 1 of Test 15, Figure 61.

Test 20 was conducted without a lightbomb to differentiate between light originating from backlighting and from charge, jet, and target self-illumination. And since the event in previous tests had appeared well advanced by the time of first frame exposure, the delay of cap initiation time was increased from 10 to 50 μs in Test 20. Results were similar to Test 15, with Frame 1 similar to Frame 1 of Figure 15 (Figure 61) and the rest of the frames grossly overexposed. Therefore backlighting had not been responsible for overexposure in tests using shaped charges. Also, increasing time delay of cap firing didn't prevent well developed

charge light appearing on first frame. The delay was increased to 300 μsec in Test 21 and to 1,000 μsec in Test 22, yet results were the same with identical charge light appearing on the first frame even though the cap was supposed to be firing up to a 1,000 μsec after the start of the 250 μsec camera coverage sequence. So it was assumed that either the delay networks were not functioning properly or light was coming through the Kerr cells when they weren't being pulsed. Test 23 was conducted to differentiate between these two possibilities by not pulsing the first two camera framing channels. The first frame picture was identical to the first frames of Tests 21 and 22, and light could be visually observed coming through the Frame 2 camera. It was therefore concluded that most of the foregoing timing ambiguities had arisen from light leakage through the Kerr cells. These were therefore adjusted to minimum light transmission with the polarizers in the cross-polarized position.

Results of Test 24 were indeterminate since some of the frames had been exposed during adjustment of polarizers. Test 25 was the first to perform, at least qualitatively, as would be expected, that is, no exposure on first frame and building up gradually to peak intensity on Frame 5 (Figure 61) and deterioration to a gas cloud on Frame 6. However the light should have appeared on Frame 1, since exposure of the latter occurred 10 μsec after cap initiation and charge detonation should be underway in about 10 μsec. Also flash duration appeared short, lasting about 25 μsec.

A tetryl booster was used between cap and charge of Test 26, but had no apparent effect on starting detonation earlier as the frame by frame exposure of Test 26 was virtually identical to Test 25. No relative cap-camera delay was used in Test 27 and a thicker charge was used, resulting in the light peaking at about 75 μsec instead of 90 μsec as for the two previous tests. For Test 28 the camera sequence was delayed to expose Frame 1 80 μsec after cap initiation. This should have placed Frame 1 at nearly the same time sequence as Frame 4 of Test 27. However approximately the same exposure resulted as in Test 27 with nothing but apparent light leakage on the first three frames and the bright light not appearing until Frame 4. Therefore all frames were set to be exposed at the same time (20 μsec after cap initiation in Test 29). The first three frames were the same as before, but four and five were much dimmer than in Test 28 in which they had virtually the same delays. Frame delays were reversed in Test 30, relative to those used in Test 28, and results were essentially the same except the light transmitting capability of Kerr cells 4, 5, and 6 deteriorated since Test 28. And apparently cells 1, 2, and 3 had transmitted essentially nothing except light leakage after adjustment of their polarizers.

A resume of the foregoing test results indicate the following. Light leakage through the Kerr cells, and an internal discrepancy in relative timing of cap initiation and starting of the camera framing sequence, through Test 23 produced such ambiguous results that it wasn't possible to set up proper timing and backlighting intensity. Whenever a shaped charge was used, exposures similar to Frame 1 of Test 15 in Figure 61

resulted which apparently was nothing more than light leakage through the Kerr cells that occurred at peak intensity of the light source regardless of delay settings for the camera frames. The same was probably true when the M112A1 photoflash cartridges were used. They may not have even come on until long after the time coverage of the frame delay settings, but light leakage overexposed the frames. The best lighting and timing resulted in Test 14, and from then on (with the possible exception of Test 18) through Test 30 the pulsed light transmission characteristics of the Kerr cells appeared to progressively detiorate, first with frames 1, 2, and 3, then with 4, 5, and 6, until virtually nothing except light leakage was being transmitted by all cells in Test 30.

Another observation which may be made concerns the amount of backlighting available from a bare charge in the partial vacuum of the back chamber. For example Test 18 produced fairly good light intensity (Figure 61) in the back chamber partial vacuum without benefit of being enclosed in a plastic tube(Figure 59). Therefore if a charge produced this much light, a jet would produce more (e.g., see comparative charge and jet light intensities in Figure 54); so in order to use this method of backlighting to obtain silhouette pictures of jet elements it will be necessary to reduce the chamber pressure to a level that will prevent the jet from being self luminous, and use light bombs of the type shown in Figure 59 for backlighting.

TARGET DATA

A qualitative measure of jet mass and cohesion was indicated by the hole size and the depth of penetration of the jet in the various targets used. The type of targets used and the target damage for each test shot is contained in Appendix II with the exception of the IRECO vacuum range tests for which target data is listed in Table 6. Photographs of typical target damage are shown in Figures 33, 41, 42, 51, and 57.

CONCLUSIONS AND SUGGESTED FUTURE INVESTIGATIONS

The pertinent results of the investigation reported herein is summarized in Table 13 which lists the average performance of the various categories of liners, as well as test conditions relating to the use of waveshapers and jet inhibitors. After averaging the maximum and minimum velocities for each category, the velocity range, ΔV, was divided by the average jet length to provide an index of velocity gradient. The latter expresses average velocity gradient per unit length of jet, thereby reducing the varying factors to a common reference.

Due to the high initial velocity gradient present in most shaped charge jets (e.g., Figures 31 and 32), use of jet inhibitors is not ordinarily

TABLE 13. Summary of performance of the various liners used in constant-velocity jet tests.

Liner		Wave		AVERAGE PERFORMANCE					
Type	Identity	Shaper	Inhibitor	Max. Jet Velocity (km/sec)	Min. Jet Velocity (km/sec)	ΔV Vel. Range (km/sec)	Jet Length (cm)	Vel. Grad. Index (km/sec/cm)	No. Shots
Conic	68°	Yes	No	14.0	4.3	9.7	6.5	1.50	6
Conic	45°	Yes	No	15.2	3.2	12.0	9.8	1.22	5
Conic	45°	No	No	8.4	2.6	5.8	4.9	1.18	1
Conic	20°	Yes	No	14.4	4.9	9.5	12.1	0.76	1
Conic	20°	No	No	11.8	3.1	8.7	6.2	1.40	6
Cylinder	0°	Yes	No	22.8	8.0	14.8	2.0	7.40	1
Hemisphere		Yes	No	12.3	3.1	9.2	9.2	1.00	4
Conic	C-1	Yes	No	13.0	5.9	7.1	8.3	0.86	8
Conic	C-1	Yes	Yes	14.3	6.3	10.0	2.6	3.85	7
Conic	C-2	Yes	No	15.0	6.8	8.2	6.2	1.32	5
Conic	C-3	Yes	No	13.8	7.9	5.9	7.8	0.76	7
Paraboloid	C-11	Yes	No	13.3	5.5	7.8	6.2	1.26	11
Paraboloid	C-11	Yes	Yes	13.6	7.9	5.7	0.2	25.90	2
Paraboloid	C-12	Yes	No	12.3	6.7	5.6	2.5	2.24	4
Paraboloid	C-13	Yes	No	12.4	7.5	4.9	2.8	1.75	4
Paraboloid	C-14	Yes	No	12.7	9.6	3.1	1.6	1.96	4
Paraboloid	C-15	Yes	No	13.7	5.5	8.2	6.5	1.26	6
Paraboloid	C-15	Yes	Yes	14.0	13.8	0.2	0.4	0.50	1
Conic	C-37-a	No	No	8.5	5.2	3.3	6.0	0.55	1
Conic	C-38	Yes	No	11.7	6.0	5.7	5.9	0.97	3
Conic	C-38	Yes	Yes	12.2	8.6	3.6	3.8	0.95	3
Conic	C-38-a	Yes	No	12.9	4.3	8.6	15.1	0.57	1
Conic	C-38-a	Yes	Yes	12.1	1.3	10.8	10.2	1.06	1
Conic	C-38-b	Yes	No	12.2	3.8	8.4	4.6	1.83	1
Conic	C-38-c	Yes	No	19.6	4.6	15.0	10.4	1.44	1
Conic	C-38-d	Yes	No	24.3	7.0	17.3	2.0	8.65	1
Conic	C-38-e	No	No	9.1	3.9	5.2	7.0	0.74	1
Conic	C-39	No	No	9.4	3.2	6.2	8.0	0.78	1
Conic	C-39-a	Yes	No	16.0	4.6	11.4	11.7	0.97	1
Conic	*C-42	Yes	No	10.0	3.8	6.2	7.8	0.80	1
Conic	C-42	No	No	11.4	8.6	2.8	3.4	0.82	1
Conic	C-43	No	No	9.6	6.1	3.5	5.1	0.69	1
Conic	**C-43	No	No	9.5	7.7	1.8	7.7	0.23	1
Conic	C-43-a	No	Yes	9.8	5.9	3.9	4.4	0.89	1
Conic	**C-43-a	No	Yes	10.4	3.8	6.6	8.8	0.75	1

** Confined Charges

* $Ba(NO_3)_2$/TNT = 60/40, all others octol

effective in reducing the velocity gradient except when only the extreme leading element is allowed to pass. However when a jet possesses a low velocity gradient over an appreciable jet length, as Test E-86 showed (Figure 30), then cutting off the trailing segment of high gradient velocity with a jet inhibitor resulted in a jet that was 0.4 cm long and a velocity that dropped only 0.2 km/sec from the initial 14.0 km/sec (Test E-126, Figure 32). Thus by careful choice of liner and charge parameters, the use of a jet inhibitor will produce the desired low gradient jet of the required velocity. A comparison of target damage resulting from Tests E-86 and E-126 (Appendix II), indicate that most of the damage resulted from the high-velocity leading segments of the jets.

The lowest velocity gradient obtained was accomplished by confining the shaped charge, and this was achieved without a jet inhibitor which permitted the entire jet length and mass to come through with a relatively low overall index (see C-43**, Table 13). However the velocity of this test was below requirements and further investigation will be needed to vary such parameters as charge configuration, liner size and shape, degree of confinement, etc. to obtain optimum performance from this approach towards lower velocity gradient jets at higher velocity.

Reducing the "S" distance between top of charge and liner apex, especially to the extent of truncating the conic liner, greatly increases the initial velocity when a waveshaper is used to provide near-optimum detonation wave impulse angle with the wall at the top of the liner (e.g., C-38-c and C-38-d, Table 13). However this is accomplished at the expense of increased velocity gradient as the impulse angle rapidly decreases from apex to base of liner (Figure 44).

Conversely, elimination of waveshaper and employment of an appreciable "S" distance decreases the initial velocities but also decreases velocity gradient significantly (e.g. C-37-a and C-39 of Table 13).

The advantage of more optimum detonation wave impulse angle throughout the length of the liner, without the foregoing attendant disadvantage of increased jet velocity gradient, may be simultaneously realized by modifying the charge configuration from a conventional cylinder to a disc shape. When the latter is symmetrically initiated around its periphery there occurs a much higher velocity jet of apparent shorter length and smaller velocity gradient. Results of disc-shaped charge jets are not listed in Table 13 since the multiple plate method of determining jet segment velocities and lengths did not lend itself very well to disc-shaped charges when shot in air. For example in Test No. E-151, 3.3" of air had a greater effect upon reducing the jet velocity than did the 1/16" thick steel plate (see Figure 50 and Table 7). Therefore conclusions on jet lengths and velocity gradients have been qualitatively deduced from target damage and streak camera film records.

Further development of the foregoing approach, of which the disc-shaped charge is but a first step, could results, ideally, in a spherically-shaped jet of still higher velocities and virtually zero velocity gradient

as an inherent corollary of the jet's shape. Such a jet would more closely simulate the maximum velocities and shape of meteors, than do the elongated jets from cylindrical charges, and would therefore provide more accurate simulation of meteor impact phenomena for cratering studies.

The contract requirement of developing shaped charge jet velocities approaching 14 km/sec has been met with various types of liners. For example the C-1 conic type liner consistantly produced jets having maximum velocities near or above 14 km/sec (Figure 25). And of the paraboloid type liners the C-11 and C-15 liners also produced jets within the required velocity range (Figure 30 and 32). Moreover, maximum jet velocities up to 24.3 km/sec from conventional cylindrical charges have been achieved (E-189, Figure 44), and which produced fair target damage (Appendix II). And finally, jet velocities up to 32.7 km/sec were attained with a disc-shaped charge (E-151, Table 7) using a 20° conic liner (Figure 49).

Compliance with the contract requirement of an essentially zero gradient jet at velocities approaching 14 km/sec was most closely realized with Test No. E-126 in which a C-15 paraboloid liner with jet inhibitor produced a jet 0.4 cm long having an initial velocity of 14.0 km/sec and a final velocity of 13.8 km/sec (Figure 32). This represents a velocity variation of $\pm$ 0.72% of a mean velocity of 13.9 km/sec. Target damage and streak camera data indicate that jets from disc-charges may have low velocity gradients, however further investigation and improved experimental techniques will need to be developed in order for this to be resolved.

Although jet cohesion was not an initial contract requirement, difficulties arising from attempts to x-ray shaped charge jets at extended standoff distances caused lateral dispersion of jet elements to become an important factor. After discovering that even the more massive liners produced jets with excessive lateral dispersion at the standoff distances involved*, a decision was made to attempt photographing jets at reduced standoff distances≠. Then, when jets from shaped charges are used in cratering studies, employment of an adequate barricade between the shaped charge and target would minimize target damage due to the blast from the charge and thereby isolate damage due to the jet. This was considered a more practical approach because efforts to reduce jet dispersion out to extended standoff distances would probably entail an investigation within itself.

---

* Page 101
≠ Page 102

APPENDIX I

Sample Pulse Delay Calculations to Provide Maximum Velocity Range for Three Orthogonal X-ray Stations of Fig. 55.

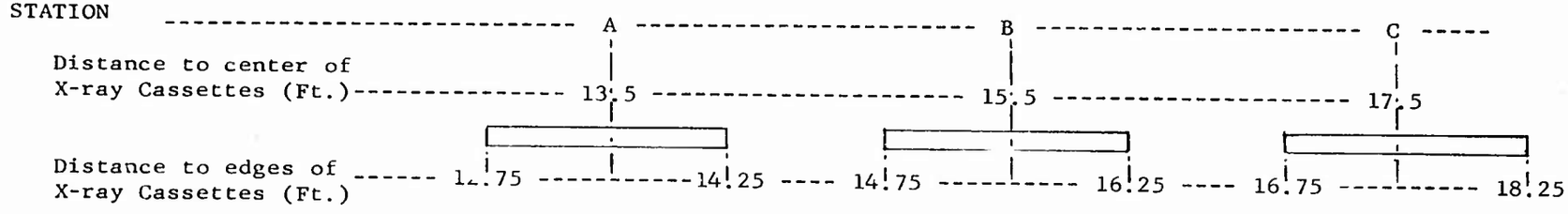

H	Velocity*	35.8 (4)	40.0 (1)	29.1 (12)	32.0 (9)	24.2 (20)	26.4 (17)
	Flight Time≠	356 (3)	356 (2)	507 (11)	507 (10)	692 (19)	692 (18)
V	Velocity*	32.0 (8)	35.8 (5)	26.4 (16)	29.1 (13)	22.2 (24)	24.2 (21)
	Flight Time≠	398 (7)	398 (6)	559 (15)	559 (14)	754 (23)	754 (22)

In this example 40,000 ft/sec is selected as the maximum velocity for which coverage is required. All delay times and all other velocities are based on this selected velocity.
Calculations are made from the equation: Velocity = distance/time, in the order shown in parenthesis.

Example: (1) Selected velocity (40,000 ft/sec maximum)

(2) $t = \frac{s}{v} = \frac{14.25 \text{ feet}}{40{,}000 \text{ ft/sec}} \times \frac{10^6 \text{ } \mu\text{seconds}}{\text{second}} = 356 \text{ } \mu\text{seconds}$

(3) Equals same time as (2)

(4) $v = \frac{s}{t} = \frac{12.75}{356} \times 10^6 = 35.8 \times 10^3$

(5) Equals same velocity as (4) etc.

Delay Time = Flight time + time from charge initiation to jet formation = flight time + 30 seconds.

*in thousands of feet/second, ≠in μseconds.

APPENDIX II

Target data for all shots except IRECO vacuum shots

NOTES:

Target schedule data are given on page

* Indicates that mutilated or missing target plates prevented obtaining data.

≠ Indicates that disc charge jets didn't penetrate first plate and that first plate was obliterated.

Omitted test numbers are due to charges that were assigned numbers and never fired or to charge failures or failure to form a jet resulted in no target data.

			TARGET DAMAGE DIMENSION (cm)		
				HOLE SIZES	
Test No.	Target Schedule	Standoff (inches)	Depth of Penetration	Maximum Diameter	Maximum Diameter
E-1	0	4	2.6	1.0	--
E-2	0	4	0.2	0.3	--
E-3	0	4	1.1	0.8	--
E-4	0	4	1.0	2.0	--
E-5	0	4	1.0	1.7	--
E-6	0	4	0.8	1.0	--
E-7	0	4	0.4	0.6	--
E-8	P	3.9	0.6	>2.0	2.0
E-11	P	3.9	1.9	1.1	0.6
E-12	P	3.9	1.9	1.2	0.4
E-13	P	3.9	1.4	1.2	0.2
E-14	P	3.9	0.7	0.8	0.4
E-15	P	3.9	1.7	1.1	0.4
E-16	K	3.9	0.5	3.2	1.5
E-17	K	3.9	>6	2.6	<1.6
E-18	A	3.9	No Data		
E-19	A	3.9	>3.5	2.5	1.4
E-20	A	3.9	2.4	2.2	0.6
E-21	A	3.9	2.4	2.2	1.5
E-22	A	3.6	2.6	2.0	1.0
E-23	A	3.6	3.0	1.7	0.5
E-24	A	3.6	2.4	1.4	0.8
E-25	A	3.6	2.3	1.4	0.9

Test No.	Target Schedule	Standoff (inches)	TARGET DAMAGE DIMENSION (cm)		
			Depth of Penetration	HOLE SIZES Maximum Diameter	Maximum Diameter
E-26	A	3.6	>3.0	1.6	1.0
E-27	A	3.6	>3.0	1.5	1.1
E-28	A	3.6	2.4	1.5	0.8
E-29	A	3.6	2.4	2.1	0.9
E-30	A	3.6	2.4	2.0	1.0
E-31		3.6	>3.0	2.5	1.0
E-32	A	3.9	2.4	4.0	1.2
E-33	A	3.9	>3.0	3.8	1.1
E-34	A	3.9	>3.0	3.5	1.0
E-35	A	4.1	2.4	1.5	0.8
E-36	A	4.1	2.4	1.2	1.1
E-37	A	4.1	1.4	3.0	0.5
E-38	A	4.0	1.8	1.7	1.4
E-39			>3.0	1.5	1.3
E-40			2.4	2.5	1.4
E-41	D	3.5	>2.4	3.6	1.0
E-42	D	3.5	2.4	3.0	0.2
E-43	D	3.4	2.6	1.3	0.4
E-44	D	3.4	2.0	3.7	<3.7
E-45	Dx	3.5	1.1	3.0	2.0
E-46	D	3.5	>3.7	3.3	1.0
E-47	D	3.5	>1.1	1.4	1.1
E-48	D	3.5	>1.1	1.3	0.5
E-49x	D	3.5	1.9	1.2	1.0
E-50	D	3.5	0.5	0.4	<0.4
E-51	D	3.5	>1.1	1.3	<1.3
E-52	D	3.5	1.2	1.2	<1.2
E-53	D	3.5			
E-54	D	3.5	1.1	2.0	1.1
E-55					
E-56					
E-57					
E-58	D	3.5	>1.1	1.2	<1.2
E-59	D	3.5	>1.1	1.2	<1.2
E-60	D	3.5	1.1	3.0	1.2
E-61	D		1.3	1.2	<1.2

Test No.	Target Schedule	Standoff (inches)	TARGET DAMAGE DIMENSION (cm) Depth of Penetration	HOLE SIZES Maximum Diameter	Maximum Diameter
E-62	E	3.2	>1.1	>1.4	1.4
E-63	E	3.2	>0.8	>3.1	3.1
E-64	E	3.2	1.1	2.0	~2.0
E-65	E	3.2	>0.8	>3.5	3.1
E-66	E	3.2	>0.8	>2.5	2.5
E-67	E	3.2	>0.8	>3.0	~3.0
E-68	E	3.2	>0.8	>2.5	2.5
E-69	E	3.2	>0.8	5.5	2.3
E-70	E	3.2	0.5	>1.0	~1.0
E-71	E	3.2	0.5	>1.5	~1.5
E-72	E	3.2	0.7	>1.5	1.5
E-73	E	3.2	0.5	~5.0	0.4
E-74	E	3.2	0.5	3.7	~0.8
E-75	E	3.2	0.6	3.5	~1.0
E-76	E	3.2	0.5	2.5	~1.2
E-77	E	3.2	0.5	~6.0	0.4
E-78	E	3.2	3.1	>3.4	1.3
E-79	E	3.2	~1.0	4.0	3.0
E-80	F	3.4	1.6	>1	~0.5
E-81	F	3.4	1.3	>1.5	0.5
E-82	F	3.4	1.3	>0.8	0.4
E-83	F	3.4	1.4	>1.3	0.8
E-84	F	3.4	1.3	>4	4
E-85	F	3.4	1.2	>4	1
E-86	F	3.4	1.2	>1.7	0.9
E-87	F	3.4	1.3	>2	0.7
E-88	F	3.4	1.3	>1.6	~1.5
E-89	E	3.4	2.1	>3.5	1.2
E-90	E	3.4	2.2	>2.5	1.7
E-92	E	3.4	1.5	>2.5	2.5
E-100	S	228	0	Scattered Craters	
E-101	Q	212	0	"	"
E-102	Q	212	0	"	"
E-103	Q	212	0	"	"
E-104	Q	212	0	"	"
E-111	Q	212	0	"	"
E-112	R	212	1.3	0.25	--

Test No.	Target Schedule	Standoff (inches)	TARGET DAMAGE DIMENSION (cm) Depth of Penetration	HOLE SIZES Maximum Diameter	HOLE SIZES Maximum Diameter
E-113	D	3.2	>3.7	>2.5	0.6
E-114	D	3.2	1.1	>2.8	2.0
E-115	E	3.2	>3.4	>2.5	0.8
E-116	E	3.2	1.5	>2.5	≈0.5
E-117	E	3.2	0.8	3.5	≈1.5
E-118	E	3.2	0.8	*	*
E-119	E	3.2	0.8	>2.5	≈2.5
E-120	E	3.2	0.9	>2	≈2
E-121	F	3.2	0.9	>3.5	3.5
E-122	F	3.2	0.7	≈4	≈1.8
E-123	F	3.2	1.2	>2.7	0.3
E-124	F	3.2	0.6	*	*
E-125	F	3.2	0.9	>2.5	2.5
E-126	F	3.2	0.9	*	*
E-127	F	3.2	0.9	>2	2
E-128	F	3.2	0.8	*	*
E-130	D	3.5	>3.4	3.0	1.0
E-131	H	3.3	0.4	>0.5	0.5
E-132	I	160	0.2	0.5	0.1
E-133	I	160	0.2	0.3	0.1
E-134	I	160	0	0	0
E-135	*	160	0.2	0.6	0.1
E-153	H	3.3	1.3	1.3	1.3
E-154	E	3.3	>3.4	≈2	0.7
E-155	H	3.3	0.8	>1	≈1
E-158	J	3.3	>3.8	2.4	1.2
E-151	H	3.3	>0.2	≠	≠
E-152	E	3.3	≠	≠	≠
E-156	H	3.3	>1	≠	≠
E-157	H	3.3	>0.7	≠	≠
E-163	Q	217	>0.3	1	0.5
E-164	Q	217	>0.3	7.6	0.5
E-165	Q	217	>0.3	7.6	0.5
E-166	Q	217	--	--	--
E-167	S	217	1	--	--
E-168	S	217	0.8	--	--
E-171	H	3.3	2.0	*	*
E-173	L	3.3	5.1	3.5	1.0
E-180	H	3.3	1.0	*	*

Test No.	Target Schedule	Standoff (inches)	TARGET DAMAGE DIMENSION (cm)		
				HOLE SIZES	
			Depth of Penetration	Maximum Diameter	Maximum Diameter'
E-182	J	3.3	1.9	*	*
E-184	H	3.3	≠	≠	≠
E-185	H	3.3	1.7	>2.3	1.0
E-186	J	3.3	2.6	5.0	2.5
E-187	J	3.3	1.1	*	*
E-188	E	3.3	0.8	*	*
E-189	E	3.3	0.8	>1	1.0
E-190	D	3.3	2.4	>3	1.5
E-192	K	3.3	>6	4.2	3.0
E-196	C	3.3	>5	3.0	0.2
E-198	D	3.3	1.1	*	*'
E-199	E	3.3	2.7	*	*
E-200	D	3.3	1.8	*	*
E-201	T	8.5	>10	3.2	--
E-202	T	8.5	>10	∿4	--
E-203	R	216	<0.6	Scattered Craters	
E-204	R	216	>1.3	∿4.7	--
E-205	R	216	1.3	1.3	--
E-206	R	216	>1.3	∿9	--
E-208	N	3.3	0.4	3.5	0.7
E-209	N	3.3	2.5	1.7	0.8
E-210	E	3.3	2.1	>1.5	1.3
E-211	D	3.3	>3.5	2.5	1.7
E-212	R	27	>1.3	∿2.5	--
E-218	R	73	∿0.5	Scattered Craters	
E-225	R	45	>1.3	∿3.5	--
E-226	R	23.5	>1.3	3.2	--

TARGET SCHEDULES

SCHEDULE	A	C	D	Dx	E	F	H	I	J	K	L	P
Plate Size:	3x3	3x3	3x3	3x3	3x3	3x3		18x18	3x3	3x3	3x3	3x3
Thickness of Plate No.												
1	1/16	1/16	1/16	1/16	1/16	1/16	1/16	1/16	1/8	1/8	1/4	1/8
2	1/8	1/8	1/8	1/8	1/8	1/16	1/16	1/8	1/8	1/4	1/4	1/8
3	1/4	1/4	1/4	1/4	1/8	1/16	1/16	1/4	1/4	1/2	1/4	1/8
4	1/4	1/2	1/4	1/4	1/4	1/8	1/16	--	1/4	1/2	1/4	1/8
5	1/4	1/2	1/4	1/4	1/4	1/8	1/8	--	1/4	1/2	1/4	1/8
6	1/4	1/2	1/2	1/2	1/2	1/4	1/4	--	1/2	1/2	1/2	1/8
Slug				3/4								
Stopper Plates				3/4 (1/4" dia hole in each plate)								

Schedule 0: 2" dia steel rod, 5" long
Schedule Q: 18 x 18 x 0.1" thick
Schedule R: 18 x 18 x 0.5" thick
Schedule S: 18 x 18 x 2" thick
Schedule T: 18 x 18 x 4" thick

All target plates of steel except Schedule Q, R, S, and T which were of aluminum.

BIBLIOGRAPHY

1. "Special Explosive Projectors", Kreyenhagen, et.al., Sixth Symposium on Hypervelocity Impact, August 1963, Vol. 1, pp. 349-373.

2. "Inhibited Jet Charge", S. Kronman and A. Merendino, Sixth Symposium on Hypervelocity Impact, August 1963, Vol. 1, pp. 331-348.

3. Cook, M. A., "The Science of High Explosives", Reinhold Publishing Corp., 1958, p. 224.

4. Birkhoof, G, Mac Dougal, D. P., Pugh, E.M., and Taylor, G., Journal Applied Physics, 19, 563 (1948).

5. Report APGC-TR-61-42, Air Proving Ground Center, Eglin Air Force Base, Figure 77, Table I, and p. 40.

6. Gainer, M. K., "The Application of Radioactive Tracers to Shaped Charge Liners", Ballistic Research Laboratories Report No. 1242, January 1960, Figure 4.

7. Opik, E., "Physics of Meteor Flight in Atmosphere", Interscience Publishers, Inc., New York and London, 1958, pp. 174.

8. McKinley, W. R., "Meteor Science and Engineering", McGraw Hill Book Company, Inc., 1961, p. 174.

9. Cook, M. A., "The Science of High Explosives", Reinhold Publishing Corp., 1958, p. 226-227.

INITIAL DISTRIBUTION

1 DOD (DIAAP-1K2)
1 Hq USAF (AFTAC)
1 Hq USAF (AFCIN-3K2)
2 Hq USAF (AFRDC)
1 Hq USAF (AFRAE-E, L/C Hicks)
1 Hq USAF (AFTST-EL/CS, Maj Myers)
1 USAF (AFRST-PM/ME, Maj Geiseman)
1 Hq USAF (AFXPDK-NI)
1 AFSC (SCRWA)
1 AFSC (SCTA, Mr R Fiek)
2 BSD (Col Brassfield)
1 AFFDL (FDTS) Mr Parmley
2 ASD (ASAD-Lib)
1 ASD (ASRNGW, Don Lewis)
2 AFSWC (Tech Info Div)
1 AFCRL (CRQST-2)
1 AFOSR
1 AFOSR (SRHP, Dr M M Slawsky)
1 AFOSR (SRHP, Dr J F Masi)
1 AFOSR (Dr A G Horney)
1 AFOSR (SRHP, Dr R Reed)
1 AFOSR (Dr M A Cook)
1 OOAMA (OOYD)
1 NASA
1 NASA (Ofc of Adv Rsch)
2 NASA (Tech Lib)
1 NASA, Rsch Ctr (W H Kinard)
1 NASA, Rsch Ctr (J Stack)
4 NASA, Ames Rsch Ctr (Tech Lib)
1 Marshall Space Flight Center (W D Murphree)
1 Marshall Space Flight Center Adv Rsch Proj Lab (Dr W Johnson)
1 Adv Rsch Proj Agency (Dr C Bates)
1 Dir of Def Rsch & Engr (Tech Lib)
2 Dir of Def Rsch & Engr (Dr R M Yates)
1 Armour Rsch Foundation (Mr G H Strohmeir)
1 Aberdeen Proving Ground (Tech Lib)
1 White Sands Missile Range
1 Univ of Chicago (Lib)
2 Franklin Institute of the State of Penn
2 SSD (SSTRG/LC W Levin)
1 Calif Inst of Tech, Jet Propulsion Lab
2 John Hopkins Univ (Applied Rsch Lab)
1 OAR (RROSA/Maj Davis)
1 OAR (RRCSA/Lt Col Williams)
20 DDC
3 Lewis Rsch Ctr
2 Dir, IDA/WPNS Sys Eval Gp
1 Dir, USAF PROJ RAND (Tech Lib)
3 Army Materiel Command Rsch Directorate (MCR)
2 Picatinny Arsenal (SMUPA-DW6)
1 Aberdeen Proving Ground (Dr Eichelberger)
1 Aberdeen Proving Ground (J Kineke)
1 Aberdeen Proving Ground (F E Allison)
1 Redstone Scientific Info Ctr
1 Frankford Arsenal (Lib)
1 Frankford (Pitman-Dunn Lab)
2 Springfield Armory (R&D Div)
2 Watertown Arsenal
1 Rock Island Arsenal
1 Army Engr Rsch and Dev Lab (Tech Doc Ctr)
1 Dir of Spec Wpns Div (C.I. Peterson)
1 Army Rsch Ofc - Durham (Dr A S Galbraith)
4 Bureau of Naval Weapons (R-12)
4 Bureau of Naval Weapons (DLI)

1 US Naval Rsch Lab
(Code 130/Mr WV Atkins)
2 US Naval Ord Test Stn
(Mr L Cosner)
2 US Naval Ord Test Stn
(Tech Lib)
1 US Naval Ord Lab
(Tech Lib)
2 US Naval Wpns Lab
(Tech Lib)
1 US Naval Wpns Lab (Dr Soper)
1 AFMTC (MTBAT)
4 TAC (DORQ)
1 General Electric Company
APGC
4 PGBSP-4
3 PGPI
1 PGOW
RTD Det 4
2 ATTR
1 ATWF
1 ATTR
1 ATB
20 ATBT
1 Intermountain Research and Engineering Co
1 Air University Library
1 US Army, Edgewood Arsenal (Operations Research Gp)
1 US Naval Weapons Evaluation Facility (NEWS-1)
1 Wright-Patterson AFB, Ohio (SEPI)

DOCUMENT CONTROL DATA - R&D

(Security classification of title, body of abstract and indexing annotation must be entered when the overall report is classified)

1. ORIGINATING ACTIVITY (Corporate author): Intermountain Research and Engineering Co., Inc., Salt Lake City, Utah	2a. REPORT SECURITY CLASSIFICATION: UNCLASSIFIED 2b. GROUP: N/A

3. REPORT TITLE

CONSTANT VELOCITY JETS FOR QUANTITATIVE ULTRA - HIGH VELOCITY CRATERING STUDIES

4. DESCRIPTIVE NOTES (Type of report and inclusive dates)

Final Report (5 June 1963 - 28 January 1965)

5. AUTHOR(S) (Last name, first name, initial)

Pack, Douglas H.

6. REPORT DATE	7a. TOTAL NO. OF PAGES	7b. NO. OF REFS
March 1965	135	9

8a. CONTRACT OR GRANT NO.	9a. ORIGINATOR'S REPORT NUMBER(S)
AF 08(635)-3668 b. PROJECT NO. 5841 c. d.	None 9b. OTHER REPORT NO(S) (Any other numbers that may be assigned this report) ATL-TR-65-24

10. AVAILABILITY/LIMITATION NOTICES

Qualified requesters may obtain copies of this report from DDC.

11. SUPPLEMENTARY NOTES	12. SPONSORING MILITARY ACTIVITY
	Ballistics Division Det 4, RTD (ATB) Eglin AFB, Fla.

13. ABSTRACT

Experiments were carried out to produce a constant velocity jet from shaped charges. Tests were conducted in atmosphere and at reduced pressures. Liner geometries, types of explosive, and wave shaping techniques were varied systematically to produce an elongated jet which approached a velocity of 14.0 km/sec.

DD FORM 1 JAN 64 1473

14 KEY WORDS	LINK A		LINK B		LINK C	
	ROLE	WT	ROLE	WT	ROLE	WT
Shaped Charge Detonation Physics						

INSTRUCTIONS

1. ORIGINATING ACTIVITY: Enter the name and address of the contractor, subcontractor, grantee, Department of Defense activity or other organization *(corporate author)* issuing the report.

2a. REPORT SECURITY CLASSIFICATION: Enter the overall security classification of the report. Indicate whether "Restricted Data" is included. Marking is to be in accordance with appropriate security regulations.

2b. GROUP: Automatic downgrading is specified in DoD Directive 5200.10 and Armed Forces Industrial Manual. Enter the group number. Also, when applicable, show that optional markings have been used for Group 3 and Group 4 as authorized.

3. REPORT TITLE: Enter the complete report title in all capital letters. Titles in all cases should be unclassified. If a meaningful title cannot be selected without classification, show title classification in all capitals in parenthesis immediately following the title.

4. DESCRIPTIVE NOTES: If appropriate, enter the type of report, e.g., interim, progress, summary, annual, or final. Give the inclusive dates when a specific reporting period is covered.

5. AUTHOR(S): Enter the name(s) of author(s) as shown on or in the report. Enter last name, first name, middle initial. If military, show rank and branch of service. The name of the principal author is an absolute minimum requirement.

6. REPORT DATE: Enter the date of the report as day, month, year, or month, year. If more than one date appears on the report, use date of publication.

7a. TOTAL NUMBER OF PAGES: The total page count should follow normal pagination procedures, i.e., enter the number of pages containing information.

7b. NUMBER OF REFERENCES: Enter the total number of references cited in the report.

8a. CONTRACT OR GRANT NUMBER: If appropriate, enter the applicable number of the contract or grant under which the report was written.

8b, 8c, & 8d. PROJECT NUMBER: Enter the appropriate military department identification, such as project number, subproject number, system numbers, task number, etc.

9a. ORIGINATOR'S REPORT NUMBER(S): Enter the official report number by which the document will be identified and controlled by the originating activity. This number must be unique to this report.

9b. OTHER REPORT NUMBER(S): If the report has been assigned any other report numbers *(either by the originator or by the sponsor)*, also enter this number(s).

10. AVAILABILITY/LIMITATION NOTICES: Enter any limitations on further dissemination of the report, other than those imposed by security classification, using standard statements such as:

(1) "Qualified requesters may obtain copies of this report from DDC."

(2) "Foreign announcement and dissemination of this report by DDC is not authorized."

(3) "U. S. Government agencies may obtain copies of this report directly from DDC. Other qualified DDC users shall request through

_____."

(4) "U. S. military agencies may obtain copies of this report directly from DDC. Other qualified users shall request through

_____."

(5) "All distribution of this report is controlled. Qualified DDC users shall request through

_____."

If the report has been furnished to the Office of Technical Services, Department of Commerce, for sale to the public, indicate this fact and enter the price, if known.

11. SUPPLEMENTARY NOTES: Use for additional explanatory notes.

12. SPONSORING MILITARY ACTIVITY: Enter the name of the departmental project office or laboratory sponsoring *(paying for)* the research and development. Include address.

13 ABSTRACT: Enter an abstract giving a brief and factual summary of the document indicative of the report, even though it may also appear elsewhere in the body of the technical report. If additional space is required, a continuation sheet shall be attached.

It is highly desirable that the abstract of classified reports be unclassified. Each paragraph of the abstract shall end with an indication of the military security classification of the information in the paragraph, represented as *(TS), (S), (C), or (U)*

There is no limitation on the length of the abstract. However, the suggested length is from 150 to 225 words.

14. KEY WORDS: Key words are technically meaningful terms or short phrases that characterize a report and may be used as index entries for cataloging the report. Key words must be selected so that no security classification is required. Identifiers, such as equipment model designation, trade name, military project code name, geographic location, may be used as key words but will be followed by an indication of technical context. The assignment of links, rules, and weights is optional.